Title	Construction of Metallosupramolecular Frameworks Based on an Anionic Pentanuclear Complex with D-Penicillaminate
Author(s)	Surinwong, Sireenart
Citation	大阪大学, 2016, 博士論文
Version Type	VoR
URL	https://doi.org/10.18910/59531
rights	
Note	

Construction of Metallosupramolecular Frameworks Based on an Anionic Pentanuclear Complex with D-Penicillaminate

(D-ペニシラミンをもつアニオン性五核錯体をベースとする
金属超分子フレームワークの構築)

Sireenart Surinwong

Department of Chemistry, Graduate School of Science
Osaka University

2016

<p style="text-align:center">Contents</p>

Chapter III. Combination of $Co^{III}_2Au^{I}_3$ complex anions and aqua zinc(II) cations.

General Introduction.

Over the past decades, supramolecular chemistry has become one of the most attractive fields in modern chemistry. In supramolecular systems, molecules are recognized as 'building blocks' that are self-assembled *via* weak noncovalent interactions such as van der Waals interaction, electrostatic interaction, and hydrogen-bonding interaction, leading to highly organized frameworks.[1] An expansion of supramolecular chemistry involving metal coordinations, which is termed as 'metallosupramolecular chemistry', has been developed regarding synthetic routes and characterization methods for coordination compounds.[2] A number of metallosupramolecular frameworks have been created by using coordination compounds as a building block, illustrating unique structures and intriguing properties, which thanks to the diversity of coordination geometries of metal ions and the flexibility of noncovalent interactions.[3,4]

A variety of well-designed building blocks consisting of metal ions and organic ligands such as 4,4'-bipyridine, pyrazine, and 1,4-benzenedicarboxylate have been exploited toward a construction of plenty metallosupramolecular frameworks mainly based on coordination bonds between metal ions and ligands, especially for metal–organic frameworks (MOFs) and coordination polymers (CPs).[5,6] They are qualified due to the directionality and the stability of coordination bonds together with the versatility of organic ligands. However, their rigid characteristics cause not only the low coordination flexibility but also the low structural dynamics.[5,6] One of the powerful approaches that can ease these drawbacks is a utilization of hydrogen bonds, in which the flexibility can be served, nevertheless the hydrogen-bonding interactions generally lack of robustness, leading to the low stability of their frameworks.[7] A common synthetic strategy to construct the metallosupramolecular frameworks that introduces both coordination and hydrogen bonds is the use of more than one kind of building blocks within a structure, for example, the framework of [$Zn_2(bdc)_2(dabco)$] reported by Burrows contains 1,4-benzenedicarboxylate (bdc) and 1,4-diazabicyclo[2.2.2]octane (dabco).[8] However, such a strategy often results in low chemical selectivity and systematic complexity which arise from the presence of multiple components. Moreover, such problems often make difficulties in the utilization of further applications through the introduction of undesired functional groups.[8] Consequently, researches on a rational methodology for the construction of novel metallosupramolecular frameworks illustrating high flexibility and stability, in which both coordination and hydrogen bonds can be fully utilized, have been still

a challenge.

As an attempt to expand the strategy, the use of multinuclear metal complexes having multiple carboxylate groups with a well-designed molecular shape as a molecular building block is one of potential methodologies. Multinuclear metal complexes, in particular heterometallic multinuclear complexes, have attracted much attention in recent years owning to their fascinating properties based on the cooperative effects between different metal ions, which arise from a combination of inherent natures of each metal ion.[9] The introduction of heterometallic multinuclear building units into metallosupramolecular frameworks potentially provides not only larger pores but also additional functions to achieve multifunctional properties, including excellent gas storage, ion exchange, and chiral selective sorption.[10] In addition, the most fascinating point of heterometallic multinuclear complexes is a variety of geometries and directionalities that cannot be provided from single metal ion or even a multidirectional organic ligand.[11] Some studies on the creation of metallosupramolecular frameworks based on heterometallic multinuclear complexes with multiple carboxylate groups have been developed, in which a possibility of dimensional and functional extensions of metallosupramolecular complexes was disclosed.[10] For examples, a pH-controlled construction of cluster-based metallosupramolecular frameworks composed of D-penicillaminato $Cu^I_8Cu^{II}_6$ complex anions, $[Cu^I_8Cu^{II}_6(\text{D-pen-}N,S)_{12}Cl]^{5-}$ (D-H$_2$pen = D-penicillamine), which contain twelve carboxylate arms and hexaaqua cobalt(II) cation, has been reported.[12] In this system, several diverse dimensional structures ranging from zero-dimensional (0D) to two-dimensional (2D) architectures constructed by both coordination and hydrogen bonds have been obtained. However, their frameworks commonly showed a closely packed arrangement, which limits the use for further applications, especially for those expected for a porous material. This is due to a nature of spherical shape of the anionic $Cu^I_8Cu^{II}_6$ multinuclear complex. An attempt to use the rod-shaped L-cysteinato $Co^{III}_2Au^I_3$ pentanuclear complex, $(\Delta)_2\text{-}[Co^{III}_2Au^I_3(\text{L-cys-}N,S)_6]^{3-}$ (L-cys = L-cysteinate), which has six carboxylate arms in a combination with $[Co_3(aet)_6]^{3+}$ trinuclear-complex cation, was investigated by Lee *et al*.[13] Nonetheless, a chiral inversion that induces a molecular dimerization of the molecular building units was observed in this case. This indicated that the employed L-cysteinato $Co^{III}_2Au^I_3$ pentanuclear complex is not suitable for the construction of stable metallosupramolecular frameworks.

Recently, an anionic rod-shaped $Co^{III}_2Au^I_3$ pentanuclear complex with D-penicillaminate, $(\Lambda)_2\text{-}[Co^{III}_2Au^I_3(\text{D-pen-}N,S)_6]^{3-}$ having six carboxylate arms, composed of two chiral

Λ-[Co^{III}(D-pen-N,S)$_6$]$^{3-}$ octahedral units that are linked by three linear Au^I ions through sulfur bridges was synthesized by Konno *et al*.[14] It has been reported that this anionic Co$^{III}_2$Au$^I_3$ pentanuclear complex crystallized with Na^I cations, leading to the formation of a metallosupramolecular framework with retention of the structural chiral pentanuclear building units. Based on this result, the chiral Co$^{III}_2$Au$^I_3$ pentanuclear complex, in which a well-fixed conformation and multiple carboxylate groups are offered, has a potential to construct chiral metallosupramolecular frameworks. Therefore, a wide diversity of frameworks together with a high stability can be anticipated. However, study on this kind of well-designed heterometallic multinuclear complex has been less explored with a limited number in the literatures. Consequently, an interest in the exploration of chiral metallosupramolecular frameworks, based on the rod-shaped Co$^{III}_2$Au$^I_3$ pentanuclear-complex anion especially in combination with aqua metal cations that offer a feasibility to form both coordination and hydrogen bonds, has been motivated in this thesis (Chart 1). A variety of intermolecular interactions potentially leads to the formation of unique metallosupramolecular frameworks presenting diverse structures that are restricted for general metallosupramolecular frameworks produced by using common mono- and dicarboxylate ligands. Furthermore, the anionic Co$^{III}_2$Au$^I_3$ pentanuclear complex also illustrates high solubility in water. In this context, one of the advantages is that the synthetic conditions can be modified in an extremely wide range of varied synthetic parameters such as pH, concentration, and metal species.

The studies presented in this thesis are aimed at the construction of diverse metallosupramolecular frameworks, in which a variety of intermolecular interactions including coordination and hydrogen bonds can be utilized, based on the rod-shaped, anionic Co$^{III}_2$Au$^I_3$ pentanuclear complex, [Co$^{III}_2$Au$^I_3$(D-pen-N,S)$_6$]$^{3-}$ ([**1**]$^{3-}$), as a molecular building unit (Chart 2). The combination of [**1**]$^{3-}$ and the simple aqua transition metal cations, [M(H$_2$O)$_n$]$^{2+}$ (M = Co^{2+}, Ni^{2+}, Mn^{2+}, Zn^{2+}), is presented and discussed. Cobalt(II) ion with 3d^7 electron configuration is one of the most favorable metal ions to investigate the formation of various metallosupramolecular frameworks owning to its potentiality to form stable interactions with many inorganic ligands such as water, ammonia, and chloride ion, etc.[15,16] In the case of nickel(II) ion with 3d^8 electron configuration, it is also intriguing because nickel(II) ion can adopt both octahedral and square-planar coordination geometries depending on the character of ligands.[15,17] Manganese(II) ion with 3d^5 electron configuration is characterized by its larger ionic radius (0.83 Å), compared with those of cobalt(II) and nickel(II) ions (0.74 Å and 0.69 Å, respectively), together with its faster rate of water

exchange reactions.[15,17] While zinc(II) ion gives no information about the d electron structure, some of $3d^{10}$ closed-shell metal ion allow resulting metallosupramolecular complexes to show luminescence are reported in previous studies.[15,17,18] This thesis reveals a successful production of a fascinating series of novel metallosupramolecular frameworks, presenting not only porous ionic frameworks but also dense coordination frameworks, which are dependent on the nature of metal ions and synthetic conditions.

In Chapter I, an excellent example of a kinetic synthesis of highly porous metallosupramolecular frameworks is presented, which are created by using a combination of the rod-shaped $Co^{III}_2Au^I_3$ complex ($[\mathbf{1}]^{3-}$) and aqua cobalt(II) species ($[Co(H_2O)_n]^{2+}$) under controlled synthetic conditions. Impressively, the resulting ionic crystals displayed an extremely porous metallosupramolecular framework with a porosity of *ca.* 80%. Such a high porosity has not been found in the previously reported frameworks consisting of cationic and anionic species without the formation of coordination bonds. Not only the crystallographic study but also the structural conversion phenomena are also examined. In Chapter II, an attempt to use other transition metals as cationic species was investigated in order to obtain more information to reach more understanding about the influences of different metal ions on resulting metallosupramolecular frameworks. It was found that four metallosupramolecular frameworks are produced from the combination of $[\mathbf{1}]^{3-}$ and $[Ni(H_2O)_n]^{2+}$ or $[Mn(H_2O)_n]^{2+}$. The structural conversion phenomena occurred for the Mn^{II} complexes were found to be different from those for Co^{II} and Ni^{II} complexes, leading to the production of different frameworks. In Chapter III, a systematic study on a pH-controlled construction of metallosupramolecular frameworks consisting of $[\mathbf{1}]^{3-}$ and $[Zn(H_2O)_n]^{2+}$ was investigated. It was found that two different frameworks with remarkably different porosities are successfully produced by controlling only a slight pH change. The effect of solution pH on the resulting metallosupramolecular frameworks, as well as the interconversion phenomena, are discussed. The obtained crystals were characterized on the basis of electronic absorption, circular dichroism (CD), X-ray fluorescence, IR, and NMR spectroscopies, together with elemental analysis. Their crystal structures were examined and discussed in detail, based on single-crystal X-ray diffraction analysis, besides the investigation of sorption behavior toward small molecules such as CO_2, N_2, and H_2O.

References.

[1]   J. M. Lehn, *Supramolecular Chemistry: Concepts and Perspectives*, VCH, Weinheim,

1995.

[2]   (a) H.-J. Schneider, H. Dürr, *Frontiers in Supramolecular Organic Chemistry and Photochemistry*, VCH, **1991**. (b) J. L. Atwood, J. E. D. Davies, D. D. Manicol. F. Vogtle, *Comprehensive Supramolecular Chemistry*, Pergamon, **1996**.

[3]   (a) G. F. Swiegers, T. J. Malefetse, *Chem. Rev.* **2000**, *100*, 3483-3537. (b) J. A. Thomas, *Chem. Soc. Rev.* **2007**, *36*, 856-868.

[4]   (a) S. Kitagawa, S. Noro, *Coordination Polymer: Infinite systems*, In *Comprehensive Coordination Chemistry II-From Biology to Nanotechnology*; J. A. McCleverty, T. B. Meyers, Eds.; Elsevier Ltd.: Oxford, U.K., **2004**; vol. 7, pp 231-261. (b) S. Kitagawa, R. Matsuda, *Coord. Chem. Rev.* **2007**, *251*, 2490-2509. (c) S. S. Han, J. L. Mendoza-Cortés, W. A. Goddard III, *Chem. Soc. Rev.* **2009**, *38*, 1460-1476.

[5]   (a) N. Guillou , Q. Gao, P. M. Forster, J. S. Chang, M. Noguès, S. E. Park, G. Férey, A. K. Cheetham, *Angew. Chem., Int. Ed.* **2001**, *40*, 2831-2834. (b) S. Kitagawa, R. Kitaura, S. Noro, *Angew. Chem., Int. Ed.* **2004**, *43*, 2334-2375. (c) A. Proust, R. Thouvenot, P. Gouzerh, *Chem. Commun.* **2008**, 1837-1852. (d) J. Lee, O. K. Farha, J. Roberts, K. A. Scheidt, S. T. Nguyen, J. T. Hupp, *Chem. Soc. Rev.* **2009**, *38*, 1450-1459. (e) J.-R. Li, R. J. Kuppler, H.-C. Zhou, *Chem. Soc. Rev.* **2009**, *38*, 1477-1504. (f) G. Rogez, N. Viart, M. Drillon, *Angew. Chem., Int. Ed.* **2010**, *49*, 1921-1923. (g) J. M. Clemente-Juan, E. Coronado, A. Gaita-Ariño, *Chem. Soc. Rev.* **2012**, *41*, 7464-7478. (h) H. Furukawa, K. E. Cordova, M. O'Keeffe, O. M. Yaghi, *Science* **2013**, *341*, 974-986.

[6]   (a) G. S. Papaefstathiou, L. R. MacGillivray, *Coord. Chem. Rev.* **2003**, *246*, 169-184. (b) D. Bradshaw, J. B. Claridge, E. J. Cussen, T. J. Prior, M. J. Rosseinsky, *Acc. Chem. Rev.* **2005**, *38*, 273-282. (c) R. Chakrabarty, P. S. Mukherjee, P. J. Stang, *Chem. Rev.* **2011**, *111*, 6810-6918. (d) T. R. Cook, Y.-R. Zheng, P. J. Stang, *Chem. Rev.* **2013**, *113*, 734-777.

[7]   (a) M. M. Conn, J. Rebek, Jr., *Chem. Rev.* **1997**, *97*, 1647-1668. (b) S. Uchida, M. Hashimoto, N. Mizuno, *Angew. Chem., Int. Ed.* **2002**, *41*, 2814-2817. (c) D. M. P. Mingos, *Supramolecular Assembly via Hydrogen Bonds*, Springer-Verlag, Berlin, **2004**; vol. 1–2. (d) S. Uchida, N. Mizuno, *Coord. Chem. Rev.* **2007**, *251*, 2537-2546. (e) S. Takamizawa, T. Akatsuka, T. Ueda, *Angew. Chem., Int. Ed.* **2008**, *47*, 1689-1692. (f) K. Suzuki, Y. Kikukawa, S. Uchida, H. Tokoro, K. Imoto, S. Ohkoshi, N. Mizuno, *Angew. Chem., Int. Ed.* **2012**, *51*, 1597-1601. (g) R. Kawahara, S. Uchida, N. Mizuno, *Inorg. Chem.* **2014**, *53*, 3655-3661. (h) R. Kawahara, S. Uchida, N. Mizuno, *Chem. Mater.*

2015, *27*, 2092-2099.

[8] (a) R. W. Saalfrank, H. Maid, A. Scheurer, *Angew. Chem., Int. Ed.* **2008**, *47*, 8794-8824. (b) S. Hiraoka, M. Goda, M. Shionoya, *J. Am. Chem. Soc.* **2009**, *131*, 4592-4593. (c) A. D. Burrows, *CrystEngComm* **2011**, *13*, 3623-3642. (d) S. De, K. Mahata, M. Schmittel, *Chem. Soc. Rev.* **2010**, *39*, 1555-1575. (e) M. M. J. Smulders, I. A. Riddell, C. Browne, J. R. Nitschke, *Chem. Soc. Rev.* **2013**, *42*, 1728-1754.

[9] (a) L. H. Gade, *Angew. Chem. Int. Ed.* **2000**, *39*, 2658-2678. (b) E. J. L. McInnes, S. Piligkos, G. A. Timco, R. E. P. Winpenny, *Coord. Chem. Rev.* **2005**, *249*, 2577-2590. (c) H. Li, T. J. Marks, *Proc. Natl. Acad. Sci. U. S. A.* **2006**, *103*, 15295-15302. (d) M. D. Ward, *Coord. Chem. Rev.* **2007**, *251*, 1663-1677. (e) H. Hofneier, U. S. Schubert, *Chem. Soc. Rev.* **2004**, *33*, 373-399. (f) C. F. Yocum, *Coord. Chem. Rev.* **2008**, *252*, 296-305. (g) Y.-G. Huang, F.-L. Jiang, M.-C. Hong, *Coord. Chem. Rev.* **2009**, *253*, 2814-2834. (h) T. Nabeshima, *Bull. Chem. Soc. Jpn.* **2010**, *83*, 969-991.

[10] (a) O. M. Yaghi, H. Li, *J. Am. Chem. Soc.* **1995**, *117*, 10401-10402. (b) J. S. Seo, D. Whang, H. Lee, S. I. Jun, J. Oh, Y. J. Jeon, K. Kim, *Nature* **2000**, *404*, 982-986. (c) O. M. Yaghi, M. O'Keeffe, N. W. Ockwig, H. K. Chae, M. Eddaoudi, J. Kim, *Nature* **2003**, *423*, 705-714. (d) O. Delgado-Friedrichs, M. O'Keeffe, O. M. Yaghi, *Phys. Chem. Chem. Phys.* **2007**, *9*, 1035-1043. (e) J. J. Perry IV, J. A. Perman, M. J. Zaworotko, *Chem. Soc. Rev.* **2009**, *38*, 1400-1417.

[11] D. J. Tranchemontagne, J. L. Mendoza-Cortés, M. O'Keeffe, O. M. Yaghi, *Chem. Soc. Rev.* **2009**, *38*, 1257-1283, and references therein.

[12] N. Yoshinari, K. Tatsumi, A. Igashira-Kamiyama, T. Konno, *Chem. Eur. J.* **2010**, *16*, 14252-14255.

[13] P. Lee, A. Igashira-Kamiyama, N. Kuwamura, N. Yoshinari, T. Konno, *Chem. Eur. J.* **2014**, *20*, 6646-6649.

[14] T. Konno, A. Toyota, A. Igashira-Kamiyama, *J. Chin. Chem. Soc.* **2009**, *56*, 26-33.

[15] (a) F. Basolo, R. C. Johnson, *Coordination Chemisry; the Chemistry of Metal Complexes*, Benjamin, NY, **1964**. (b) D. F. Shriver, P. W. Atkins, *Inorganic Chemistry* (Third edition), Oxford University Press, **1999**.

[16] T. Ishii, S. Tsuboi, G. Sakane, M. Yamashita, B. K. Breedlove, *Dalton Trans.* **2009**, 680-687.

[17] R. J. Deeth, *Coord. Chem. Rev.* **2001**, *212*, 11-34.

[18] (a) A. Vogler, H. Kunkely, *Coord. Chem. Rev.* **2001**, *219-221*, 489-507. (b) V. W.-W.

Yam, E. C.-C. Cheng, *Chem. Soc. Rev.* **2008**, *37*, 1806-1813. (c) E. R. T. Tiekink, J.-G. Kang, *Coord. Chem. Rev.* **2009**, *253*, 1627-1648. (d) X. He, V. W.-W. Yam, *Coord. Chem. Rev.* **2011**, *255*, 2111-2123.
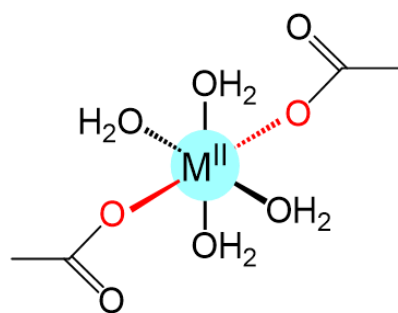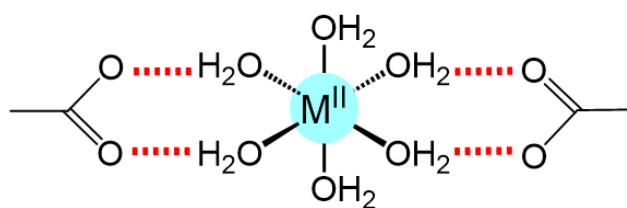
Chart 1. Feasible interactions of ᴅ-pen carboxyl groups and aqua metal cation. Dashed lines indicate hydrogen bonds.

Advantages
- rigidity
- directionality
- stability

only coordination bonds

Disadvantages
- low coordination flexibility
- low structural dynamic
- insolubility
- irreproducibility

structural dynamic

stability

reproducibility

coordination flexibility

solubility

directionality

combination of coordination and hydrogen bonds

Advantages
- coordination flexibility
- structural dynamic
- high solubility
- reproducibility

only hydrogen bonds

Disadvantages
- fragility
- low stability
- copresence of undesired products

$\equiv$ $[Co_2Au_3(D\text{-pen-}N,S)_6]^{3-}$ ($[\mathbf{1}]^{3-}$)

$\equiv$ $[M(H_2O)_n]^{2+}$
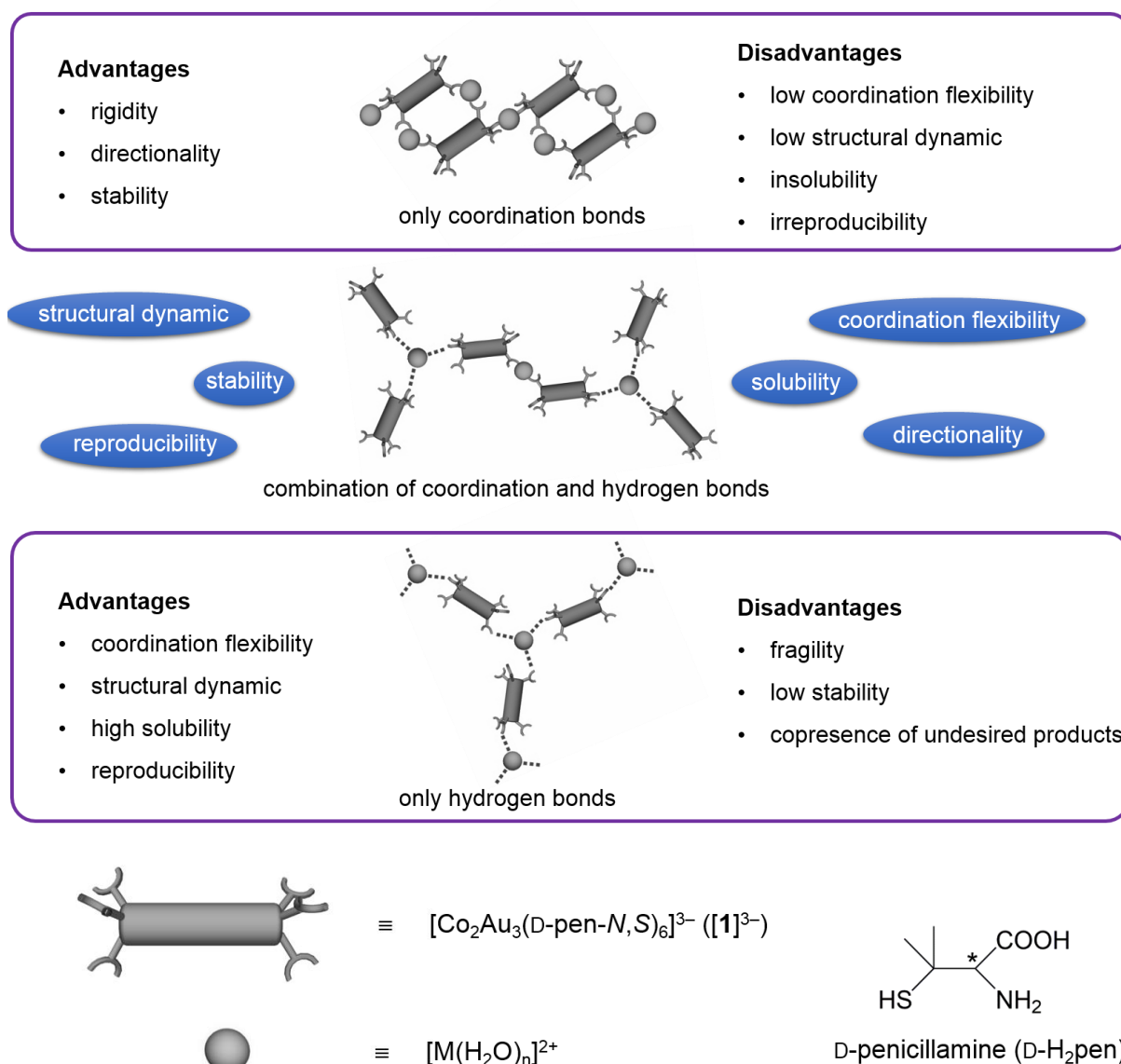
D-penicillamine (D-H$_2$pen)

Chart 2. Proposed metallosupramolecular frameworks constructed from only coordination bonds (top), a combination of coordination and hydrogen bonds (middle), and only hydrogen bonds (bottom). Dashed lines indicate hydrogen bonds.

Chapter I. Combination of Co$^{III}_2$Au$^I_3$ complex anions and aqua cobalt(II) cations.

I-1. Introduction.

Porous ionic crystals, in which discrete cations and anions are arranged in a crystal lattice with large intermolecular spaces, have been known as a new class of alternative porous crystalline materials.[1] This is because these compounds can exhibit strong electrostatic interactions on internal surfaces and are easily reproduced by recrystallization from solvents. One of the simple approaches for the synthesis of this class of porous frameworks is the use of spherical nanometer-sized discrete ions, such as polyoxometalates and S-bridged multinuclear metal clusters as components, which naturally expand their intermolecular spaces.[2,3] However, so far, the highest reported porosities have been limited to *ca.* 50%, mainly due to the closely packed arrangement of their spherically shaped ionic components. An alternative approach, in which the number of connectivity among cationic and anionic species decreased through directionally controlled hydrogen-bonding interactions, has been proposed for the synthesis of highly porous ionic frameworks.[4] With this approach, the ionic crystal with a high porosity up to 63% has been reported for [Co(H$_2$bim)$_3$](TMA) (H$_2$bim = 2,2'-biimidazol; H$_3$TMA = 1,3,5-benzenetricarboxylic acid), in which the planar TMA^{3-} anions are hydrogen-bonded with the [Co(H$_2$bim)$_3$]$^{3+}$ cations, thus forming a 2D sheet-like structure with a 3-connected net.[5] Although this reported porosity of 63% is higher than that expected for the 6-connected primitive lattice (48%) and is comparable with that for the 4-connected diamondoid lattice (66%),[6] it is still lower than the porosity values found in several highly porous metal–organic frameworks (MOFs) formed by coordination bonds between metal ions and organic or inorganic ligands.[7] Thus, an exploration of efficient methodologies for the rational production of highly porous ionic crystals has been still a challenge.

Studies of the chemistry of MOFs have established that a kinetic product is quickly formed through an accelerating polymerization process under highly concentrated conditions and tends to have a more porous framework compared with a thermodynamic product.[8] This is simply explained by the lower stability of more highly porous frameworks compared with dense frameworks. However, the kinetic product is usually formed as crystalline powders or microcrystals which are not suitable for single-crystal X-ray diffraction analyses. In addition,

kinetic products may transform to more stable compounds which are thermodynamic products.

In this chapter, an excellent example of a kinetic synthesis of highly porous metallosupramolecular frameworks is presented by using the well-designed anionic $Co^{III}_2Au^I_3$ pentanuclear complex with six carboxylate arms, $[Co^{III}_2Au^I_3(D\text{-}pen\text{-}N,S)_6]^{3-}$ ($[1]^{3-}$; D-H2pen = D-penicillamine),[9] as a molecular building block. This anionic pentanuclear complex has a potential to form manifold interactions with hexaaqua metal cations, possibly leading to the frameworks with high porosities. A combination of $[1]^{3-}$ anions and aqua cobalt(II) cations, $[Co(H_2O)_n]^{2+}$, produced an extremely porous ionic crystal with a high porosity of *ca.* 80%, $[Co(H_2O)_6]_3[Co_2Au_3(D\text{-}pen\text{-}N,S)_6]_2$ (**2a**), in which the rod-shaped $[1]^{3-}$ anions are alternately hydrogen-bonded with $[Co(H_2O)_6]^{2+}$ cations to form a 3D metallosupramolecular framework. Remarkably, crystal **2a** was found to stepwise convert to two types of crystals that are suitable for X-ray diffraction, $[Co(H_2O)_6]_2[\{Co(H_2O)_4\}\{Co_2Au_3(D\text{-}pen\text{-}N,S)_6\}_2]$ (**2b**) and $[\{Co(H_2O)_4\}_3\{Co_2Au_3(D\text{-}pen\text{-}N,S)_6\}_2]$ (**2c**), which are thermodynamically metastable and stable products with decreased porosities of *ca.* 60% and *ca.* 30%, respectively (Scheme I-1). The crystallographic data of the obtained crystals were fully studied by single-crystal X-ray diffraction analyses. In addition, the physical characterizations on the basis of electronic absorption, circular dichroism (CD), IR, and NMR spectra, in addition to X-ray fluorescence and elemental analyses, were performed.

I-2. Experimental section.

I-2-1. Materials.

$NH_4[Au(D\text{-}Hpen)_2]\cdot3.5H_2O$ and $Na_3[Co(CO_3)_3]\cdot3H_2O$ were prepared according to the methods described in literatures.[9,10] All other chemicals and solvents were commercially available and used without further purification.

I-2-2. Synthesis of Na3[Co2Au3(D-pen-*N*,*S*)6] (Na3[1]).

To a colorless solution of $NH_4[Au(D\text{-}Hpen)_2]\cdot3.5H_2O$ (500 mg, 0.871 mmol) in H_2O 50 mL was added $Na_3[Co(CO_3)_3]\cdot3H_2O$ (210 mg, 0.580 mmol). The mixture was stirred at room temperature for 1 hour, which gave a dark purple solution. The reaction solution was evaporated to dryness by a rotary evaporator, and then an aqueous NaOAc solution (1 M, 5 mL), followed by 10 mL of MeOH was added. The resulting dark purple solution was allowed

to stand in the refrigerator for 1 day, and the obtained purple powder was collected by filtration. Yield: 440 mg (80%). Anal. Calcd for $Na_3[Co_2Au_3(D\text{-pen-}N,S)_6]\cdot13H_2O$ = $C_{30}H_{80}N_6S_6O_{25}Co_2Au_3Na_3$: C, 19.01; H, 4.25; N, 4.43%. Found: C, 18.98; H, 4.00; N, 4.19%. IR spectrum (cm^{-1}, KBr disk): 1609 (ν_{COO}). ^1H NMR spectrum (ppm from DSS, D_2O): δ 1.47 (s, 3H), 1.64 (s, 3H), 3.21 (s, 1H).

I-2-3. Crystallization of $[Co(H_2O)_6]_3[Co_2Au_3(D\text{-pen-}N,S)_6]_2$ (2a).

To a purple solution of $Na_3[Co_2Au_3(D\text{-pen-}N,S)_6]\cdot13H_2O$ (100 mg, 0.0602 mmol) in H_2O (3 mL) was added 1 M aqueous $(NH_4)_2CO_3$ (400 μL). The solution was stirred at room temperature for 10 min, and then a pink solution of $Co(OAc)_2\cdot4H_2O$ (26 mg, 0.10 mmol) in H_2O (1.6 mL) was added to it. After stirring at room temperature for a few minutes, the mixture was allowed to stand at room temperature for 12 hours. The resulting purple platelet crystals (2a), one of which was used for single-crystal X-ray analysis, were collected by filtration and washed with acetone. Yield: 48 mg (39%). Anal. Calcd for $[Co(H_2O)_6]_3[Co_2Au_3(D\text{-pen-}N,S)_6]_2\cdot23H_2O$ = $C_{60}H_{190}N_{12}S_{12}O_{65}Co_7Au_6$: C, 17.58; H, 4.67; N, 4.10%. Found: C, 17.55; H, 4.44; N, 4.14%. IR spectrum (cm^{-1}, KBr disk): 1609 (ν_{COO}). ^1H NMR spectrum (ppm from DSS, D_2O): δ 1.49 (s, 3H), 1.64 (s, 3H), 3.27 (s, 1H).

I-2-4. Structural conversions.

(a) Conversion from 2a to $[Co(H_2O)_6]_2[\{Co(H_2O)_4\}\{Co_2Au_3(D\text{-pen-}N,S)_6\}_2]$ (2b).

The resulting purple hexagonal platelet crystals of 2a were stored in the mother liquor for several days in a closed vessel. A change in crystal shape was clearly observed, in which purple hexagonal block crystals (2b) appeared instead of 2a after 5 days. One of the purple hexagonal block crystals of 2b was used for single-crystal X-ray diffraction analysis. The resulting purple hexagonal block crystals were collected by filtration and washed with acetone. Yield: 28 mg (24%). Anal. Calcd for $[Co(H_2O)_6]_2[\{Co(H_2O)_4\}\{Co_2Au_3(D\text{-pen-}N,S)_6\}_2]\cdot15H_2O$ = $C_{60}H_{170}N_{12}S_{12}O_{55}Co_7Au_6$: C, 18.39; H, 4.37; N, 4.29%. Found: C, 18.31; H, 4.29; N, 4.26%. IR spectrum (cm^{-1}, KBr disk): 1603 (ν_{COO}). ^1H NMR spectrum (ppm from DSS, D_2O): δ 1.49 (s, 3H), 1.64 (s, 3H), 3.29 (s, 1H).

(b) Conversion from 2b to $[\{Co(H_2O)_4\}_3\{Co_2Au_3(D\text{-pen-}N,S)_6\}_2]$ (2c).

After the purple hexagonal block crystals of **2b** appeared, these crystals were continuously stored in the mother liquor for several days in a closed vessel. When the storing time was extended to 7 days, the second change in crystal shape was obviously observed. The purple needle crystals (**2c**) that are almost insoluble in water appeared instead of **2b**. One of the purple needle crystals of **2c** was used for single-crystal X-ray diffraction analysis. The resulting purple needle crystals were collected by filtration and washed with acetone. Yield: 42 mg (38%). Anal. Calcd for [{Co(H$_2$O)$_4$}$_3$\{Co$_2$Au$_3$(D-pen-N,S)$_6$\}$_2$]·5H$_2$O = C$_{60}$H$_{142}$N$_{12}$S$_{12}$O$_{41}$Co$_7$Au$_6$: C, 19.65; H, 3.90; N, 4.58%. Found: C, 19.89; H, 3.68; N, 4.54%. IR spectrum (cm^{-1}, KBr disk): 1604 (ν_{COO}).

I-2-5. Physical measurements.

The electronic absorption spectra were measured with a JASCO V-660 UV/Vis spectrometer at room temperature. The circular dichroism (CD) spectra were measured with a JASCO J-820 spectropolarimeter at room temperature. The IR spectra were recorded with a JASCO FT/IR-4100 infrared spectrometer using KBr disks at room temperature. Elemental analyses (C, H, N) were performed using a Yanaco CHN Corder MT-5. The X-ray fluorescence analyses were conducted using a SHIMADZU Rayny EDX-720 spectrometer. The ^{1}H NMR spectra were recorded with a JEOL ECAMX-500SP spectrometer in D$_2$O. Sodium 4,4-dimethyl-4-silapentane-1-sulfonate (DSS) was used as the internal reference. All NMR measurements were performed at room temperature. The sorption isotherms of N$_2$ and CO$_2$ were measured with a BELSORP-mini II volumetric adsorption instrument. N$_2$ and CO$_2$ gases of high purity (99.9999%) were used. The sorption isotherms for H$_2$O, EtOH, and acetone were performed on a BELSORP-max volumetric adsorption instrument. High quality powder X-ray diffraction (PXRD) patterns were recorded at room temperature, in transmission mode [synchrotron radiation λ = 0.999115(18) Å; 2θ range = 0–78°; step width = 0.01°; data collection time = 5 min] on a diffractometer equipped with a white imaging plate detector at SPring-8 BL02B2 beamline. The crystals were stored in the mother liquor for several days for time-dependent observation of the powder X-ray diffraction. The crystals were loaded into glass capillary tubes (diameter = 0.3 mm) with their mother liquor. The samples were rotated during the measurements. The diffraction patterns were collected with a large Debye-Scherrer camera. The powder simulation patterns were generated from the single-crystal X-ray structures using Mercury 3.8. Variable-temperature magnetic susceptibility measurements were made using the SQUID magnetometer MPMS XL7AC

(Quantum Design).

I-2-6. X-ray structural determinations.

Single-crystal X-ray diffraction data for **2a** were recorded on an ADSC Q210 CCD area detector with a synchrotron radiation (λ = 0.7000 Å) at 2D beamline in Pohang Accelerator Laboratory (PAL). The intensity data were collected by the ω-scan and the diffraction images were processed by HKL3000.[11] Absorption correction was performed by HKL3000.[11] The structure of **2a** was solved by direct methods using SHELXS-2014.[12] The structure refinements were carried out using full-matrix least-squares (SHELXL-2014).[12] All calculations were performed using the Yadokari-XG software package.[13] All non-hydrogen atoms except for $[Co(H_2O)_6]^{2+}$ cations were refined anisotropically, while the others were refined isotropically. Hydrogen atoms were included in the calculated positions except those of water molecules. All $[Co(H_2O)_6]^{2+}$ cations were refined using DFIX restraints. The solvated water molecules and a part of $[Co(H_2O)_6]^{2+}$ ions are severely disordered and could not be modeled; their contribution was excluded using the SQUEEZE in the PLATON package.[14]

The diffraction data for **2b** were recorded on a Rigaku Mercury 2 CCD detector with a synchrotron radiation (λ = 0.6997 Å) at BL02B1 beamline in SPring-8 with the approval of the Japan Synchrotron Radiation Research Institute (JASRI). The intensity data were collected by the ω-scan technique and were processed with a Rapid Auto software program. The structure of **2b** was solved by direct methods using SHELXS-2014.[12] The structure refinements were carried out using full-matrix least-squares (SHELXL-2014).[12] All calculations were performed using the Yadokari-XG software package.[13] All non-hydrogen atoms were refined anisotropically. Hydrogen atoms were included in the calculated positions except those of water molecules. The solvated water molecules and a part of $[Co(H_2O)_6]^{2+}$ ions are severely disordered and could not be modeled; their contribution was excluded using the SQUEEZE in the PLATON package.[14]

Single-crystal X-ray diffraction experiment for **2c** was performed on a Rigaku R-AXIS 7 imaging plate area detector with graphite-monochromated Mo Kα radiation (λ = 0.71075 Å) at 180 K. The intensity data were collected by the ω-scan and were empirically corrected for absorption. The collected diffraction data were processed with a Rapid Auto software program. The structure of **2c** was solved by direct methods using SHELXS-2014.[12] The structure refinements were carried out using full-matrix least-squares (SHELXL-2014).[12] All

14

calculations were performed using the Yadokari-XG software package.[13] All non-hydrogen atoms, except the disordered carboxylate groups, C, N, and S atoms of D-pen ligands, one Co, and one Au atoms in the complex anion and water molecules, were refined anisotropically, while the others were refined isotropically. Hydrogen atoms were included in the calculated positions except those of water molecules. EADP constraints and ISOR restraints were used to model a part of disordered D-pen ligands. Crystal data are summarized in Table I-1.

I-3. Results and discussion.

I-3-1. Syntheses, characterizations, and structural conversions.

(a) Na$_3$[Co$_2$Au$_3$(D-pen-*N,S*)$_6$] (Na$_3$[1]).

A preparation of Na$_3$[1] was reported by Konno *et al.*[9] According to the previous method, the reaction of NH$_4$[Au(D-Hpen)$_2$] and CoCl$_2 \cdot$6H$_2$O in an acetate buffer solution, followed by air oxidation gave a mixture of anionic Co$^{III}_2$Au$^I_3$ and neutral Co$^{III}_3$Au$^I_3$ multinuclear complexes, [Co$_2$Au$_3$(D-pen-*N,S*)$_6$]$^{3-}$ ([1]$^{3-}$) and [Co$_3$Au$_3$(D-pen-*N,O,S*)$_6$], respectively. A separation by anion-exchange column chromatography was required in order to isolate the desired anionic [1]$^{3-}$ pentanuclear complex. In this thesis, the synthetic procedure was modified by using Co^{III} instead of Co^{II}. A treatment of NH$_4$[Au(D-Hpen)$_2$] with Na$_3$[Co(CO$_3$)$_3$] in a 3:2 ratio, followed by an isolation with MeOH, gave purple powder of Na$_3$[1] with a high yield of 80%. The electronic absorption spectrum of Na$_3$[1] in water presents the characteristic intense *d-d* transition band at 561 nm and its CD spectrum shows an optical active feature with positive and negative CD bands at 584 and 459 nm, respectively (Figure I-1), indicative of the selective formation of (Λ)$_2$-[1]$^{3-}$ pentanuclear species. The similar observed results have previously been found in the S-bridged pentanuclear complexes, such as, (Λ)$_2$-[Co$_2$Au$_3$(L-cys-*N,S*)$_6$]$^{3-}$ (L-cys = L-cysteinate) and (Δ)$_2$-[Co$_2$Au$_3$(L-pen-*N,S*)$_6$]$^{3-}$ (L-pen = L-penicillamine).[15] The results from X-ray fluorescence and elemental analyses match well with the existence of Co and Au atoms in a 2:3 ratio. In addition, the IR spectrum illustrates an intense ν_{COO} band at 1609 cm^{-1} (Figure I-2), indicating the presence of fully deprotonated form of D-pen carboxyl groups in Na$_3$[1].[16]

(b) [Co(H$_2$O)$_6$]$_3$[Co$_2$Au$_3$(D-pen-*N,S*)$_6$]$_2$ (2a).

The ionic crystal **2a** was successfully obtained in the form of highly water-soluble purple

hexagonal platelet crystals from a highly concentrated aqueous solution containing Na$_3$[**1**] (10 mM) and Co(OAc)$_2$ (20 mM) in a 1:2 ratio. The crystallization of **2a** occurred within 12 hours with a yield of 39%. The electronic absorption spectrum of **2a** in water shows the characteristic *d-d* transition band at 560 nm and its CD spectrum shows positive, and negative CD bands at 587 and 467 nm, respectively (Figure I-1). These spectral features are the same as those for parental Na$_3$[**1**], indicating that **2a** is composed of [**1**]$^{3-}$ as the anionic building blocks. X-ray fluorescence and elemental analysis data are in good agreement with the formula for a 2:3 adduct of [**1**]$^{3-}$ and Co^{2+}. The presence of the high-spin octahedral Co^{2+} species in **2a** in this ratio was supported by the magnetic susceptibility measurement with the observed $\chi_M T$ value at 300 K of 8.87 cm^3 K mol^{-1} and the calculated *g* value of 2.51 (Figure I-3). The IR spectrum displays an intense ν_{COO} band at 1609 cm^{-1} (Figure I-2), indicative of the complete deprotonation of the D-pen carboxyl groups in **2a**.[16]

To check the stability of the ionic crystal **2a**, the obtained purple hexagonal platelet crystals of **2a** were stored in a mother liquor for several days in a closed vessel (Figure I-4a). A change in the crystal shape was clearly noticed after 5 days with the appearance of purple hexagonal block crystals (**2b**) (Figure I-4b). As shown in Figure I-4d, a stepwise structural conversion could be observed from the PXRD investigation. A pure phase of **2a** was retained for 3 days in a mother liquor with the subsequent conversion to a pure phase of **2b** after 5 days. The structural conversion from **2a** to **2b** implied that **2a** is a kinetic product, whereas **2b** is more thermodynamically stable product compared to **2a**. The connectivity between the cations and anions indicates that **2a** contains only the hydrogen bonds between [Co(H$_2$O)$_6$]$^{2+}$ cations and [**1**]$^{3-}$ anions (*vide infra*). In contrast, **2b** contains coordination bonds between [Co(H$_2$O)$_4$]$^{2+}$ cations and [**1**]$^{3-}$ anions in addition to the hydrogen bonds between [Co(H$_2$O)$_6$]$^{2+}$ cations and [**1**]$^{3-}$ anions. Therefore, the kinetic product **2a** preferentially converted to the thermodynamic product **2b** through the replacement of hydrogen bonds by coordination bonds that have a greater binding energy.[17] The observed structural conversion could be explained by the dissolution–recrystallization process allowing the kinetic product **2a** to be transformed toward more thermodynamically stable product **2b**.[18] At this point, the single-crystal-to-single-crystal transformation is unconcerned because the structural conversion phenomena occurred only when the crystals of **2a** were kept in the mother liquor. In addition, it was found that a reproducibility of highly porous ionic crystal **2a** could be achieved after the ionic crystal **2b** was dissolved in water, followed by column separation. Crystal **2b** thus reverted back to **2a** by the dissolution and the subsequent crystallization

procedures. This result is a beneficial advantage for the ionic crystals over other porous coordination polymers which are commonly insoluble in most solvents and thus are not reproducible.

(c) [Co(H$_2$O)$_6$]$_2$[{Co(H$_2$O)$_4$}{Co$_2$Au$_3$(D-pen-*N,S*)$_6$}$_2$] (2b).

The ionic crystal **2b** was successfully obtained in the form of water-soluble purple hexagonal block crystals from a structural conversion of crystal **2a** as mentioned above. The formation of **2b** occurred with a yield of 24% after crystals of **2a** were stored in a mother liquor in a closed vessel for 5 days. The diffuse reflection spectrum of **2b** and the solid state CD spectrum are similar to those of Na$_3$[**1**], indicating that the S-bridged pentanuclear structure of [**1**]$^{3-}$ anionic building blocks retained in **2b** (Figure I-5 and Figure I-6). The results from X-ray fluorescence and elemental analyses match well with the formula for a 2:3 adduct of [**1**]$^{3-}$ and Co^{2+}. The presence of the high-spin octahedral Co^{2+} species in **2b** in this ratio was supported by the magnetic susceptibility measurement with the observed $\chi_M T$ value at 300 K of 8.77 cm^3 K mol^{-1} and the calculated *g* value of 2.50 (Figure I-7). The IR spectrum shows an intense ν_{COO} band at 1603 cm^{-1} (Figure I-2), indicative of the complete deprotonation of the D-pen carboxyl groups in **2b**.[16]

To investigate the stability of the ionic crystal **2b**, the purple hexagonal block crystals of **2b** were continuously stored in a mother liquor for several days in a closed vessel. Interestingly, the second change in crystal shape was obviously observed when the storing time reached to 7 days. The purple needle crystals (**2c**) (Figure I-4c) that are almost insoluble in water appeared instead of **2b**. As shown in Figure I-4d, a unique two-step structural conversion could be observed from the PXRD investigation. A pure phase of **2b** was retained for 2 days in a mother liquor with the subsequent conversion to a pure phase of **2c** after 7 days counted from when the mixing of Na$_3$[**1**] and Co(OAc)$_2$ was started. The structural conversion from **2b** to **2c** indicated that **2b** is a thermodynamically metastable product, whereas **2c** is more thermodynamically stable product compared to **2b**. The connectivity between the cations and anions shows that **2b** has not only coordination bonds between [Co(H$_2$O)$_4$]$^{2+}$ cations and [**1**]$^{3-}$ anions but also the hydrogen bonds between [Co(H$_2$O)$_6$]$^{2+}$ cations and [**1**]$^{3-}$ anions (*vide infra*). On the other hand, only the coordination bonds between [Co(H$_2$O)$_4$]$^{2+}$ cations and [**1**]$^{3-}$ anions are involved in **2c**. Thus, the metastable product **2b** is reasonably converted to the thermodynamic product **2c** through the replacement of all hydrogen bonds by coordination bonds which have a greater binding energy.[17] Similar to the structural

conversion from **2a** to **2b**, this structural conversion could also be explained by the dissolution–recrystallization process allowing the thermodynamically metastable product **2b** transforms toward more thermodynamically stable product **2c**.[18] In addition, the structural conversion from **2b** to **2c** also occurred only when the crystals of **2b** were stored in the mother liquor.

(d) [{Co(H₂O)₄}₃{Co₂Au₃(D-pen-*N*,*S*)₆}₂] (2c).

The crystal **2c** was successfully obtained in the form of water-insoluble purple needle crystals from a structural conversion of crystal **2b**. A production of **2c** occurred with a yield of 38% after crystals of **2b** were continuously kept in a mother liquor for several days in a closed vessel. When the storing time was extended to 7 days, a change in crystal shape was obviously observed. The purple needle crystals of **2c** which are almost insoluble in water appeared instead of **2b**. The diffuse reflection and solid state CD spectra of **2c** are essentially similar to those of Na₃[**1**], indicating that the S-bridged pentanuclear structure of [**1**]$^{3-}$ anionic building blocks retained in **2c** (Figure I-5 and Figure I-6). X-ray fluorescence and elemental analysis data are in good agreement with the formula for a 2:3 adduct of [**1**]$^{3-}$ and Co^{2+}. Additionally, a presence of the high-spin octahedral Co^{2+} species in **2c** in this ratio was supported by the magnetic susceptibility measurement with the observed $\chi_M T$ value at 300 K of 9.15 cm^3 K mol^{-1} and the calculated *g* value of 2.55 (Figure I-8). The IR spectrum of **2c** illustrates an intense ν_{COO} band at 1604 cm^{-1} (Figure I-2), indicative of the complete deprotonation of the D-pen carboxyl groups in **2c**.[16]

The stability of the crystal **2c** was also investigated. The obtained purple needle crystals of **2c** were continuously stored in a mother liquor in a closed vessel for 1 month, but no further conversion was observed by PXRD investigation. This result is reasonable because the structural conversion occurred *via* a dissolution–recrystallization process in this studied system. Crystal **2c** that is almost insoluble in water, thus could not undergo a conversion in the mother liquor containing water as solvent. Consequently, crystal **2c** is supposed to be the most thermodynamically stable product in the studied system.

I-3-2. Crystal structures.

(a) [Co(H₂O)₆]₃[Co₂Au₃(D-pen-*N*,*S*)₆]₂ (2a).

The crystal structure of **2a** was established by single-crystal X-ray analysis. Crystal **2a**

consists of rod-shaped $[1]^{3-}$ anions and octahedral $[Co(H_2O)_6]^{2+}$ cations in addition to the water molecules of crystallization. A part of $[Co(H_2O)_6]^{2+}$ cations in **2a** could not be modeled in the crystal structure, presumably due to the severe disorder in the large void space. The overall structure of the entire complex anion in **2a** is nearly the same as that of $Na_3[1]$,[9] in which two Λ-$[Co(D\text{-pen-}N,S)_6]^{3-}$ octahedral units with free COO^- groups are linked by three Au^I ions with linear coordination structure through sulfur bridges. In **2a**, $[Co(H_2O)_6]^{2+}$ cations and $[1]^{3-}$ anions are alternately arranged and thus form $OH_2\cdots OOC$ hydrogen bonds with an average $O\cdots O$ distance of 2.84 Å. Each $[Co(H_2O)_6]^{2+}$ cation is surrounded by three $[1]^{3-}$ anions in a right-handed screw form, whereas each complex anion is surrounded by four $[Co(H_2O)_6]^{2+}$ cations (Figure I-9). As a result, a three-dimensional, 3-connected net consisting of 10-membered rings composed of ten $[Co(H_2O)_6]^{2+}$ cations as nodes and ten $[1]^{3-}$ anions as edges, was constructed (Figure I-10). This 3-connected net exhibits large opening channels with a maximum diameter of *ca.* 35 Å in all directions (Figure I-11), giving an extremely high porosity of *ca.* 80%, as calculated by PLATON.[19] The homogeneity of the bulk sample **2a** was confirmed by PXRD result. It was found that the experimental diffraction pattern matches well with the simulated pattern calculated based on the single-crystal X-ray data (Figure I-12).

(b) $[Co(H_2O)_6]_2[\{Co(H_2O)_4\}\{Co_2Au_3(D\text{-pen-}N,S)_6\}_2]$ (2b).

The crystal structure of **2b** was determined by single-crystal X-ray analysis. Crystal **2b** contains *trans*-$[Co(H_2O)_4]^{2+}$ cations, each of which connects two $[1]^{3-}$ anions, and isolated $[Co(H_2O)_6]^{2+}$ cations, in addition to the water molecules of crystallization (Figure I-13). A part of $[Co(H_2O)_6]^{2+}$ cations in **2b** could not be modeled in the crystal structure, presumably due to the severe disorder in the large void space. In **2b**, the $[1]^{3-}$ anions are hydrogen-bonded to each other (av. $N\cdots O$ = 2.92 Å), thus forming a six-fold helix with right handedness along the *c* axis. In addition, the two helices are bridged by the *trans*-$[Co(H_2O)_4]^{2+}$ cations through coordination bonds (av. $Co-OOC$ = 2.05 Å), resulting in a double helix structure with a large 1D pore with a diameter of *ca.* 18 Å (Figure I-14). The double helices are further connected by $[1]^{3-}$ anions through $NH_2\cdots OOC$ hydrogen bonds (av. $N\cdots O$ = 2.92 Å), completing a 1D channel structure (Figure I-15 and Figure I-16) with a porosity of *ca.* 60%, as calculated by PLATON.[19] This 1D channel structure is sustained by the isolated $[Co(H_2O)_6]^{2+}$ cations, each of which is hydrogen-bonded to two $[1]^{3-}$ anions in the double helix and one $[1]^{3-}$ anion that connects the double helix (av. $O\cdots O$ = 2.72 Å). The $[1]^{3-}$ anion is hydrogen-bonded with two $[Co(H_2O)_6]^{2+}$ cations in addition to another *trans*-$[Co(H_2O)_4]^{2+}$ cation through coordination

bond (Figure I-17), while the connecting mode of each $[Co(H_2O)_6]^{2+}$ cation by three $[1]^{3-}$ anions is the same as that found in **2a** (Figure I-18).

(c) [{Co(H$_2$O)$_4$}$_3${Co$_2$Au$_3$(D-pen-*N*,*S*)$_6$}$_2$] (2c).

The crystal structure of **2c** was also determined by single-crystal X-ray analysis. Crystal **2c** does not have the isolated $[Co(H_2O)_6]^{2+}$ cations, but contains the *cis*- and *trans*-$[Co(H_2O)_4]^{2+}$ cations that are directly bound to $[1]^{3-}$ anions (Figure I-19 and Figure I-20). The $[1]^{3-}$ anion is connected with four $[Co(H_2O)_4]^{2+}$ cations through coordination bonds in addition to another $[Co(H_2O)_4]^{2+}$ cation which is located nearby through $OH_2 \cdots OOC$ hydrogen bonds (av. $O \cdots O = 2.72$ Å) (Figure II-21). In **2c**, the $[1]^{3-}$ anions are alternately connected by the *cis*-$[Co(H_2O)_4]^{2+}$ cations through coordination bonds (av. Co–OOC = 2.06 Å), forming a 2-fold helix along the *b* axis. In addition, the two helices are connected to each other through $OH_2 \cdots OOC$ hydrogen bonds (av. $O \cdots O = 2.86$ Å), thus forming a right-handed double helix structure (Figure I-22 and Figure I-23). The double helices are connected by the *trans*-$[Co(H_2O)_4]^{2+}$ cations through coordination bonds (av. Co–OOC = 2.03 Å) in a 2D sheet-like structure. Finally, the 2D sheets are stacked through the $NH_2 \cdots OOC$ and $OH_2 \cdots OOC$ hydrogen bonds (av. $N \cdots O = 3.01$ Å, $O \cdots O = 2.69$ Å), completing a 3D dense framework (Figure I-24) with a low porosity of *ca.* 30%, as calculated by PLATON.[19]

I-3-3. Sorption behavior.

To investigate the adsorption characteristics of **2a**, **2b**, and **2c** toward small molecules, their adsorption isotherms for H_2O, EtOH, and acetone vapors were measured at 298 K. As shown in Figure I-25, a high H_2O adsorption capacity was observed for **2a** with a value of 45 mol mol^{-1} at $P/P_0 = 0.90$. A clear hysteresis loop was observed in an adsorption–desorption cycle for **2a**, indicative of the strong host–guest interactions accompanied by a structural transformation during the adsorption process.[20] Although a similar H_2O adsorption isotherm with a clear hysteresis loop was observed for **2b**, the adsorption amount (38 mol mol^{-1} at P/P_0 = 0.99) was smaller, consistently with its lower porosity (Figure I-26). The amount of adsorbed H_2O was further decreased (14 mol mol^{-1} at $P/P_0 = 0.96$) for **2c** with no hysteresis loop obtained because of its rigid framework with a low porosity (Figure I-27). Remarkably, all obtained metallosupramolecular frameworks (**2a**, **2b**, and **2c**) showed no appreciable adsorption capability toward EtOH and acetone vapors (Figure I-25, Figure I-26, and Figure I-27). This is attributed to the superhydrophilic character of their opening channels,[21]

surrounded not only by the amine and carboxylate groups of D-pen but also by the aqua groups in $[Co(H_2O)_6]^{2+}$ cations. The adsorption isotherms for CO_2 and N_2 gases were also measured. The CO_2 adsorption isotherm for **2a** at 195 K displayed a gradual increase and reached a value of 18.0 cm^3 g^{-1} at $P/P_0 = 0.96$ (Figure I-28). Similar CO_2 adsorption isotherms were observed for **2b** and **2c**, but the adsorption amount decreased in parallel with the decrease in their porosities (Figure I-29 and Figure I-30). In contrast, the adsorption capacities of N_2 gas for **2a**, **2b**, and **2c** are all poor at 77 K (<2.4 cm^3 g^{-1}), reflecting the superhydrophilic character of their frameworks.

I-3-4. Kinetic control of highly porous frameworks.

As described previously, crystal **2a** was successfully produced under a highly concentrated condition containing 10 mM $Na_3[1]$ and 20 mM $Co(OAc)_2$. This employed high concentration encouraged a rapid crystallization leading to a formation of the highly porous ionic framework of **2a**. Generally, a product that obtained under such a high concentration usually forms as crystalline powder or microcrystals, in which a crystallographic study cannot be achieved by single-crystal X-ray diffraction analysis. However, both cationic and anionic species which are the aqua cobalt(II) cation and the $Co^{III}_2Au^I_3$ pentanuclear-complex anion, respectively, involved in the system are highly soluble in water. This property plays an important role for decelerating of the crystallization process, resulting in the formation of X-ray quality crystals, instead of the undesired forms such as crystalline powder and microcrystals.[8] In addition, it was found that **2a** could not be obtained from a similar reaction of $Na_3[1]$ and $Co(OAc)_2$ under a slightly diluted condition. Instead of **2a**, crystals of **2b** were directly produced with a prolonged crystallization time. This result supports that a kinetically controlled synthesis could be rationally applied for a creation of the desired highly porous frameworks, in which a controlled high concentration of the employed reaction solutions plays an important role.

From the PXRD investigation, a unique two-step structural conversion was clearly observed (Figure I-4d). The structural conversions from **2a** to **2b**, and to **2c** implied that **2a** is a kinetic product, whereas **2b** and **2c** are thermodynamically metastable and stable products, respectively. The connectivity between the cations and anions indicates that **2a** contains only the hydrogen bonds between $[Co(H_2O)_6]^{2+}$ and $[1]^{3-}$. In contrast, **2b** contains coordination bonds between $[Co(H_2O)_4]^{2+}$ and $[1]^{3-}$ in addition to the hydrogen bonds between $[Co(H_2O)_6]^{2+}$ and $[1]^{3-}$, while only coordination bonds between $[Co(H_2O)_4]^{2+}$ and $[1]^{3-}$ are

involved in **2c**. Thus, the observed structural conversion phenomena clarified that crystal **2a**, behaving as the kinetic product, could be stepwise converted to the thermodynamic product **2c**, by way of **2b**, through the replacement of hydrogen bonds by coordination bonds that have a greater binding energy.[17] The lower porosities of **2b** (*ca.* 60%) and **2c** (*ca.* 30%), than that of **2a** (*ca.* 80%), also made a premise that the denser frameworks favor the thermodynamic stability.

I-4. Conclusion.

In this chapter, a combination of the rod-shaped $[Co_2Au_3(\text{D-pen-}N,S)_6]^{3-}$ ($[\mathbf{1}]^{3-}$) anions, as a molecular building block, and the aqua cobalt(II) cations showed an achievement in the kinetic synthesis of the porous metallosupramolecular framework of $[Co(H_2O)_6]_3[Co_2Au_3(\text{D-pen-}N,S)_6]_2$ (**2a**) with the extremely high porosity of *ca.* 80%, in which the anionic $[\mathbf{1}]^{3-}$ and cationic $[Co(H_2O)_6]^{2+}$ species are alternately linked solely by COO···HO hydrogen bonds. The success in the kinetically controlled synthesis thanks to the presence of terminal, non-coordinating carboxylate groups in the rod-shaped chiral $[\mathbf{1}]^{3-}$ anion that forms screwed, 3-connected hydrogen bonds around the aqua groups in the octahedral $[Co(H_2O)_6]^{2+}$ cation. Notably, such a high porosity has not been found in the previously reported ionic crystals consisting of cationic and anionic species without the formation of coordination bonds. Crystal **2a** was kinetically produced and stepwise converted to the thermodynamically more stable products with denser frameworks, $[Co(H_2O)_6]_2[\{Co(H_2O)_4\}\{Co_2Au_3(\text{D-pen-}N,S)_6\}_2]$ (**2b**; porosity *ca.* 60%) and $[\{Co(H_2O)_4\}_3\{Co_2Au_3(\text{D-pen-}N,S)_6\}_2]$ (**2c**; porosity *ca.* 30%), induced by the coordination of the carboxylate groups toward the Co^{II} centers. Such a unique stepwise conversion, in which all the three solid phases were crystallographically characterized, is quite rare. In addition, the selective capture of H_2O over EtOH or acetone, together with that of CO_2 over N_2, was recognized for **2a**, which is ascribed to its highly porous framework with superhydrophilic opening channels.
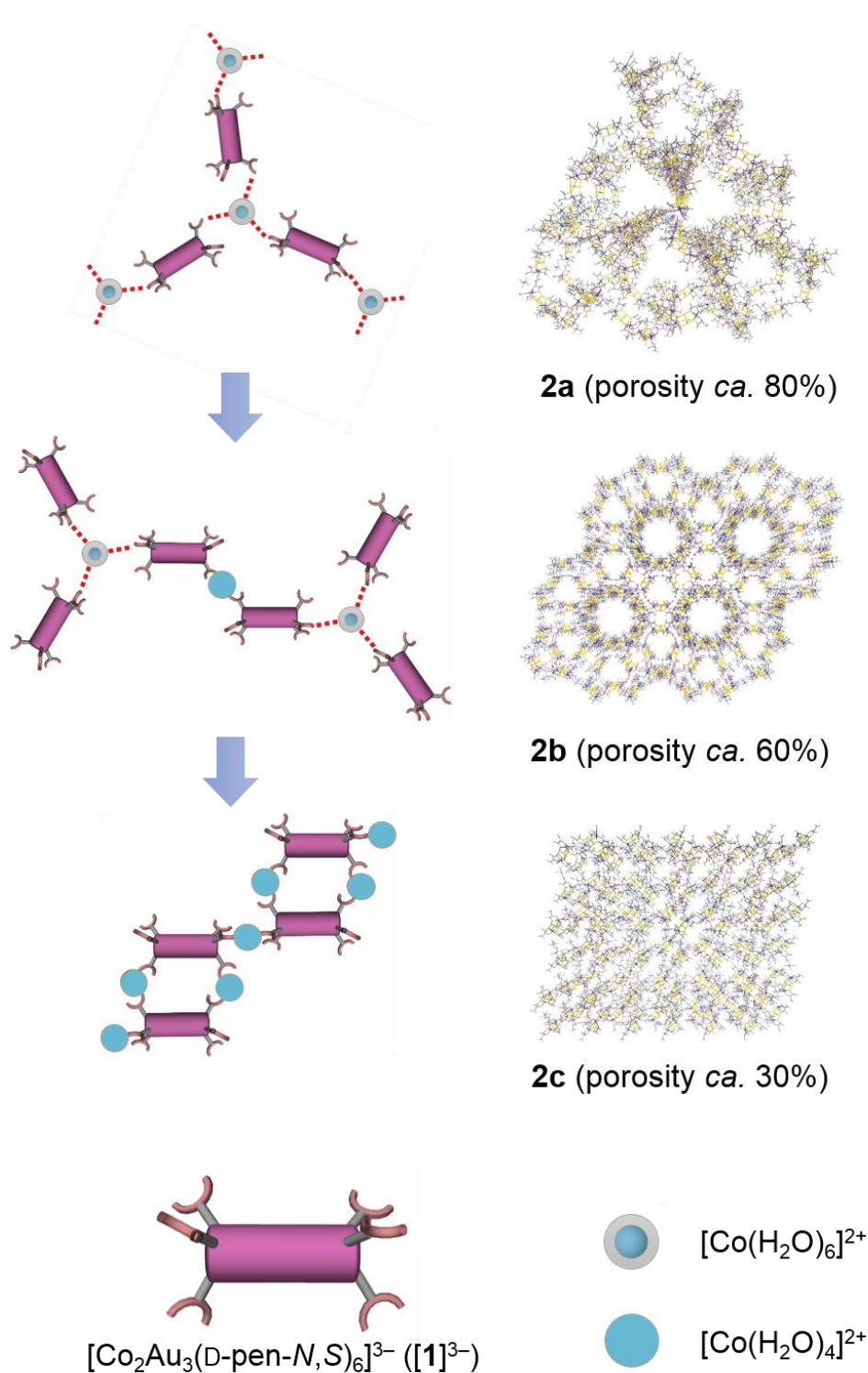
In order to reach more understanding about the effects of aqua metal ions on a construction of metallosupramolecular frameworks, an attempt to use other metals as cationic species should be made. The construction of metallosupramolecular frameworks based on a combination of D-penicillaminato Co^{III}_2Au^{I}_3 pentanuclear-complex anion and aqua nickel(II) or aqua manganese(II) cations, as representatives of aqua metal cations other than cobalt, will

be shown in Chapter II.

I-5. References.

[1]   (a) S. Uchida, N. Mizuno, *Coord. Chem. Rev.* **2007**, *251*, 2537-2546. (b) S. Takamizawa, T. Akatsuka, T. Ueda, *Angew. Chem., Int. Ed.* **2008**, *47*, 1689-1692.

[2]   (a) S. Uchida, M. Hashimoto, N. Mizuno, *Angew. Chem., Int. Ed.* **2002**, *41*, 2814-2817. (b) K. Suzuki, Y. Kikukawa, S. Uchida, H. Tokoro, K. Imoto, S. Ohkoshi, N. Mizuno, *Angew. Chem., Int. Ed.* **2012**, *51*, 1597-1601. (c) R. Eguchi, S. Uchida, N. Mizuno, *Angew. Chem., Int. Ed.* **2012**, *51*, 1635-1639. (d) R. Kawahara, S. Uchida, N. Mizuno, *Inorg. Chem.* **2014**, *53*, 3655-3661. (e) R. Kawahara, S. Uchida, N. Mizuno, *Chem. Mater.* **2015**, *27*, 2092-2099.

[3]   (a) N. Yoshinari, K. Tatsumi, A. Igashira-Kamiyama, T. Konno, *Chem. Eur. J.* **2010**, *16*, 14252-14255. (b) N. Yoshinari, U. Yamashita, T. Konno, *CrystEngComm* **2013**, *15*, 10016-10019.

[4]   (a) M. Tadokoro, J. Toyoda, K. Isobe, T. Itoh, A. Miyazaki, T. Enoki, K. Nakasuji, *Chem. Lett.* **1995**, *24*, 613-614. (b) M. Tadokoro, K. Isobe, H. Uekusa, Y. Ohashi, J. Toyoda, K. Tashiro, K. Nakasuji, *Angew. Chem., Int. Ed.* **1999**, *38*, 95-98. (c) M. Tadokoro, K. Nakasuji, *Coord. Chem. Rev.* **2000**, *198*, 205-218. (d) M. Tadokoro, H. Kanno, T. Kitajima, H. S. Umemoto, N. Nakanishi, K. Isobe, K. Nakasuji, *Proc. Natl. Acad. Sci. U. S. A.* **2002**, *99*, 4950-4955. (e) M. Tadokoro, Y. Tanaka, K. Noguchi, T. Sugaya, K. Isoda, *Chem. Commun.* **2012**, *48*, 7155-7157.

[5]   M. Tadokoro, S. Fukui, T. Kitajima, Y. Nagao, S. Ishimaru, H. Kitagawa, K. Isobe, K. Nakasuji, *Chem. Commun.* **2006**, 1274-1276.

[6]   (a) P. Krishna, D. Pandey, *Close-Packed Structures*, University College Cardiff Press, Cardiff, Wales, **1981**. (b) L. E. Smart, E. A. Moore, *Solid State Chemistry: An Introduction* (Fourth edition), CRC Press, Boca Raton, Florida, **2012**.

[7]   (a) H. Furukawa, N. Ko, Y. B. Go, N. Aratani, S. B. Choi, E. Choi, A. O. Yazaydin, R. Q. Snurr, M. O'Keeffe, J. Kim, O. M. Yaghi, *Science* **2010**, *329*, 424-428. (b) H. Furukawa, K. E. Cordova, M. O'Keeffe, O. M. Yaghi, *Science* **2013**, *341*, 974-986. (c) I. Senkovska, S. Kaskel, *Chem. Commun.* **2014**, *50*, 7089-7098.

[8]   (a) S. H. Jhung, J. H. Lee, P. M. Forster, G. Férey, A. K. Cheetham, J. S. Chang, *Chem. Eur. J.* **2006**, *12*, 7899-7905. (b) M. Kawano, T. Haneda, D. Hashizume, F. Izumi, M.

Fujita, *Angew. Chem., Int. Ed.* **2008**, *47*, 1269-1271. (c) J. Martí-Rujas, M. Kawano, *Acc. Chem. Res.* **2013**, *46*, 493-505.

[9] T. Konno, A. Toyota, A. Igashira-Kamiyama, *J. Chin. Chem. Soc.* **2009**, *56*, 26-33.

[10] H. F. Bauer, W. C. Drinkard, *J. Am. Chem. Soc.* **1960**, *82*, 5031-5032.

[11] Z. Otwinowski, W. Minor, *Methods Enzymol.* **1997**, *276A*, 307-326.

[12] (a) G. M. Sheldrick, *Acta Cryst.* **2008**, *A64*, 112-122. (b) G. M. Sheldrick, *Acta Cryst.* **2015**, *C71*, 3-8.

[13] C. Kabuto, S. Akine, T. Nemoto, E. Kwon, *Nihon Kessho Gakkaishi* **2009**, *51*, 218-224.

[14] A. L. Spek, *Acta Cryst.* **2009**, *D65*, 148-155.

[15] A. Igashira-Kamiyama, T. Konno, *Dalton Trans.* **2011**, *40*, 7249-7263.

[16] K. Nakamoto, *Infrared and Raman Spectra of Inorganic and Coordination Compounds*, Wiley, New York, **1997**.

[17] G. R. Desiraju, T. Steiner, *The Weak Hydrogen Bond in Structural Chemistry and Biology*, Oxford University Press, Oxford, **1999**.

[18] (a) R. J. Davey, P. T. Cardew, D. McEwan, D. E. Sadler, *Angew. J. Cryst. Growth* **1986**, *79*, 648-653. (b) J. W. Mullin, *Crystallization*, Butterworth, London, **1993**.

[19] A. L. Spek, *J. Appl. Cryst.* **2003**, *36*, 7-13.

[20] (a) J. Canivet, J. Bonnefoy, C. Daniel, A. Legrand, B. Coasne, D. Farrusseng, *New J. Chem.* **2014**, *38*, 3102-3111. (b) J. Canivet, A. Fateeva, Y. Guo, B. Coasne, D. Farrusseng, *Chem. Soc. Rev.* **2014**, *43*, 5594-5617. (c) N. C. Burtch, H. Jasuja, K. S. Walton, *Chem. Rev.* **2014**, *114*, 10575-10612.

[21] (a) A. Nalaparaju, X. S. Zhao, J. W. Jiang, *J. Phys. Chem. C* **2010**, *114*, 11542-11550. (b) R. Plessius, R. Kromhout, A. L. D. Ramos, M. Ferbinteanu, M. C. Mittelmeijer-Hazeleger, R. Krishna, G. Ronthenberg, S. Tananse, *Chem. Eur. J.* **2014**, *20*, 7922-7925. (c) J. J. Gutiérrez-Sevillano, S. Calero, R. Krishna, *J. Phys. Chem. C* **2015**, *119*, 3658-3666.

2a (porosity *ca.* 80%)

2b (porosity *ca.* 60%)

2c (porosity *ca.* 30%)

$[Co_2Au_3(D\text{-pen-}N,S)_6]^{3-}$ ($[\mathbf{1}]^{3-}$)

$[Co(H_2O)_6]^{2+}$

$[Co(H_2O)_4]^{2+}$

Scheme I-1. Stepwise structural conversion from the kinetic product **2a** to the thermodynamically stable product **2c** *via* the thermodynamically metastable product **2b**. Dashed lines indicate hydrogen bonds.
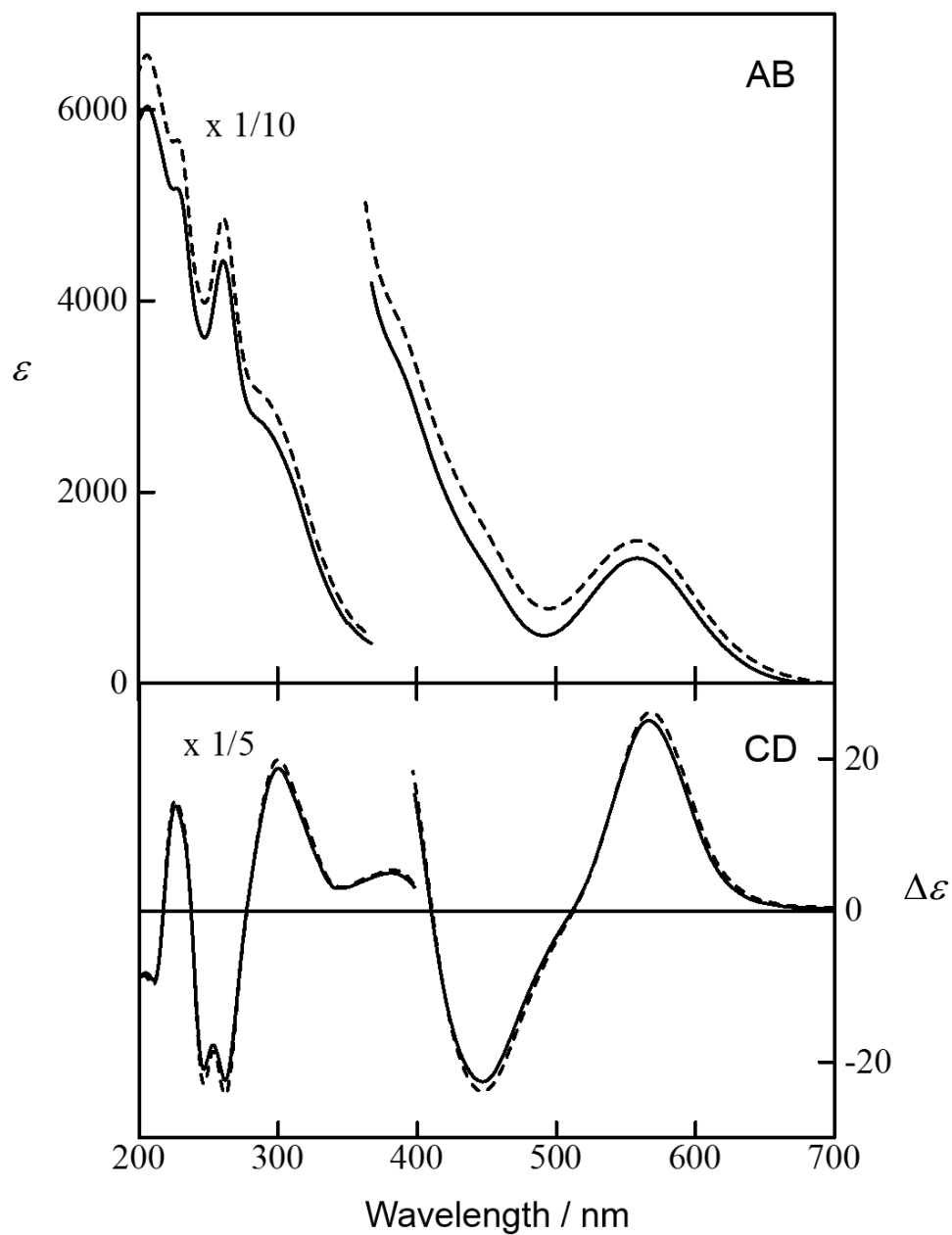
Figure I-1. Absorption (AB) and circular dichroism (CD) spectra of Na$_3$[**1**] (——) and **2a** (----) in water.
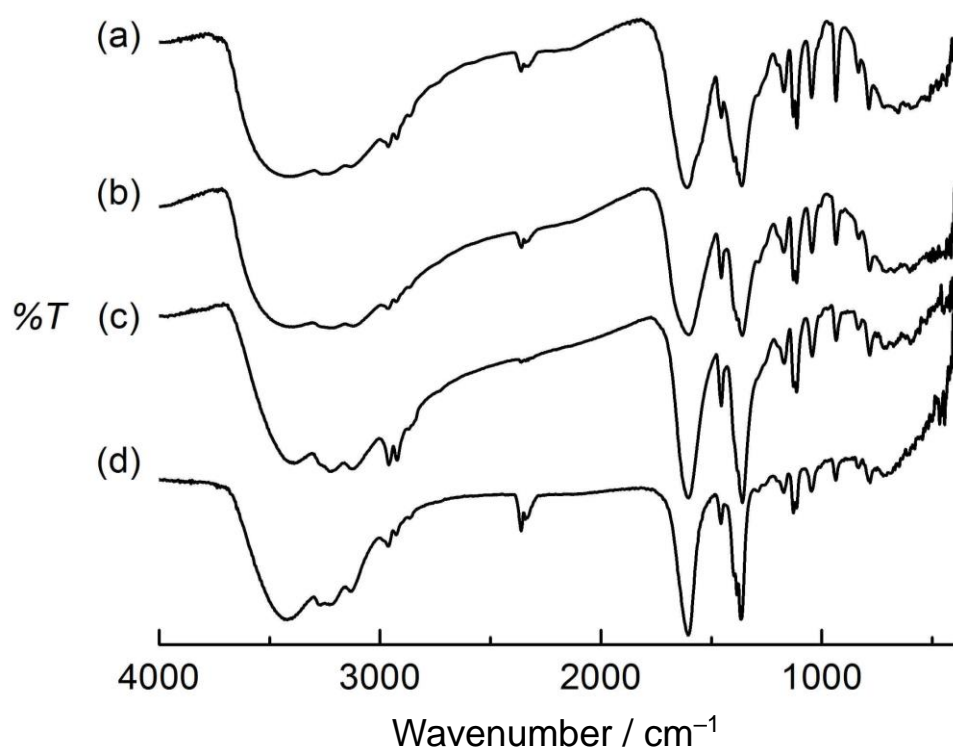
Figure I-2. IR spectra of (a) Na$_3$[**1**], (b) **2a**, (c) **2b**, and (d) **2c**.
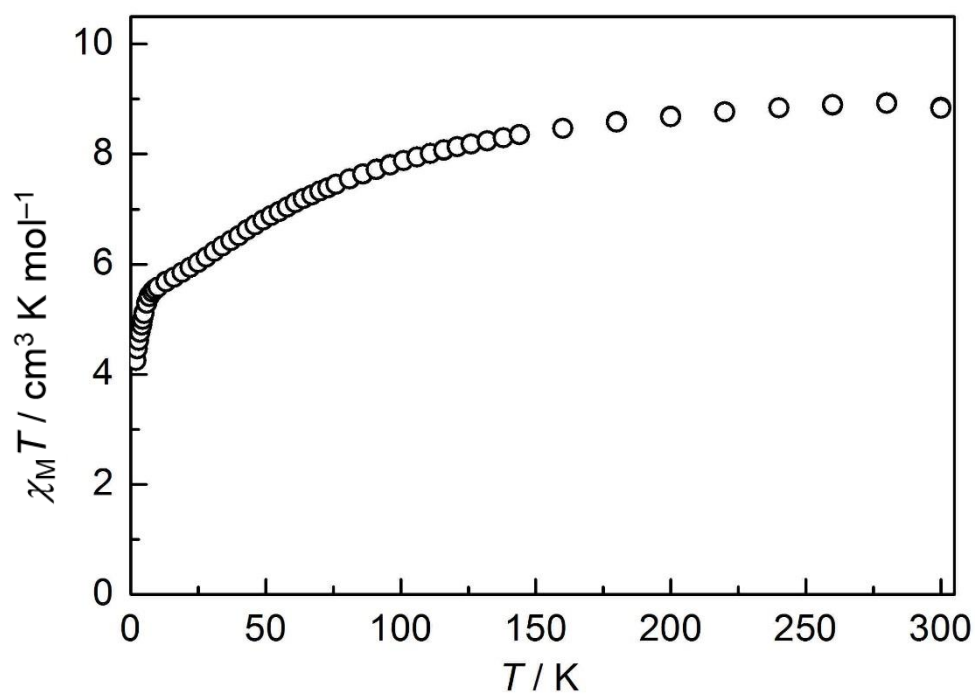
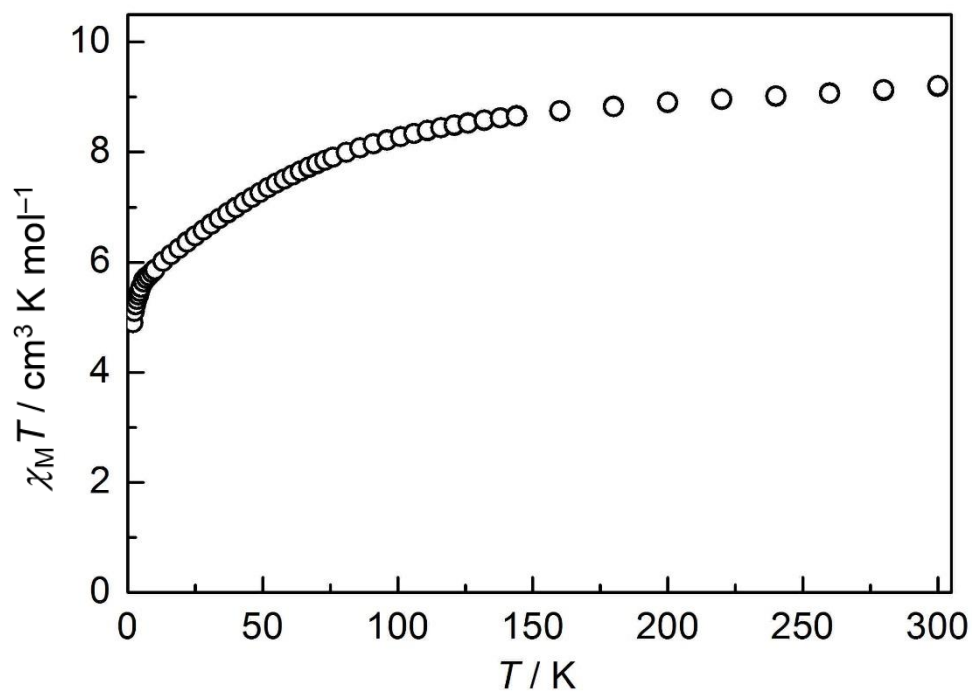**Figure I-3.** Plot of $\chi_M T$ vs. T for **2a** showing $\chi_M T$ value of 8.87 cm^3 K mol^{-1} at 300 K.
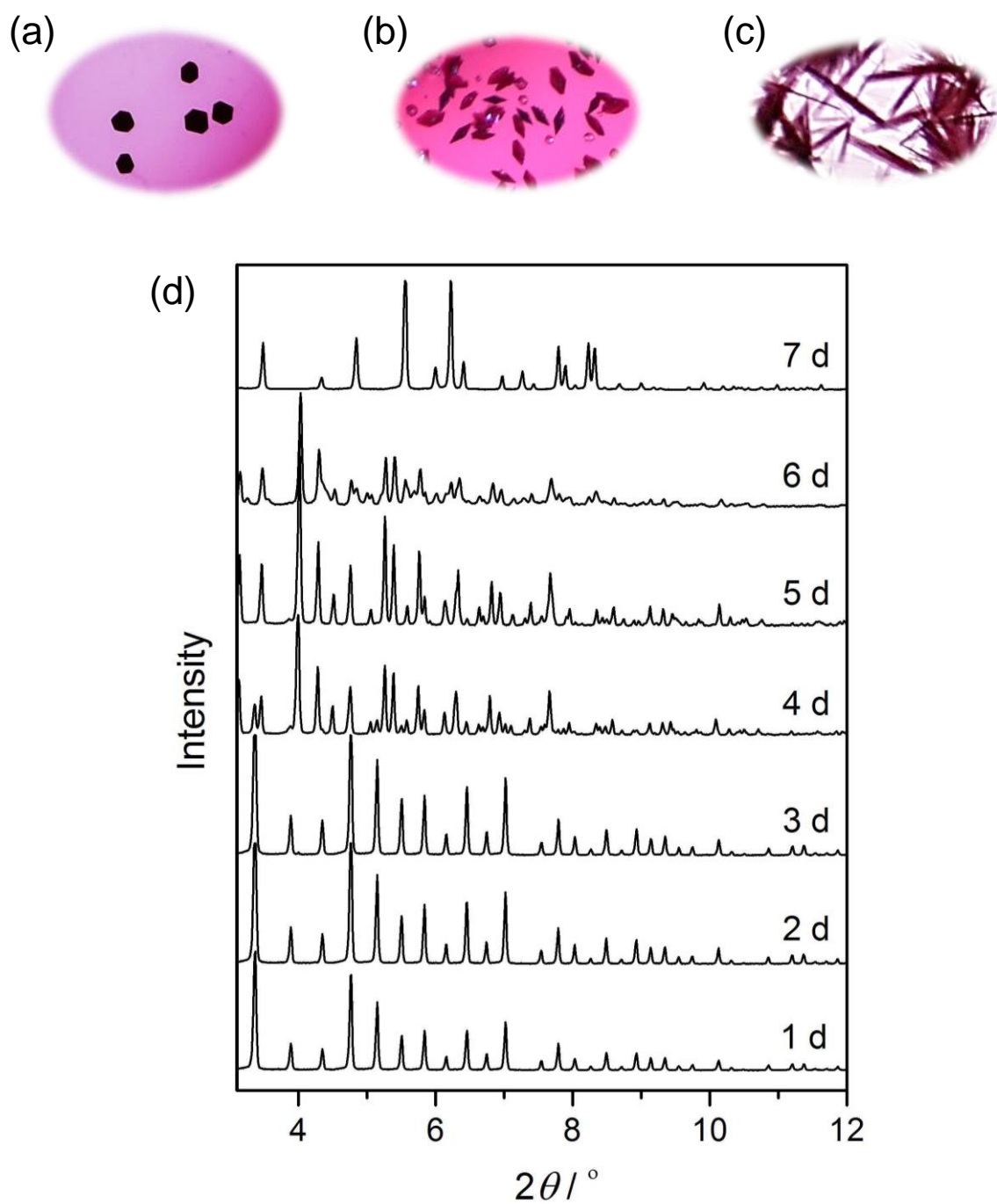
Figure I-4. Images of crystals (a) **2a**, (b) **2b**, and (c) **2c**. (d) PXRD patterns showing structural conversion of **2a** in its mother liquor. Patterns observed at 4 and 6 days matched well with the mixture of **2a** & **2b** and **2b** & **2c**, respectively.
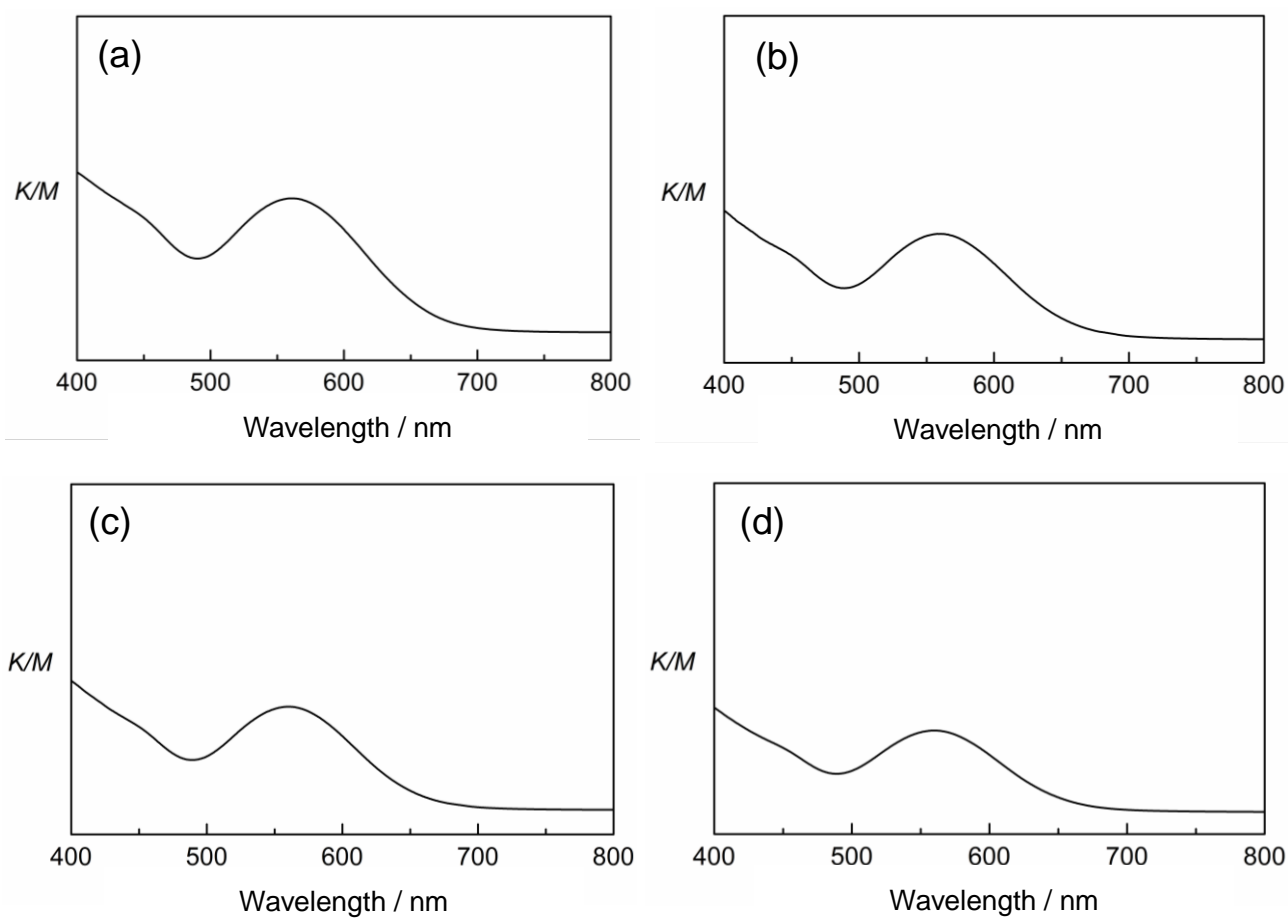
Figure I-5. Diffuse reflection spectra of (a) Na$_3$[**1**], (b) **2a**, (c) **2b**, and (d) **2c**.
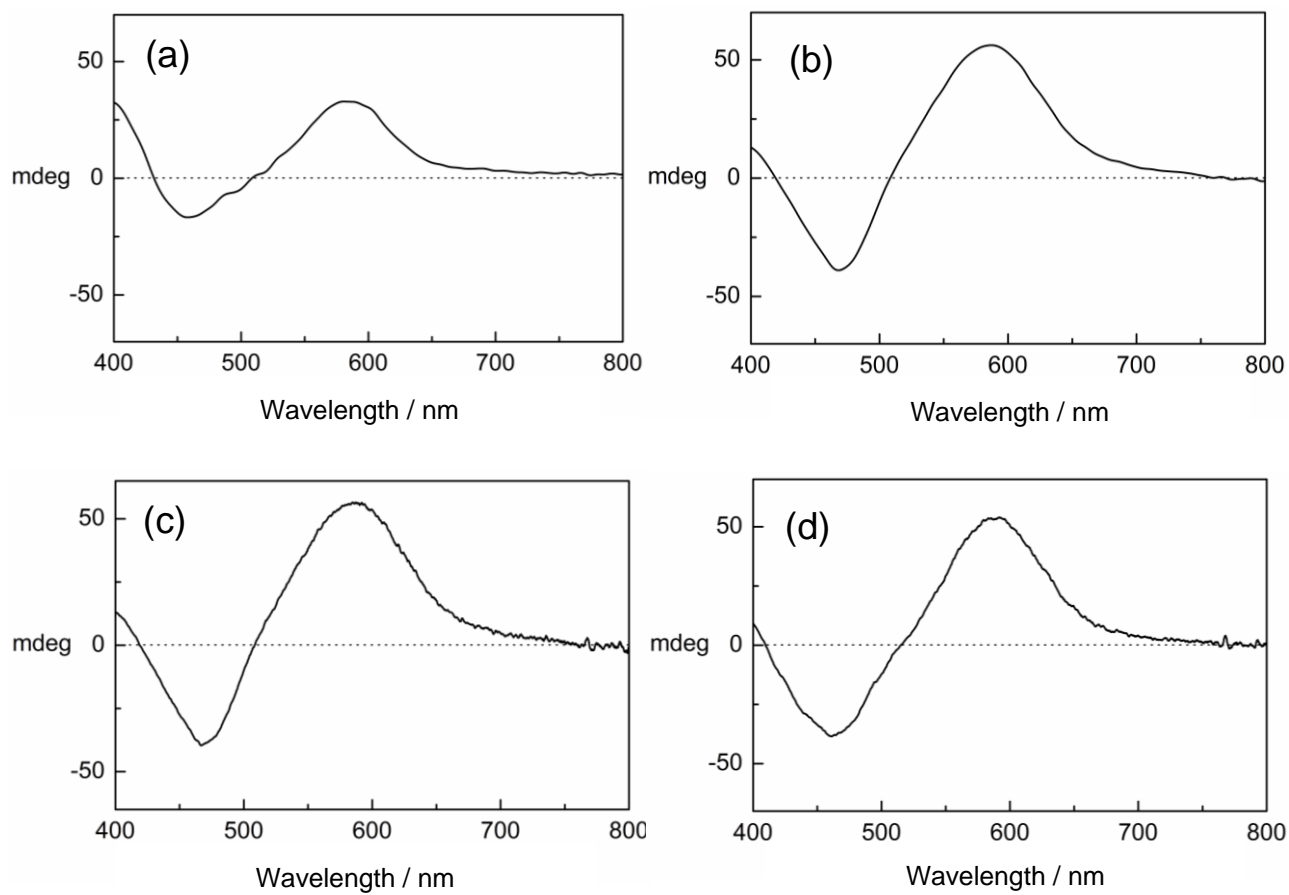
Figure I-6. Solid state CD spectra of (a) Na₃[**1**], (b) **2a**, (c) **2b**, and (d) **2c**.
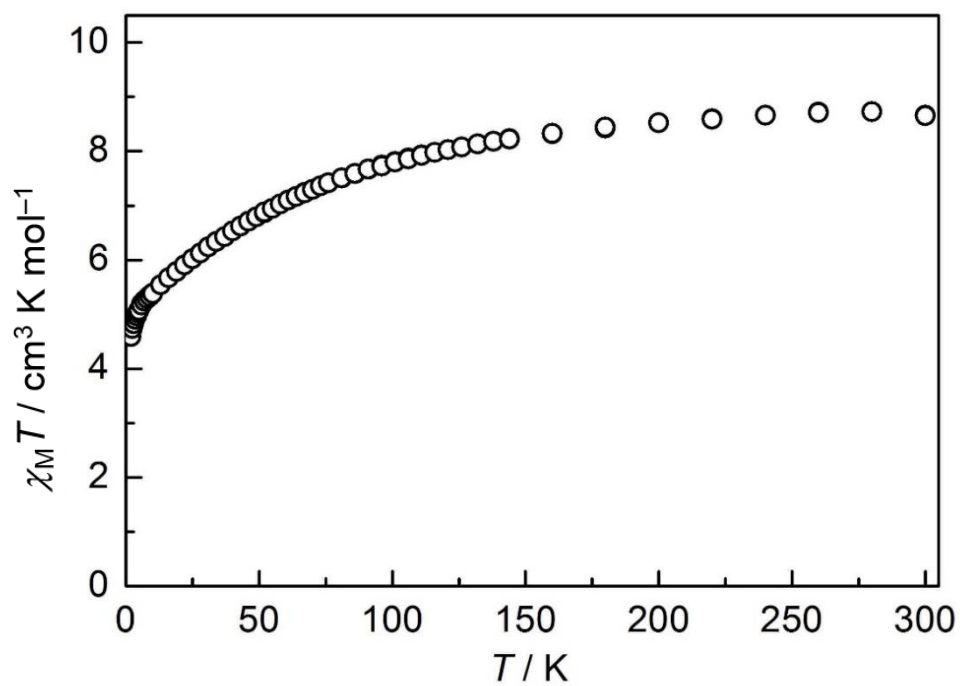
Figure I-7. Plot of $\chi_M T$ vs. T for **2b** showing $\chi_M T$ value of 8.77 cm^3 K mol^{-1} at 300 K.

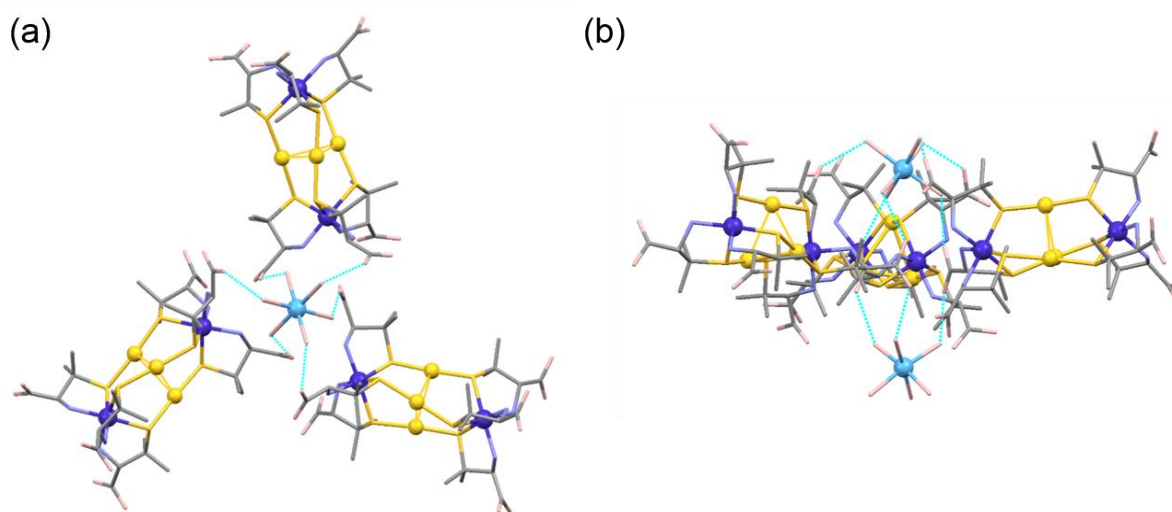**Figure I-8.** Plot of $\chi_M T$ vs. T for **2c** showing $\chi_M T$ value of 9.15 cm^3 K mol^{-1} at 300 K.

Figure I-9. (a) Top and (b) side views of the two $[Co(H_2O)_6]^{2+}$ cations connecting three complex anions in **2a**. Color codes: Co^{II}, light blue; Co^{III}, purple; Au, gold; S, yellow; O, pink; N, blue; C, gray. Dashed lines indicate hydrogen bonds.
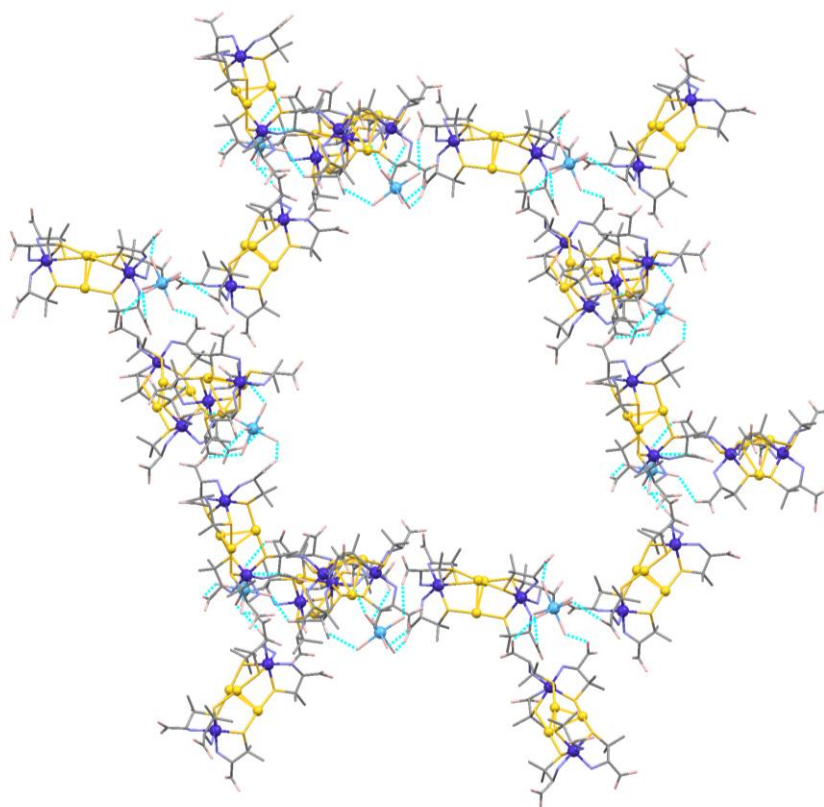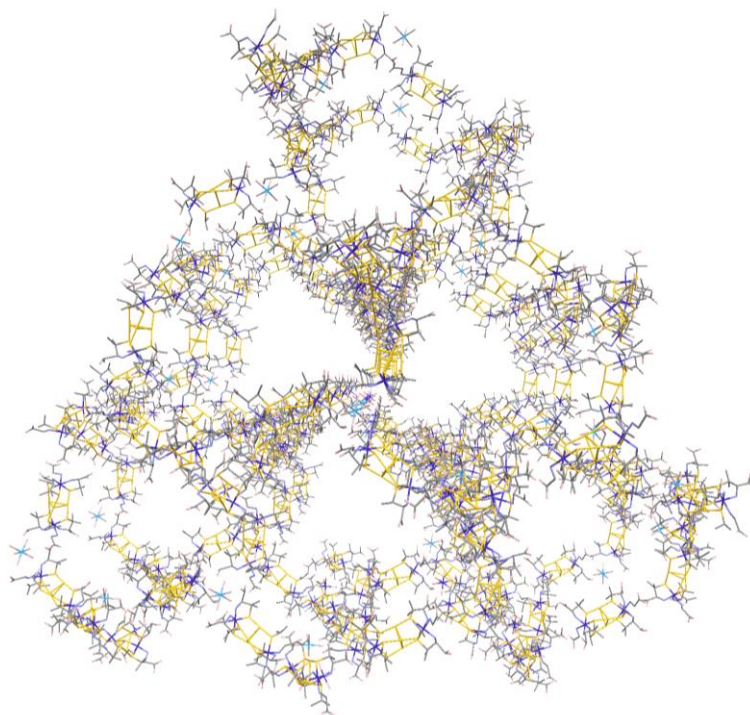

Figure I-10. A perspective view of the 10-membered ring in **2a**. Color codes: Co^{II}, light blue; Co^{III}, purple; Au, gold; S, yellow; O, pink; N, blue; C, gray. Dashed lines indicate hydrogen bonds.

Figure I-11. A perspective view of the 3D hydrogen-bonded framework in **2a**.
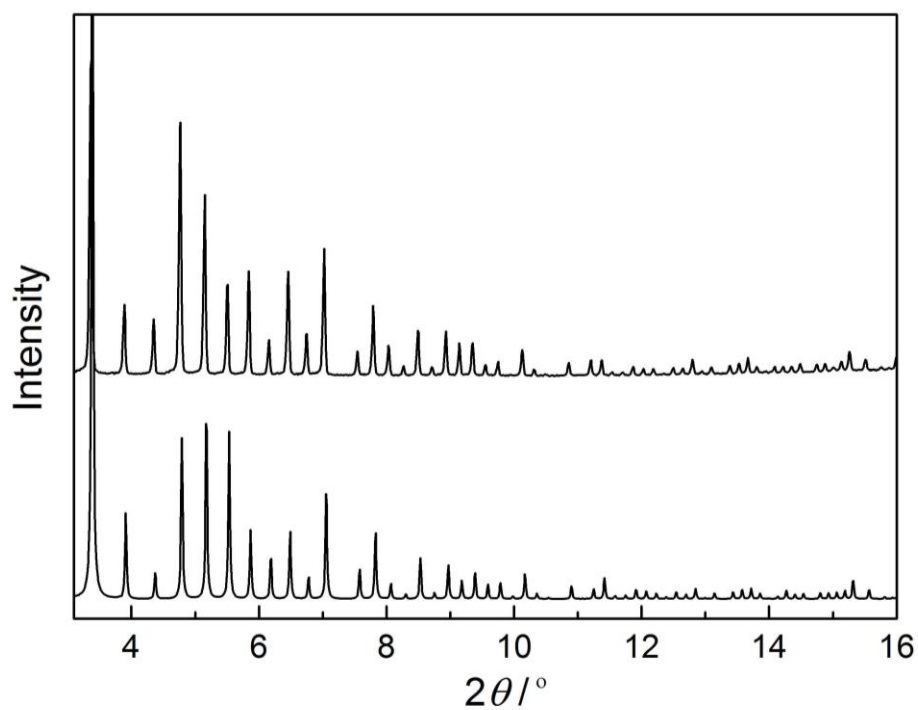

Figure I-12. Experimental (top) and simulated (bottom) PXRD patterns of **2a**.
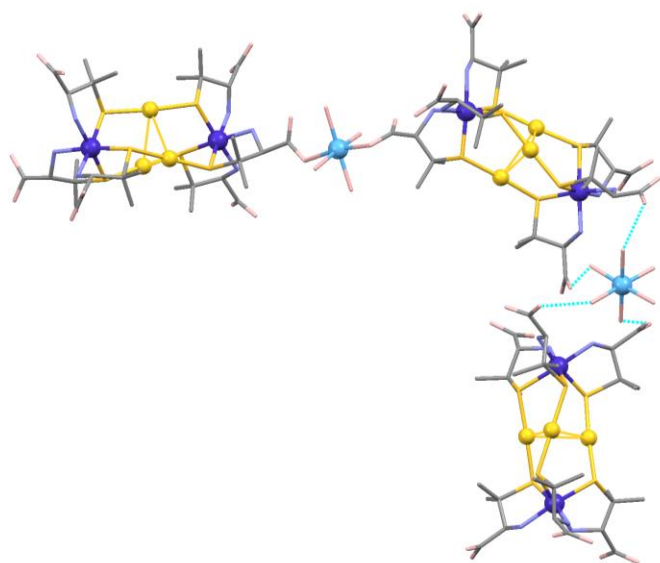
Figure I-13. A perspective view of the expanded asymmetric unit in **2b**. Color codes: Co^{II}, light blue; Co^{III}, purple; Au, gold; S, yellow; O, pink; N, blue; C, gray. Dashed lines indicate hydrogen bonds.
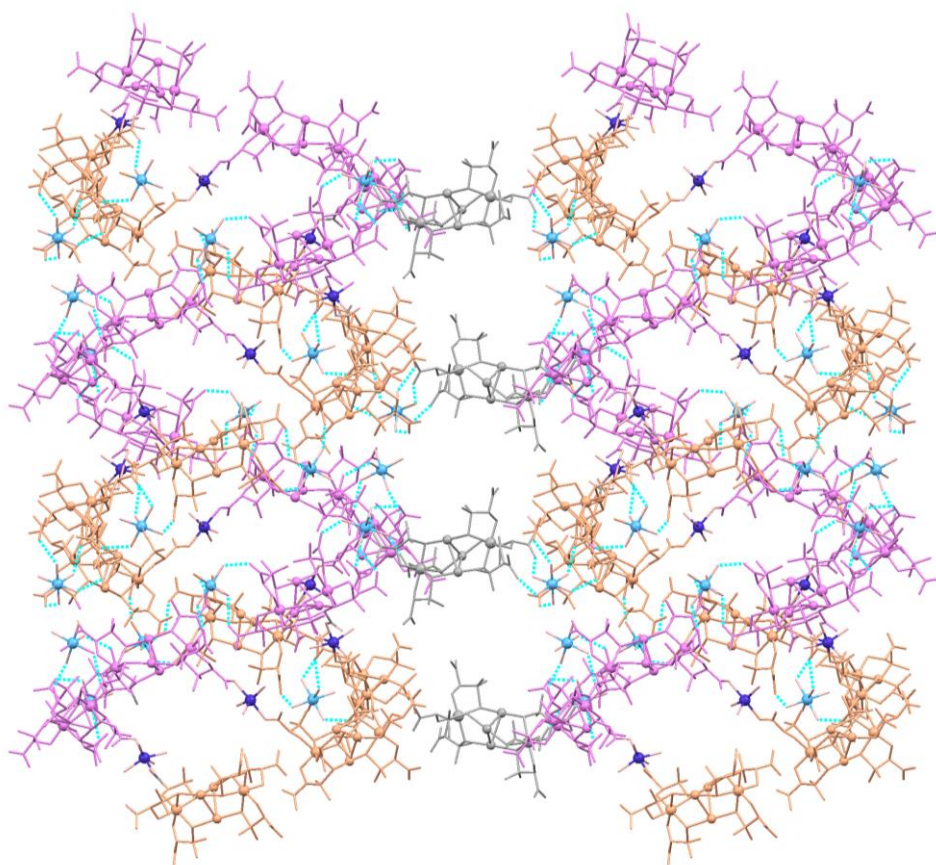

Figure I-14. A perspective view of two double helices (purple and orange) connected by [**1**]$^{3-}$ anions (gray) in **2b**. Color codes: Co^{II}, light blue; Co^{III}, purple; O, pink. Dashed lines indicate hydrogen bonds.
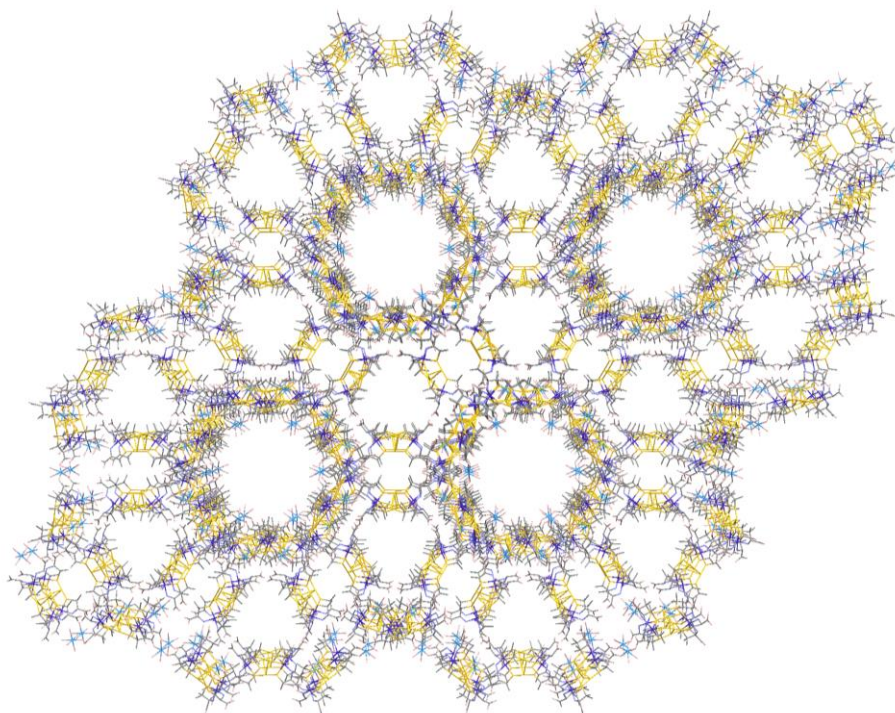
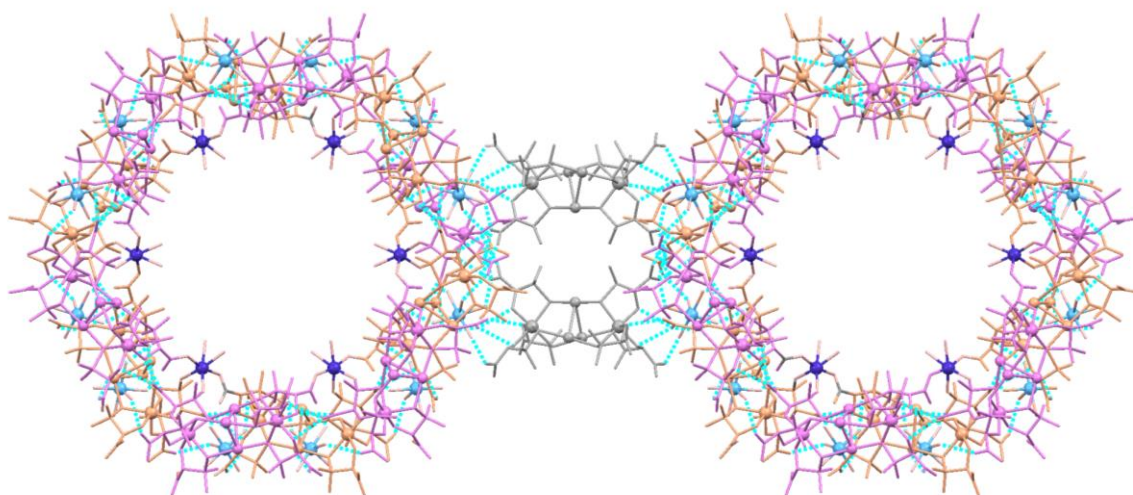**Figure I-15.** A perspective view of the 1D channel structure in **2b**.

Figure I-16. A top view of the two double helices connected by [**1**]$^{3-}$ anions in **2b**. Dashed lines indicate hydrogen bonds.
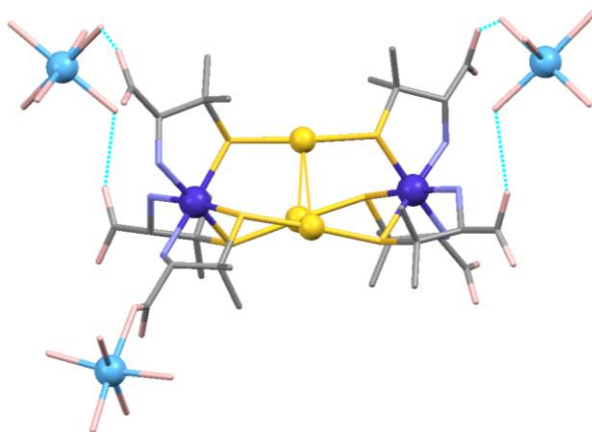
Figure I-17. A perspective view of the [**1**]$^{3-}$ anion connecting three [Co(H$_2$O)$_n$]$^{2+}$ cations through coordination bonds and hydrogen bonds in **2b**. Color codes: Co^{II}, light blue; Co^{III}, purple; Au, gold; S, yellow; O, pink; N, blue; C, gray. Dashed lines indicate hydrogen bonds.

Figure I-18. A perspective view of the [Co(H$_2$O)$_6$]$^{2+}$ cation connecting three [**1**]$^{3-}$ anions through hydrogen bonds in **2b**. Color codes: Co^{II}, light blue; Co^{III}, purple; Au, gold; S, yellow; O, pink; N, blue; C, gray. Dashed lines indicate hydrogen bonds.
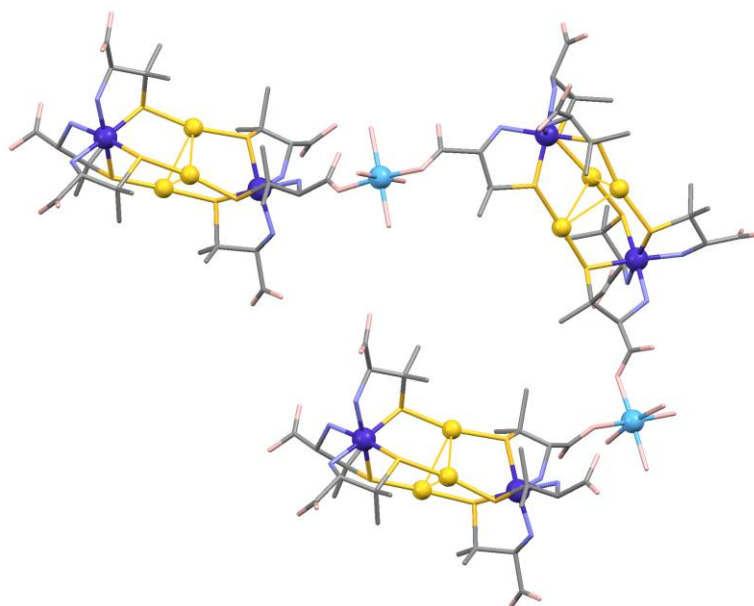
Figure I-19. A perspective view of the expanded asymmetric unit in **2c**. Color codes: Co^{II}, light blue; Co^{III}, purple; Au, gold; S, yellow; O, pink; N, blue; C, gray.

(a)

(b)
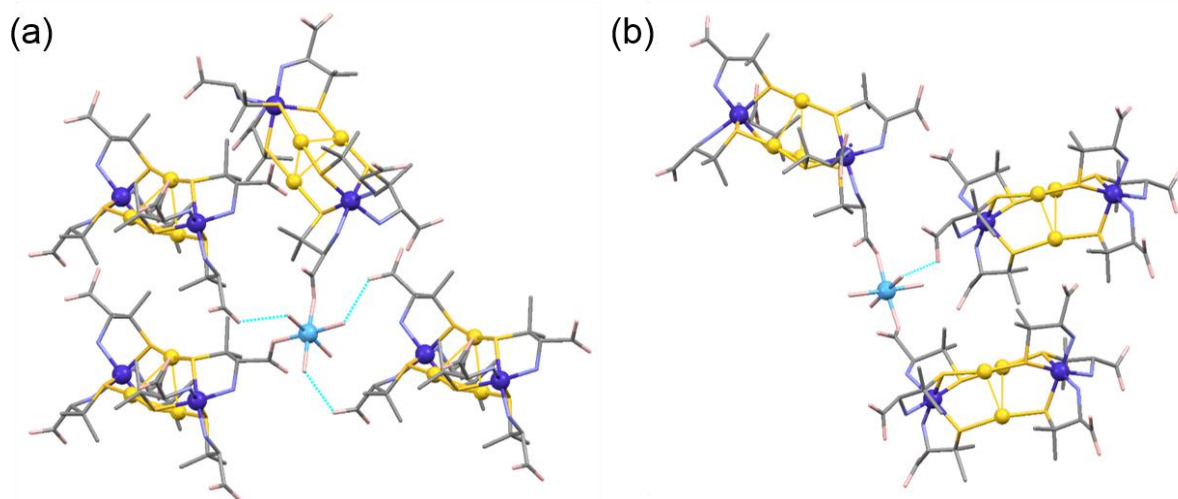
Figure I-20. Perspective views of (a) *cis*-[Co(H$_2$O)$_4$]$^{2+}$ and (b) *trans*-[Co(H$_2$O)$_4$]$^{2+}$ cations connecting complex anions in **2c**. Color codes: Co^{II}, light blue; Co^{III}, purple; Au, gold; S, yellow; O, pink; N, blue; C, gray. Dashed lines indicate hydrogen bonds.
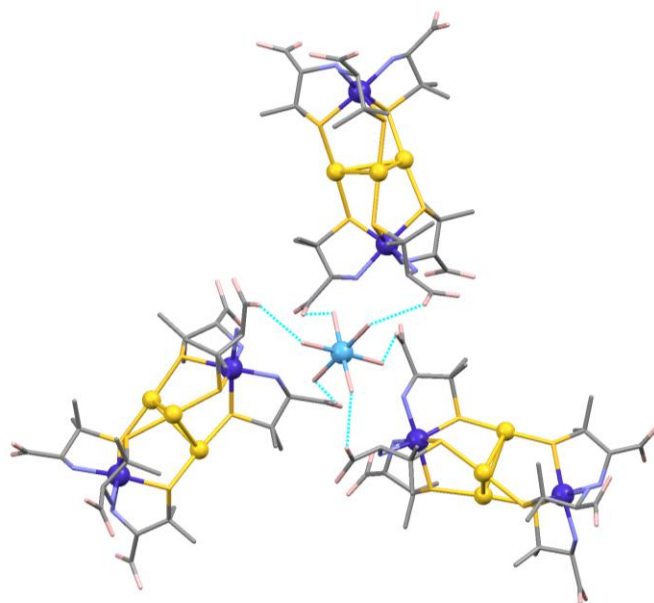
Figure I-21. A perspective view of the [**1**]$^{3-}$ anion connecting three [Co(H$_2$O)$_n$]$^{2+}$ cations through coordination bond and hydrogen bonds in **2c**. Color codes: Co^{II}, light blue; Co^{III}, purple; Au, gold; S, yellow; O, pink; N, blue; C, gray. Dashed lines indicate hydrogen bonds.
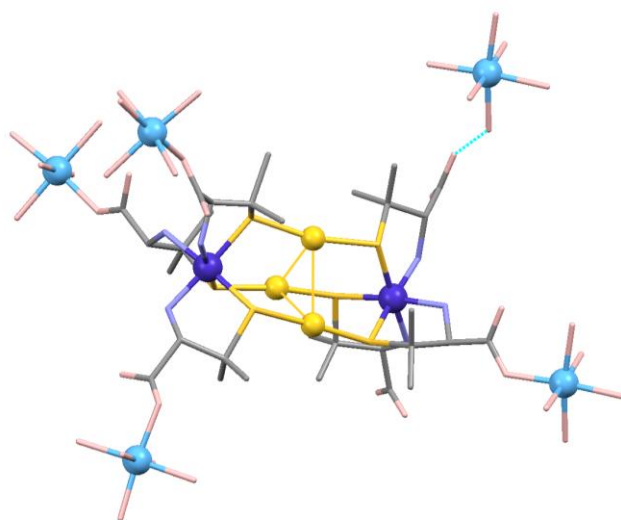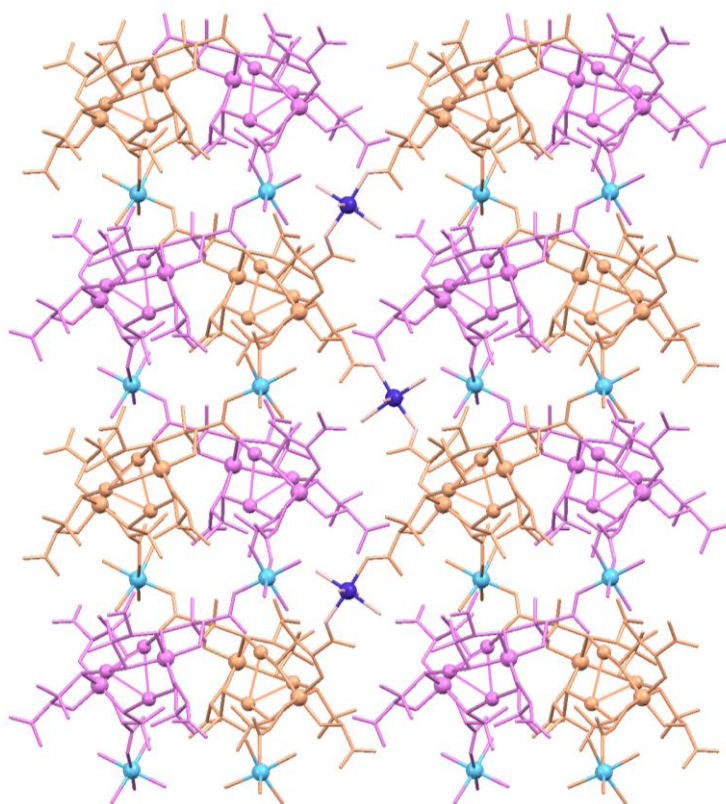

Figure I-22. A perspective view of two double helices (purple and orange) connected by *trans*-[Co(H$_2$O)$_4$]$^{2+}$ (dark purple) cations in **2c**.
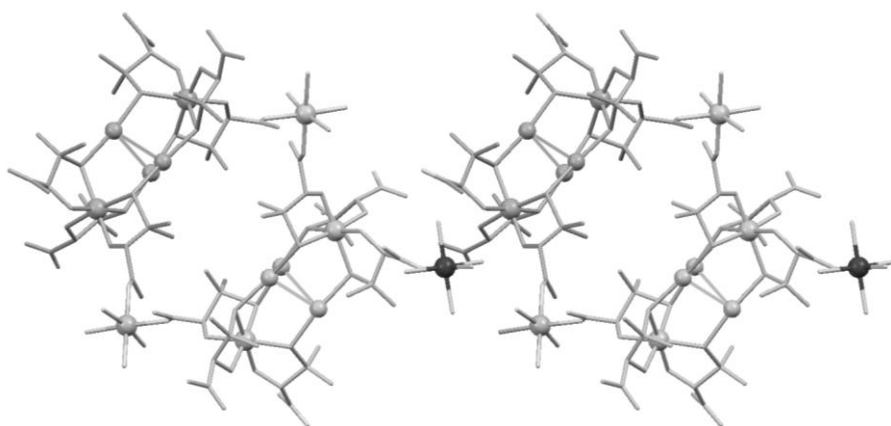
Figure I-23. A top view of two double helices connected by *trans*-[Co(H$_2$O)$_4$]$^{2+}$ (dark gray) cations in **2c**.
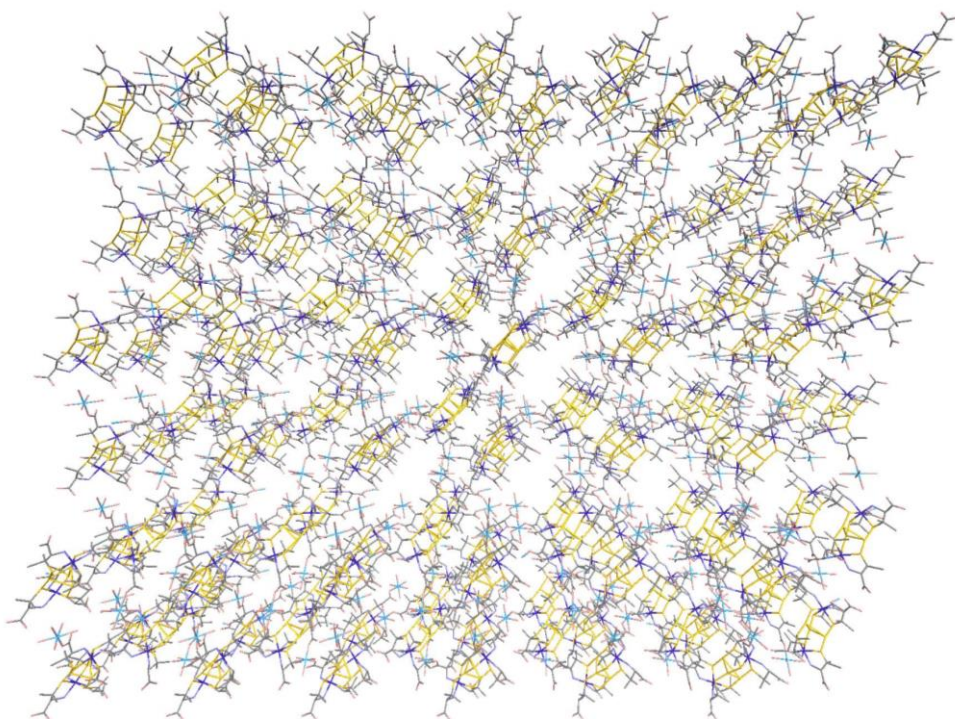
Figure I-24. A perspective view of the 3D dense structure with 2D coordination polymers in **2c**.
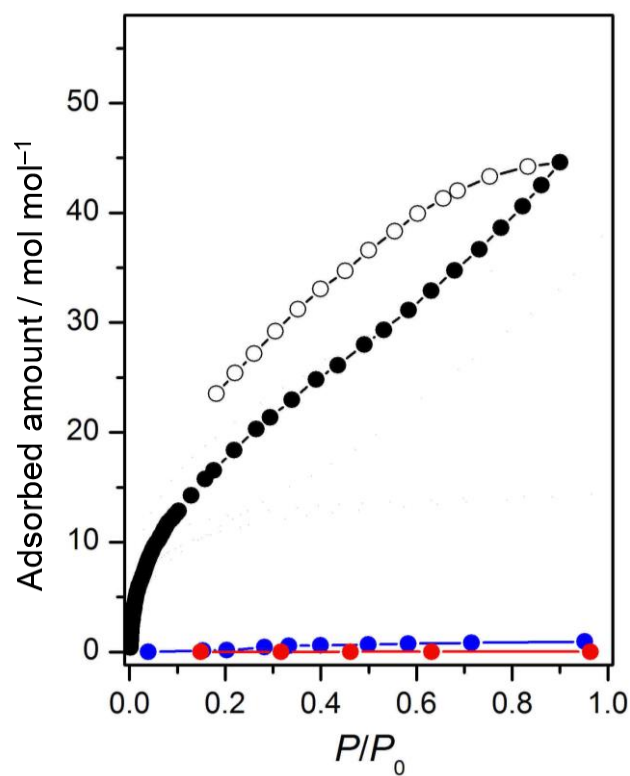
Figure I-25. Vapor adsorption (solid symbols) and desorption (open symbols) isotherms of **2a** for H_2O (black), EtOH (blue), and acetone (red) at 298 K.
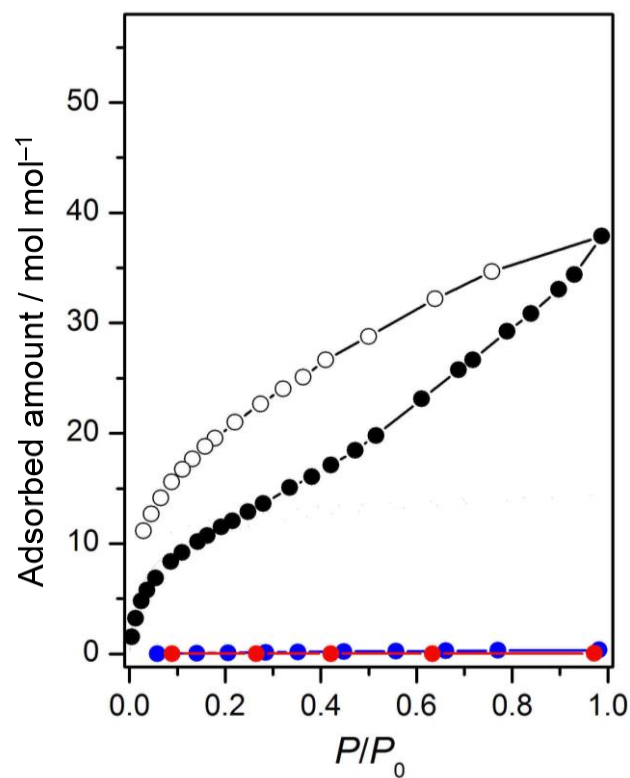
Figure I-26. Vapor adsorption (solid symbols) and desorption (open symbols) isotherms of **2b** for H_2O (black), EtOH (blue), and acetone (red) at 298 K.
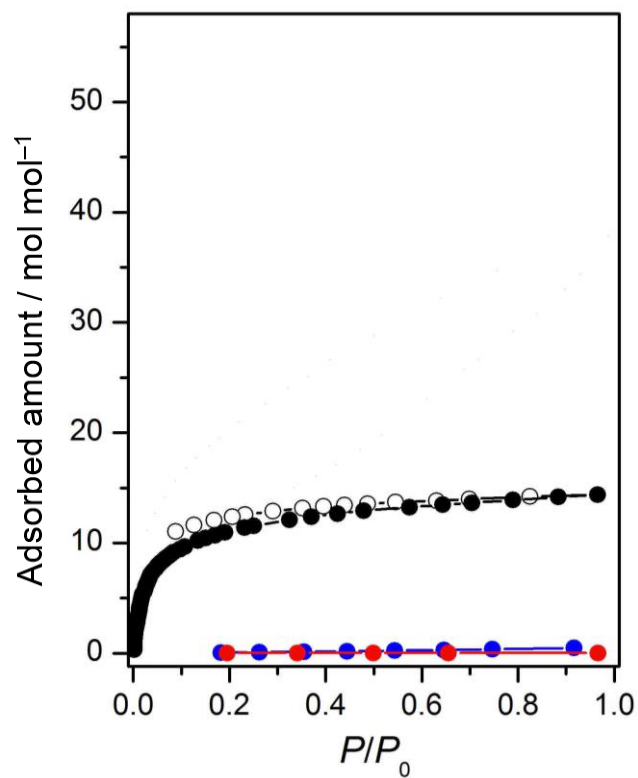
Figure I-27. Vapor adsorption (solid symbols) and desorption (open symbols) isotherms of **2c** for H$_2$O (black), EtOH (blue), and acetone (red) at 298 K.

Figure I-28. Comparison of CO$_2$ at 195 K (–●–) and N$_2$ at 77 K (–◆–) adsorption isotherms of **2a**.

Figure I-29. Comparison of CO_2 at 195 K (−●−) and N_2 at 77 K (−◆−) adsorption isotherms of **2b**.

Figure I-30. Comparison of CO_2 at 195 K (−●−) and N_2 at 77 K (−◆−) adsorption isotherms of **2c**.

Table I-1. Crystallographic data of **2a**, **2b**, and **2c**.

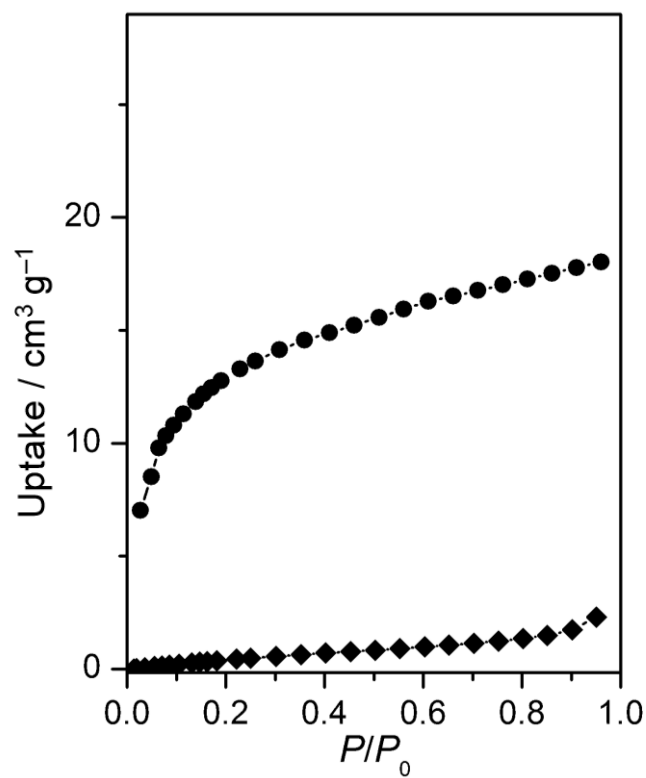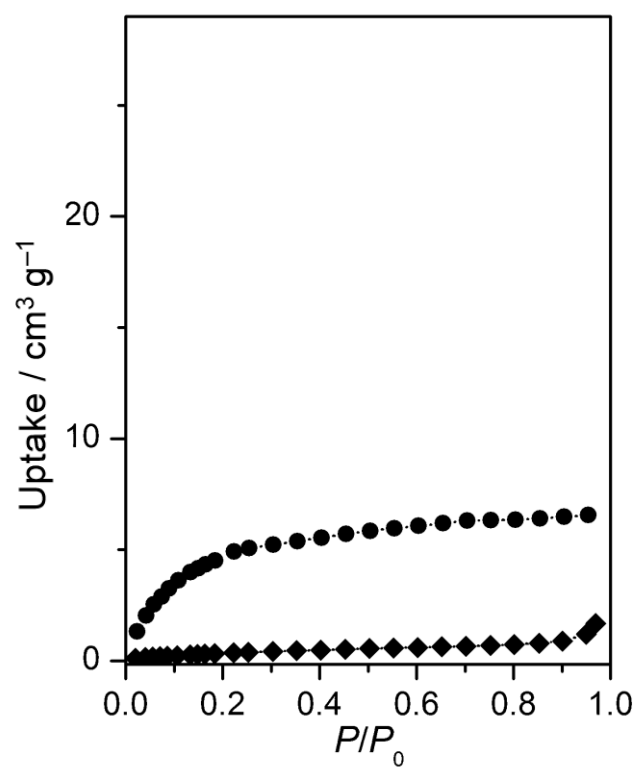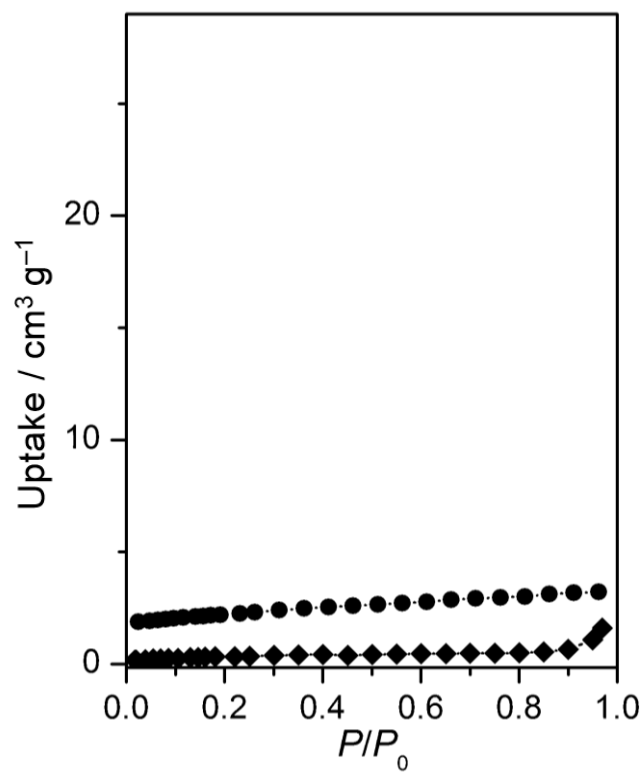|	2a	2b	2c
Formula	$C_{30}H_{54}Au_3Co_{3.33}N_6O_{20}S_6$	$C_{90}H_{162}Au_9Co_9N_{18}O_{52}S_{18}$	$C_{30}H_{54}Au_3Co_{3.5}N_6O_{29.5}S_6$
Color, form	Purple, hexagonal plate	Purple, hexagonal block	Purple, needle
Formula weight	1798.48	5208.52	1960.30
Crystal system	Cubic	Hexagonal	Monoclinic
Space group	$I2_13$	$P6_122$	$P2_1$
a / Å	41.4443(3)	45.349(3)	32.964(4)
b / Å	41.4443(3)	45.349(3)	21.5440(14)
c / Å	41.4443(3)	30.2033(9)	19.335(2)
α / °	90	90	90
β / °	90	90	96.386(7)
γ / °	90	120	90
V / Å^3	71186.0(15)	53793(6)	13646.0(15)
Z	12	6	4
T / K	100(2)	100(2)	180(2)
F(000)	10308	14916	3758
ρ_{calcd} / g cm^{-3}	0.503	0.965	1.908
μ(Mo Kα) / mm^{-1}	2.049	4.023	7.515
Crystal size / mm^3	0.13×0.13×0.11	0.03×0.03×0.02	0.10×0.03×0.01
Limiting indices	$-57 \leq h \leq 54$,	$-56 \leq h \leq 30$,	$-38 \leq h \leq 42$,
	$-57 \leq k \leq 55$,	$-47 \leq k \leq 59$,	$-13 \leq k \leq 13$,
	$-49 \leq l \leq 49$	$-41 \leq l \leq 30$	$-25 \leq l \leq 25$
$2\theta_{max}$ / °	59.02	58.14	54.97
R_1^a ($I>2\sigma(I)$)	0.0422	0.0418	0.0728
wR_2^b (all data)	0.1136	0.0763	0.1904
GOF	0.924	0.856	0.972

[a] $R_1 = (\Sigma|(|F_o| - c|F_c|)|)/(\Sigma|F_o|)$

[b] $wR_2 = [\{\Sigma w(F_o^2 - cF_c^2)^2\}/(\Sigma w|F_o^2|^2)]^{1/2}$

Chapter II. Combination of $Co^{III}_2Au^{I}_3$ complex anions and aqua nickel(II) or aqua manganese(II) cations.

II-1. Introduction.

In Chapter I, the combination of the rod-shaped $Co^{III}_2Au^{I}_3$ pentanuclear-complex anions and the aqua cobalt(II) cations was found to give the highly porous metallosupramolecular framework of $[Co(H_2O)_6]_3[Co_2Au_3(D\text{-}pen\text{-}N,S)_6]_2$ (**2a**; D-H$_2$pen = D-penicillamine), which is kinetically produced before a stepwise conversion to two more thermodynamically stable products with lower porosities, $[Co(H_2O)_6]_2[\{Co(H_2O)_4\}\{Co_2Au_3(D\text{-}pen\text{-}N,S)_6\}_2]$ (**2b**) and $[\{Co(H_2O)_4\}_3\{Co_2Au_3(D\text{-}pen\text{-}N,S)_6\}_2]$ (**2c**), through the replacement of hydrogen bonds by coordination bonds of the free carboxylate groups in $[Co_2Au_3(D\text{-}pen\text{-}N,S)_6]^{3-}$ to Co^{II} centers. Based on the fact that each metal ion has its own chemistry which directly affects the formation of chemical interactions,[1,2] it is interesting to investigate whether different kinds of aqua metal ions affect the formation of metallosupramolecular frameworks, in particular, whether porous frameworks can be constructed to illustrate remarkable properties. An introduction of other transition metals for cationic species, such as Ni^{2+}, Mn^{2+}, and Zn^{2+}, should be examined in order to obtain more information about the effects of changing metal ions on the construction of metallosupramolecular frameworks. In this context, nickel(II) ion with a 3d^8 electron configuration is intriguing because it can adopt both of octahedral and square-planar coordination geometries depending on the character of ligands.[3,4] Manganese(II) ion with a 3d^5 electron configuration is also prominent owing to its larger ionic radius (0.83 Å), compared with those of cobalt(II) and nickel(II) ions (0.74 Å and 0.69 Å, respectively), together with a faster rate of water exchange reactions.[3,4]

In this chapter, a study on the construction of metallosupramolecular frameworks based on a combination of the $Co^{III}_2Au^{I}_3$ pentanuclear-complex anions, $[Co^{III}_2Au^{I}_3(D\text{-}pen\text{-}N,S)_6]^{3-}$ ($[\mathbf{1}]^{3-}$), and aqua nickel(II) or aqua manganese(II) cations is presented. A pair of isostructure of porous ionic crystals, $[Ni(H_2O)_6]_2[\{Ni(H_2O)_4\}\{Co_2Au_3(D\text{-}pen\text{-}N,S)_6\}_2]$ (**3a**) and $[Mn(H_2O)_6]_2[\{Mn(H_2O)_4\}\{Co_2Au_3(D\text{-}pen\text{-}N,S)_6\}_2]$ (**4a**), were produced under controlled synthetic conditions. Remarkably, each of them was stepwise converted to different types of X-ray quality crystals, $[\{Ni(H_2O)_4\}_3\{Co_2Au_3(D\text{-}pen\text{-}N,S)_6\}_2]$ (**3b**) and $[\{Mn(H_2O)_4\}\{Co_2Au_3(D\text{-}Hpen\text{-}N,S)(D\text{-}pen\text{-}N,S)_5\}]$ (**4b**), presenting different porosities of *ca.* 30% and *ca.* 13%, respectively (Scheme II-1 and Scheme II-2). The crystallographic data of

the obtained crystals were fully studied by single-crystal X-ray diffraction analyses. In addition, the physical characterizations on the basis of electronic absorption, CD, IR, and NMR spectra, in addition to X-ray fluorescence and elemental analyses, were performed. The influences of different aqua metal ions on the metallosupramolecular structures constructed, as well as the interconversion phenomena, are discussed. Furthermore, the sorption behavior toward small molecules are also presented.

II-2. Experimental section.

II-2-1. Materials.

The starting complex, $Na_3[Co_2Au_3(D\text{-pen-}N,S)_6]$ ($Na_3[1]$), was prepared by the method described in Chapter I. All other chemicals and solvents were commercially available and used without further purification.

II-2-2. Crystallizations.

(a) $[Ni(H_2O)_6]_2[\{Ni(H_2O)_4\}\{Co_2Au_3(D\text{-pen-}N,S)_6\}_2]$ (3a).

To a purple solution of $Na_3[1]\cdot13H_2O$ (50.0 mg, 0.0301 mmol) in H_2O (2.5 mL), a green solution of $Ni(OAc)_2\cdot4H_2O$ (11.2 mg, 0.0450 mmol) in H_2O 2.5 mL was added. After stirring at room temperature for 5 min, the mixture was allowed to stand at room temperature for 3 days. The resulting purple hexagonal block crystals (**3a**), one of which was used for single-crystal X-ray analysis, were collected by filtration and washed with acetone. Yield: 21 mg (35%). Anal. Calcd for $[Ni(H_2O)_6]_2[\{Ni(H_2O)_4\}\{Co_2Au_3(D\text{-pen-}N,S)_6\}_2]\cdot16H_2O$ = $C_{60}H_{172}N_{12}S_{12}O_{56}Co_4Au_6Ni_3$: C, 18.31; H, 4.40; N, 4.27%. Found: C, 18.34; H, 4.45; N, 4.24%. IR spectrum (cm^{-1}, KBr disk): 1604 (ν_{COO}). ^{1}H NMR spectrum (ppm from DSS, D_2O): δ 1.48 (s, 3H), 1.64 (s, 3H), 3.22 (s, 1H).

(b) $[Mn(H_2O)_6]_2[\{Mn(H_2O)_4\}\{Co_2Au_3(D\text{-pen-}N,S)_6\}_2]$ (4a).

To a purple solution of $Na_3[1]\cdot13H_2O$ (50.0 mg, 0.0301 mmol) in H_2O (2.5 mL), a pale pink solution of $Mn(OAc)_2\cdot4H_2O$ (11.0 mg, 0.0449 mmol) in H_2O 2.5 mL was added. After stirring at room temperature for 5 min, the mixture was allowed to stand at room temperature for 3 days. The resulting purple hexagonal block crystals (**4a**), one of which was used for single-crystal X-ray analysis, were collected by filtration and washed with acetone. Yield: 23

mg (39%). Anal. Calcd for $[Mn(H_2O)_6]_2[\{Mn(H_2O)_4\}\{Co_2Au_3(D\text{-}pen\text{-}N,S)_6\}_2]\cdot14H_2O$ = $C_{60}H_{168}Au_6Co_4Mn_3N_{12}O_{54}S_{12}$: C, 18.53; H, 4.35; N, 4.32%. Found: C, 18.53; H, 4.36; N, 4.20%. IR spectrum (cm^{-1}, KBr disk): 1603 (ν_{COO}). ^{1}H NMR spectrum (ppm from DSS, D$_2$O): δ 1.48 (s, 3H), 1.65 (s, 3H), 3.27 (s, 1H).

II-2-3. Structural conversions.

(a) Conversion from 3a to [{Ni(H₂O)₄}₃{Co₂Au₃(D-pen-*N,S*)₆}₂] (3b).

The obtained purple hexagonal block crystals of **3a** were stored in the mother liquor for several days in a closed vessel. A change in crystal shape was clearly observed after 9 days. The purple needle crystals (**3b**) that are almost insoluble in water, appeared instead of **3a**. One of the purple needle crystals of **3b** was used for single-crystal X-ray diffraction analysis. The resulting purple needle crystals were collected by filtration and washed with acetone. Yield: 22 mg (37%). Anal. Calcd for $[\{Ni(H_2O)_4\}_3\{Co_2Au_3(D\text{-}pen\text{-}N,S)_6\}_2]\cdot23H_2O$ = $C_{60}H_{178}N_{12}S_{12}O_{59}Co_4Au_6Ni_3$: C, 18.06; H, 4.50; N, 4.21%. Found: C, 17.97; H, 4.37; N, 4.12%. IR spectrum (cm^{-1}, KBr disk): 1600 (ν_{COO}).

The crystals were continuously stored in the mother liquor for 1 month, but no further conversion was observed.

(b) Conversion from 4a to [{Mn(H₂O)₄}{Co₂Au₃(D-Hpen-*N,S*)(D-pen-*N,S*)₅}] (4b).

The obtained purple hexagonal block crystals of **4a** were continuously stored in the mother liquor for several days in a closed vessel. A change in crystal shape was clearly observed after 13 days. The purple stick crystals (**4b**) which are insoluble in water appeared instead of **4a**. One of the purple stick crystals of **4b** was used for single-crystal X-ray diffraction analysis. The resulting purple stick crystals were collected by filtration and washed with acetone. Yield: 18 mg (33%). Anal. Calcd for $[\{Mn(H_2O)_4\}\{Co_2Au_3(D\text{-}Hpen\text{-}N,S)(D\text{-}pen\text{-}N,S)_5\}]\cdot5H_2O$ = $C_{30}H_{73}N_6S_6O_{21}Co_2Au_3Mn$: C, 19.91; H, 4.07; N, 4.64%. Found: C, 19.89; H, 4.05; N, 4.64%. IR spectrum (cm^{-1}, KBr disk): 1609 (ν_{COO}), 1717 (ν_{COOH})^{sh}.

The crystals were continuously kept in the mother liquor for 1 month, but no further conversion was observed.

II-2-4. Physical measurements.

The diffuse reflection spectra were recorded with a JASCO V-570 UV/VIS/NIR spectrometer at room temperature. The circular dichroism (CD) spectra in the solid state were performed on a JASCO J-820 spectropolarimeter at room temperature. The IR spectra were recorded with a JASCO FT/IR-4100 infrared spectrometer using KBr disks at room temperature. Elemental analyses (C, H, N) were performed using a Yanaco CHN Corder MT-5. The X-ray fluorescence analyses were conducted using a SHIMADZU Rayny EDX-720 spectrometer. The ^{1}H NMR spectra were recorded with a JEOL ECAMX-500SP spectrometer in D_2O. Sodium 4,4-dimethyl-4-silapentane-1-sulfonate (DSS) was used as the internal reference. All measurements were performed at room temperature. The sorption isotherms of N_2 and CO_2 were measured with a BELSORP-mini II volumetric adsorption instrument. N_2 and CO_2 gases of high purity (99.9999%) were used. The sorption isotherms for H_2O, EtOH, and acetone were performed on a BELSORP-max volumetric adsorption instrument. High quality powder X-ray diffraction patterns were recorded at room temperature, in transmission mode [synchrotron radiation λ = 0.999139(2) Å; 2θ range = 0–78°; step width = 0.005°; data collection time = 1 min] on a diffractometer equipped with a MYTHEN microstrip X-ray detectors (Dectris ltd.) at SPring-8 BL02B2 beamline. The crystals were stored in the mother liquor for several days for time-dependent observation of the powder X-ray diffraction. The crystals were loaded into glass capillary tubes (diameter = 0.3 mm) with their mother liquor. The samples were rotated during the measurements. The diffraction patterns were collected with a large Debye-Scherrer camera. The powder simulation patterns were generated from the single-crystal X-ray structures using Mercury 3.8. The high-quality PXRD patterns were illustrated in Figure II-4 and Figure II-5. Other PXRD measurement experiments were performed on a BRUKER D2 PHASER.

II-2-5. X-ray structural determinations.

Single-crystal X-ray diffraction data for **3a**, **3b**, and **4a** were recorded on a Rigaku Mercury 2 CCD detector with a synchrotron radiation (λ = 0.6997 Å) at BL02B1 beamline in SPring-8 with the approval of the Japan Synchrotron Radiation Research Institute (JASRI). The intensity data were collected by the ω-scan and were processed with a Rapid Auto software program. The structures of **3a**, **3b**, and **4a** were solved by direct methods using SHELXS-2014.[5] The structure refinements were carried out using full-matrix least-squares (SHELXL-2014).[5] All calculations were performed using the Yadokari-XG software package.[6] All non-hydrogen atoms were refined anisotropically. Hydrogen atoms were

included in the calculated positions except those of water molecules. For **3a** and **4a**, the crystal structures possess a large void space in a one dimensional structure composed of [**1**]$^{3-}$ anions, [Ni(H$_2$O)$_4$]$^{2+}$ or [Mn(H$_2$O)$_4$]$^{2+}$, and [Ni(H$_2$O)$_6$]$^{2+}$ or [Mn(H$_2$O)$_6$]$^{2+}$ cations. The void space should be filled by the solvated water molecules and a part of [Ni(H$_2$O)$_6$]$^{2+}$ and [Mn(H$_2$O)$_6$]$^{2+}$ cations for **3a** and **4a**, respectively, based on the results from X-ray fluorescence and elemental analyses. However, they are severely disordered and only several solvated water molecules could be modeled in the void space. The SQUEEZE reports indicated the solvent-accessible volume of 36004 A^3 and 36451 A^3 per cell for **3a** and **4a**, respectively,[7] corresponding to *ca.* 60% of the unit-cell volume for both structures.

Single-crystal X-ray diffraction experiment for **4b** was performed on a RIGAKU/MSC Mercury CCD X-ray diffractometer with a synchrotron radiation (λ = 0.6889 Å) at PF-AR (NW2A beamline) of the High Energy Accelerator Research Organization (KEK). The diffraction images were processed by HKL2000.[8] The structure of **4b** was solved by direct methods using SHELXS-2014.[5] The structure refinements were carried out using full-matrix least-squares (SHELXL-2014).[5] All calculations were performed using the Yadokari-XG software package.[6] All non-hydrogen atoms were refined anisotropically. Hydrogen atoms were included in the calculated positions except those of water molecules. Crystal data are summarized in Table II-1 and Table II-2.

II-3. Results and discussion.

II-3-1. Syntheses, characterizations, and structural conversions.

(a) [Ni(H$_2$O)$_6$]$_2$[{Ni(H$_2$O)$_4$}{Co$_2$Au$_3$(D-pen-*N,S*)$_6$}$_2$] (3a).

The ionic crystal **3a** was successfully obtained in the form of water-soluble purple hexagonal block crystals from an aqueous solution containing Na$_3$[**1**] and Ni(OAc)$_2$ in a 2:3 ratio. The crystallization of **3a** occurred within 1 day with a yield of 35%. The diffuse reflection and the solid state CD spectra of **3a** are similar to those of Na$_3$[**1**], indicating that the S-bridged pentanuclear structure of rod-shaped [**1**]$^{3-}$ retained in **3a**, as an anionic molecular building block (Figure II-1 and Figure II-2). The results from X-ray fluorescence and elemental analyses are in good agreement with the formula for a 2:3 adduct of [**1**]$^{3-}$ and Ni^{2+}. In addition, the IR spectrum of **3a** displays an intense ν_{COO} band at 1604 cm^{-1} (Figure II-3), indicative of the fully deprotonated carboxyl groups of D-pen in **3a**.[9]

To investigate the stability of the ionic crystal **3a**, the resulting purple hexagonal block crystals of **3a** were stored in the mother liquor for several days in a closed vessel (Figure II-4a). The change in the crystal shape was clearly observed after 9 days with the appearance of purple needle crystals (**3b**) (Figure II-4b) that are almost insoluble in water instead of **3a**. As shown in Figure II-4c, a structural conversion could be observed by PXRD measurements. A pure phase of **3a** was retained in its mother liquor for 6 days followed by the subsequent conversion to a pure phase of **3b** after 9 days. The PXRD patterns observed at 7 and 8 days indicate the mixture of **3a** and **3b**. The structural conversion from **3a** to **3b** implied that **3a** is a kinetic product, whereas **3b** is more thermodynamically stable compared with **3a**. The connectivity between the cations and anions shows that **3a** has not only coordination bonds between $[Ni(H_2O)_4]^{2+}$ cations and $[1]^{3-}$ anions but also the hydrogen bonds between $[Ni(H_2O)_6]^{2+}$ cations and $[1]^{3-}$ anions (*vide infra*). On the other hand, only the coordination bonds between $[Ni(H_2O)_4]^{2+}$ cations and $[1]^{3-}$ anions are involved in **3b**. Therefore, the kinetic product **3a** preferentially was converted to the thermodynamic product **3b** through the replacement of hydrogen bonds by coordination bonds that have a greater binding energy.[10] The observed structural conversion could be explained by the dissolution–recrystallization process which allows the kinetic product **3a** to be transformed toward more thermodynamically stable product **3b**.[11] At this point, the single-crystal-to-single-crystal transformation is unconcerned because the structural conversion phenomenon occurred only when the crystals of **3a** were stored in the mother liquor.

(b) $[\{Ni(H_2O)_4\}_3\{Co_2Au_3(\text{D-pen-}N,S)_6\}_2]$ (3b).

The crystal **3b** was successfully obtained in the form of water-insoluble purple needle crystals from a structural conversion of crystal **3a**. The formation of **3b** occurred after crystal **3a** was continuously stored in the mother liquor for several days in a closed vessel. When the storing time reached 9 days, a change in crystal shape was clearly observed. The purple needle crystals of **3b** which are almost insoluble in water appeared instead of the purple hexagonal block crystals of **3a**. The diffuse reflection and solid state CD spectra of **3b** are essentially similar to those of $Na_3[1]$, indicating that the S-bridged pentanuclear structure of rod-shaped $[1]^{3-}$ retained in **3b**, as an anionic molecular building block (Figure II-1 and Figure II-2). X-ray fluorescence and elemental analysis data are in good agreement with the formula for a 2:3 adduct of $[1]^{3-}$ and Ni^{2+}. Additionally, the IR spectrum of **3b** illustrates an intense ν_{COO} band at 1600 cm^{-1} (Figure II-3), indicative of the fully deprotonated carboxyl

groups of D-pen in **3b**.[9]

The stability of the crystal **3b** was also investigated. The resulting purple needle crystals of **3b** were continuously stored in the mother liquor in a closed vessel for 1 month; however, no further conversion was observed. This result is reasonable because the structural conversion phenomena in this system occurred *via* a dissolution–recrystallization process. Crystal **3b** which is almost insoluble in water, thus, could not undergo a structural conversion in its aqueous mother liquor. Consequently, crystal **3b** is suggested to be more thermodynamically stable product in the metallosupramolecular system composed of rod-shaped $Co^{III}_2Au^I_3$ pentanuclear-complex anions and aqua nickel(II) cations.

(c) $[Mn(H_2O)_6]_2[\{Mn(H_2O)_4\}\{Co_2Au_3(D\text{-}pen\text{-}N,S)_6\}_2]$ (4a).

The ionic crystal **4a** was successfully produced in the form of water-soluble purple hexagonal block crystals from an aqueous solution containing $Na_3[1]$ and $Mn(OAc)_2$ in a 2:3 ratio. The crystallization of the phase-pure **4a** completed after 3 days with a yield of 39%. The diffuse reflection and the solid state CD spectra of **4a** are the same as those for $Na_3[1]$, indicating that the S-bridged pentanuclear structure of rod-shaped $[1]^{3-}$ retained in **4a**, as an anionic molecular building block (Figure II-1 and Figure II-2). The results from X-ray fluorescence and elemental analyses match well with the formula for a 2:3 adduct of $[1]^{3-}$ and Mn^{2+}. In addition, the IR spectrum of **4a** shows an intense ν_{COO} band at 1603 cm^{-1} (Figure II-3), indicative of the fully deprotonated carboxyl groups of D-pen in **4a**.[9]

To examine the stability of the ionic crystal **4a**, the resulting purple hexagonal block crystals of **4a** were stored in the mother liquor for several days in a closed vessel (Figure II-5a). Crystals of **4a** appeared after 3 days counted from when the mixing of $Na_3[1]$ and $Mn(OAc)_2$ was started, and a change in the crystal shape was clearly observed after 13 days with the appearance of purple stick crystals (**4b**) (Figure II-5b) that are insoluble in water instead of **4a**. As shown in Figure II-5c, a stepwise structural conversion was observed by PXRD measurements. The experimental PXRD pattern of the resulting crystals within a day is reminiscent of that for the previous highly porous ionic crystal, $[Co(H_2O)_6]_3[Co_2Au_3(D\text{-}pen\text{-}N,S)_6]_2$ (**2a**), demonstrated in Chapter I. This result implied that the isostructural complex with **2a** was firstly produced, proposed to be $[Mn(H_2O)_6]_3[Co_2Au_3(D\text{-}pen\text{-}N,S)_6]_2$ (**4a***), before converted to **4a**. The structural conversion to a pure phase of **4a** was completed after 3 days, and was retained for additional 6 days in its mother liquor followed by the subsequent presence of an unidentified intermediate phase,

illustrating a low crystallinity. The unidentified intermediate phase was retained for 2 days before the gradual formation of **4b**. Finally, the conversion to the pure phase of **4b** occurred after 13 days. The structural conversion from **4a*** to **4a** and to **4b** implied that both **4a*** and **4a** are kinetic and thermodynamically metastable products, respectively, whereas **4b** is more thermodynamically stable product. Unfortunately, the full crystallographic data of **4a*** could not be accomplished due to its fragile nature that is not suitable for a single-crystal X-ray diffraction experiment. Discussion on the crystal structure of **4a*** is therefore impracticable at this state. On the other hand, crystal **4a** which is more thermodynamically stable compared with **4a*** could be fully characterized by single-crystal X-ray diffraction analysis. From the crystallographic comparison of crystal **4a** and **4b** in detail, it was revealed that the connectivity between the cations and anions in **4a** has not only coordination bonds between $[Mn(H_2O)_4]^{2+}$ cations and $[\mathbf{1}]^{3-}$ anions but also the hydrogen bonds between $[Mn(H_2O)_6]^{2+}$ cations and $[\mathbf{1}]^{3-}$ anions (*vide infra*). On the contrary, only the coordination bonds between $[Mn(H_2O)_4]^{2+}$ cations and $[\mathbf{1}]^{3-}$ anions are involved in **4b**. Thus, the thermodynamically metastable product **4a** is reasonably converted to the more thermodynamically stable product **4b** through the replacement of hydrogen bonds by coordination bonds that have a greater binding energy.[10] Similar to the previously structural conversion from **3a** to **3b**, the observed conversion from **4a*** to **4b** *via* **4a** could also be explained by the dissolution–recrystallization process allowing the kinetic and the thermodynamically metastable products of **4a*** and **4a**, respectively, were transformed to more thermodynamically stable product of **4b**.[11] The single-crystal-to-single-crystal transformation is not concerned because the structural conversion phenomenon occurred only when the crystals of **4a*** and **4a** were stored in the mother liquor.

(d) [{Mn(H₂O)₄}{Co₂Au₃(D-Hpen-*N,S*)(D-pen-*N,S*)₅}] (4b).

The crystal **4b** was successfully obtained in the form of water-insoluble purple stick crystals from the structural conversion of crystal **4a**. The production of **4b** occurred after crystal **4a** was continuously stored in the mother liquor for several days in a closed vessel. When the storing time reached to 13 days, the change in crystal shape was clearly observed, resulting in the purple stick crystals of **4b** instead of the purple hexagonal block crystals of **4a**. The diffuse reflection and solid state CD spectra of **4b** are essentially similar to those of Na₃[**1**], indicating that the S-bridged pentanuclear structure of rod-shaped $[\mathbf{1}]^{3-}$ still retained in **4b**, as an anionic molecular building block (Figure II-1 and Figure II-2). In the IR spectrum,

4b illustrates an intense C=O stretching band at 1609 cm^{-1} with the shoulder at 1717 cm^{-1}. The former and the latter correspond to the deprotonated COO$^-$ and protonated COOH groups, indicative of the partial protonation of carboxylate groups in **4b** (Figure II-3).[9] From the observed results, together with the X-ray fluorescence analysis, showing the existence of Mn, Co and Au, and the elemental analysis data, it could be expected that **4b** contains a 1:1 adduct of the monoprotonated form of Co$^{III}_2$Au$^I_3$ pentanuclear-complex anion ([Co$_2$Au$_3$(D-Hpen-*N,S*)(D-pen-*N,S*)$_5$]$^{2-}$; [H**1**]$^{2-}$) and Mn^{2+}, in which one of six D-pen carboxyl groups was protonated.

The stability of the crystal **4b** was also investigated. The obtained purple stick crystals of **4b** were continuously stored in the mother liquor in a closed vessel for 1 month; however, no further conversion was observed by PXRD investigation. The observed result is reasonable since the structural conversion phenomena in this studied system occurred *via* a dissolution–recrystallization process. Crystal **4b** which is insoluble in water thus could not undergo a conversion in its aqueous mother liquor. As a result, crystal **4b** is indicated to be the most thermodynamically stable product in this metallosupramolecular system, containing rod-shaped Co$^{III}_2$Au$^I_3$ pentanuclear-complex anions and aqua manganese(II) cations.

II-3-2. Crystal structures.

(a) [Ni(H$_2$O)$_6$]$_2$[{Ni(H$_2$O)$_4$}{Co$_2$Au$_3$(D-pen-*N,S*)$_6$}$_2$] (3a).

The crystal structure of **3a** was determined by single-crystal X-ray analysis. Crystal **3a** contains *trans*-[Ni(H$_2$O)$_4$]$^{2+}$ cations, each of which connects two [**1**]$^{3-}$ anions, and isolated [Ni(H$_2$O)$_6$]$^{2+}$ cations, in addition to the water molecules of crystallization (Figure II-6). A part of [Ni(H$_2$O)$_6$]$^{2+}$ cations in **3a** could not be modeled in the crystal structure, presumably due to the severe disorder in the large void space. In **3a**, the [**1**]$^{3-}$ anions make NH$_2$···OOC hydrogen bonds connected to each other (av. N···O = 2.93 Å), thus forming a six-fold helix with right handedness along the *c* axis. Additionally, the two helices are bridged through coordination bonds between *trans*-[Ni(H$_2$O)$_4$]$^{2+}$ cations and [**1**]$^{3-}$ anions (av. Ni–OOC = 2.16 Å), resulting in a double helix structure with a large 1D pore with a diameter of *ca.* 18 Å (Figure II-7). The double helices are further connected by [**1**]$^{3-}$ anions through NH$_2$···OOC hydrogen bonds (av. N···O = 2.93 Å) (Figure II-8), completing a 1D channel structure with a porosity of *ca.* 60%, based on the calculation with PLATON.[12] This 1D channel structure is sustained by the isolated [Ni(H$_2$O)$_6$]$^{2+}$ cations, each of which is hydrogen-bonded to two [**1**]$^{3-}$ anions in the

double helix and one [1]$^{3-}$ anion that connects the double helix (av. O$\cdots$O = 2.73 Å). Similar to the previous porous ionic crystal, [Co(H$_2$O)$_6$]$_2$[{Co(H$_2$O)$_4$}{Co$_2$Au$_3$(D-pen-*N,S*)$_6$}$_2$] (**2b**), demonstrated in Chapter I, the [1]$^{3-}$ anion is hydrogen-bonded with two [Ni(H$_2$O)$_6$]$^{2+}$ cations in addition to another *trans*-[Ni(H$_2$O)$_4$]$^{2+}$ cation through coordination bond, while each [Ni(H$_2$O)$_6$]$^{2+}$ cation is surrounded by three [1]$^{3-}$ anions (Figure II-9) through only H-bonds. Moreover, the overall packing structure of **3a** is reminiscent of that of **2b**. Crystal **3a** thus presents the isostructure with crystal **2b**.

(b) [{Ni(H$_2$O)$_4$}$_3${Co$_2$Au$_3$(D-pen-*N,S*)$_6$}$_2$] (3b).

The crystal structure of **3b** was also determined by single-crystal X-ray analysis. Crystal **3b** does not have the isolated [Ni(H$_2$O)$_6$]$^{2+}$ cations, but contains the *cis*- and *trans*-[Ni(H$_2$O)$_4$]$^{2+}$ cations that are directly bound to [1]$^{3-}$ anions (Figure II-10). The [1]$^{3-}$ anion is connected with four [Ni(H$_2$O)$_4$]$^{2+}$ cations through coordination bonds in addition to another [Ni(H$_2$O)$_4$]$^{2+}$ cation which is located nearby through OH$_2$$\cdots$OOC hydrogen bonds (av. O$\cdots$O = 2.69 Å). In **3b**, the [1]$^{3-}$ anions are alternately connected by the *cis*-[Ni(H$_2$O)$_4$]$^{2+}$ cations through coordination bonds (av. Ni–OOC = 2.01 Å), forming a 2-fold helix along the *b* axis. Furthermore, the two helices are connected to each other through OH$_2$$\cdots$OOC hydrogen bonds (av. O$\cdots$O = 2.73 Å), thus forming a right-handed double helix structure (Figure II-11 and Figure II-12). The double helices are connected by the *trans*-[Ni(H$_2$O)$_4$]$^{2+}$ cations through coordination bonds (av. Ni–OOC = 2.05 Å) in a 2D sheet-like structure. Finally, the 2D sheets are stacked through the NH$_2$$\cdots$OOC and OH$_2$$\cdots$OOC hydrogen bonds (av. N$\cdots$O = 2.95 Å, O$\cdots$O = 2.75 Å), completing a 3D dense framework (Figure II-13) with a low porosity of *ca.* 30%, based on the calculation with PLATON.[12] In addition, overall packing structure of **3b** is essentially similar to that of the previous dense framework, [{Co(H$_2$O)$_4$}$_3${Co$_2$Au$_3$(D-pen-*N,S*)$_6$}$_2$] (**2c**), demonstrated in Chapter I. Thus, crystal **3b** illustrates the isostructure with crystal **2c**.

(c) [Mn(H$_2$O)$_6$]$_2$[{Mn(H$_2$O)$_4$}{Co$_2$Au$_3$(D-pen-*N,S*)$_6$}$_2$] (4a).

The crystal structure of **4a** was studied by single-crystal X-ray analysis. Similar to crystal **3a** that was discussed previously in this chapter, crystal **4a** also contains *trans*-[Mn(H$_2$O)$_4$]$^{2+}$ cations, each of which connects two [1]$^{3-}$ anions, and isolated [Mn(H$_2$O)$_6$]$^{2+}$ cations, in addition to the water molecules of crystallization (Figure II-14). A part of [Mn(H$_2$O)$_6$]$^{2+}$ cations in **4a** could not be modeled in the crystal structure, presumably due to the severe

disorder in the large void space. In **4a**, the [**1**]$^{3-}$ anions are hydrogen-bonded to each other (av. N···O = 2.92 Å), resulting in a six-fold helix with right handedness along the *c* axis. Additionally, the two helices are bridged by the *trans*-[Mn(H$_2$O)$_4$]$^{2+}$ cations through coordination bonds (av. Mn–OOC = 2.10 Å), resulting in a double helix structure with a large 1D pore with a diameter of *ca.* 18 Å (Figure II-15). The double helices are further connected by [**1**]$^{3-}$ anions through NH$_2$···OOC hydrogen bonds (av. N···O = 2.92 Å) (Figure II-16), leading to a 1D channel structure with a porosity of *ca.* 60%, based on the calculation with PLATON.[12] The resulting 1D channel structure is supported by the isolated [Mn(H$_2$O)$_6$]$^{2+}$ cations, each of which is hydrogen-bonded to two [**1**]$^{3-}$ anions in the double helix and one [**1**]$^{3-}$ anion that connects the double helix (av. O···O = 2.71 Å). Each [Mn(H$_2$O)$_6$]$^{2+}$ cation is surrounded by three [**1**]$^{3-}$ anions (Figure II-17) which is similar to those in the previously mentioned porous ionic crystals **2b** and **3a**, demonstrated in Chapter I and this chapter, respectively. It could be revealed that the overall packing structure in **4a** is also reminiscent of those in **2b** and **3a**. Consequently, crystal **4a** presents the isostructure with both crystals **2b** and **3a**.

(d) [{Mn(H$_2$O)$_4$}{Co$_2$Au$_3$(D-Hpen-*N,S*)(D-pen-*N,S*)$_5$}] (4b).

The crystal structure of **4b** was also studied by single-crystal X-ray diffraction analysis. In addition to the water molecules of crystallization, crystal **4b** contains the *cis*-[Mn(H$_2$O)$_4$]$^{2+}$ cations that are directly bound to the rod-shaped [H**1**]$^{2-}$ anions (Figure II-18). In this context, it should be noted that the partial protonation of D-pen carboxyl groups observed in **4b**, [H**1**]$^{2-}$, did not cause a change in the conformation of Co$^{III}_2$Au$^I_3$ pentanuclear-complex anion. In **4b**, the [H**1**]$^{2-}$ anions are alternately connected by the *cis*-[Mn(H$_2$O)$_4$]$^{2+}$ cations through coordination bonds (av. Mn–OOC = 2.08 Å), forming a 2-fold helix along the crystallographic *a* axis. Additionally, the two helices are intertwined and connected to each other through OH$_2$···OOC hydrogen bonds (av. O···O = 2.69 Å), thus forming a right-handed double helix structure (Figure II-19 and Figure II-20). Each double helix makes hydrogen bonds to each other through COOH···OOC intermolecular hydrogen-bonding interactions (av. O···O = 2.88 Å) *via* the protonated D-pen carboxyl groups to form a 2D sheet-like structure (Figure II-21). Finally, the 2D sheets are stacked through the NH$_2$···OOC hydrogen bonds (av. N···O = 2.99 Å), completing a 3D dense framework (Figure II-22). The crystal porosity of **4b** without including the water molecules of crystallization was estimated to be *ca.* 13%, based on the calculation with PLATON.[12]

II-3-3. Sorption behavior.

The gas and vapor adsorption behaviors were investigated for all obtained metallosupramolecular frameworks (**3a**, **3b**, **4a**, and **4b**) (Table II-3). As shown in Figure II-23, the CO_2 adsorption isotherm for **3a** at 195 K displayed a type-I physical sorption isotherm illustrating a gradual increase and reached the amounts of 17.1 cm^3 g^{-1} at $P/P_0 =$ 0.96 with a calculated BET surface area of 50 m^2 g^{-1}. A similar CO_2 adsorption isotherm was observed for **3b**, but the adsorption amounts apparently decreased with the saturated amounts of only 2.5 cm^3 g^{-1} at $P/P_0 = 0.97$, corresponding to its lower porosity. The BET surface area calculated from the CO_2 sorption isotherm was also significantly decreased to a small amount of 5.4 m^2 g^{-1}. Remarkably, the adsorption capacities of N_2 gas for **3a** and **3b** (Figure II-24 and Figure II-25) are all poor at 77 K (<2.0 cm^3 g^{-1}). In addition, the adsorption characteristics of **3a** and **3b** toward small molecules were also studied. The adsorption isotherms for H_2O, EtOH, and acetone vapors were measured at 298 K. As shown in Figure II-26, a high H_2O adsorption capacity was observed for **3a** with a value of 34 mol mol^{-1} at $P/P_0 = 0.92$. A clear hysteresis loop was observed in an adsorption–desorption cycle for **3a**, indicative of the strong host-guest interactions accompanied by a structural transformation during the adsorption process.[13] The amount of adsorbed H_2O significantly decreased (11 mol mol^{-1} at $P/P_0 = 0.92$) for **3b** without a presence of a clear hysteresis loop because of its rigid framework with a lower porosity compared with that of **3a**. In contrast, both **3a** and **3b** showed no appreciable adsorption capability toward EtOH and acetone vapors (Figure II-27 and Figure II-28). This is attributed to the superhydrophilic character of their opening channels,[14] which are surrounded by not only the amine and carboxylate groups of D-pen but also the aqua groups in $[Ni(H_2O)_6]^{2+}$ cations. A similar superhydrophilic behavior was also observed in **2a**, **2b**, and **2c**, previously demonstrated in Chapter I. In addition, it should be noted that both isostructural pairs, **2b** & **3a** and **2c** & **3b**, displayed the similar adsorption isotherms together with the comparable adsorbed amounts for not only CO_2 gas adsorption but also H_2O vapor adsorption.

The adsorption characteristics of **4a** and **4b** were also examined. The adsorption isotherms for CO_2 and N_2 gases were measured at 195 K and 77 K, respectively. As shown in Figure II-29, the CO_2 adsorption isotherm for **4a** illustrated a type-I physical sorption isotherm showing a gradual increase and reached a saturated amounts of 32.0 cm^3 g^{-1} at P/P_0 = 0.96 with a calculated BET surface area of 77 m^2 g^{-1}. This observed value is remarkably higher than those found in **2b** (6.6 cm^3 g^{-1} at $P/P_0 = 0.95$) and **3a** (17.1 cm^3 g^{-1} at $P/P_0 =$

0.96), even though all of them (**2b**, **3a**, and **4a**) are isostructures. At this point, the stability of the frameworks after treated by heating under vacuum should be related. The PXRD results clearly showed that the stability of **4a** is different from those of **2b** and **3a** (Figure II-30). Crystal **4a** could retain its crystallinity after heating at 120°C for 2 h even though the framework partially collapsed, as demonstrated by a retention of some peaks. On the other hand, both **2b** and **3a** illustrated an amorphous phase, indicating that their frameworks completely collapsed after heating. The observed results from PXRD measurements thus support the higher stability of crystal **4a**. Furthermore, it is apparent that the CO_2 adsorption amount was much smaller for **4b** (3.2 cm^3 g^{-1} at P/P_0 = 0.96) in parallel with the decrease in its porosity. The calculated BET surface area was significantly decreased to a small amount of 4.2 m^2 g^{-1}. Similar to crystals **3a** and **3b**, both **4a** and **4b** showed the poor adsorption capacities toward N_2 gas (Figure II-31 and Figure II-32). The adsorption characteristics of **4a** and **4b** toward small molecules such as H_2O, EtOH, and, acetone were also studied. As shown in Figure II-33, an adsorption of H_2O vapor was observed for **4a** with the high amounts of 42 mol mol^{-1} at P/P_0 = 0.95 with a presence of the hysteresis loop, indicating the strong host-guest interactions during the adsorption–desorption process.[13] On the contrary, the adsorbed amount of H_2O were further decreased (6 mol mol^{-1} at P/P_0 = 0.94) for **4b** with no hysteresis loop obtained because of its rigid framework with a very low porosity. Furthermore, both of them (**4a** and **4b**) showed no preferential adsorption ability toward EtOH and acetone vapors (Figure II-34 and Figure II-35), reflecting the superhydrophilic character of their frameworks.[14]

II-3-4. Influence of aqua metal ions.

As described previously, the combination of the rod-shaped $Co^{III}_2Au^{I}_3$ pentanuclear-complex anion, $[\mathbf{1}]^{3-}$, and aqua nickel(II) cation, $[Ni(H_2O)_n]^{2+}$, firstly produced the ionic crystal **3a**, presenting the 1D channel structure with a porosity of *ca.* 60%. As shown in Figure II-4c, crystal **3a** was retained in its mother liquor for 6 days before a subsequent conversion to crystal **3b**, in which the 3D dense framework was formed together with the decrease in a porosity to *ca.* 30%. This structural conversion is reminiscent of that for **2b**, demonstrated in Chapter I. In addition to the similar structural conversion phenomena, the isostructural pairs, **2b** & **3a** and **2c** & **3b**, also displayed the similar stabilities. This is simply explained by the resemblance in their labilities and their electron configuration of $3d^7$ and $3d^8$ for Co^{2+} and Ni^{2+}, respectively.[3,15] In addition, the ionic radii of Co^{2+} (0.74 Å) and Ni^{2+} (0.69

Å) ions are quite close to each other and thus form the chemical bondings with the comparable bond strengths, in which their hydration enthalpies that are 2113 kJ mol^{-1} and 2174 kJ mol^{-1} for Co^{2+} and Ni^{2+}, respectively, do not have much difference.[3,4,15,16]

On the other hand, a different conversion was observed in the Mn complexes. Firstly, the porous ionic crystal **4a**, illustrating the isostructure with crystals **2b** and **3a**, could be produced from a combination of [**1**]$^{3-}$ anion and aqua manganese(II) cation. After crystal **4a** was continuously stored in its mother liquor for 9 days counted from a presence of phase-pure **4a**, a structural conversion to crystal **4b** was observed which was evidenced by PXRD investigation (Figure II-5c). Interestingly, crystal **4b** does not possess the similar framework to those of **2c** and **3b**. The structural conversion thus yielded the different product in this case. From the X-ray fluorescence and elemental analyses together with IR result, it was found that **4b** contains a 1:1 adduct of Mn^{2+} and [H**1**]$^{2-}$, in which one of six D-pen carboxyl groups was protonated leading to a formation of the strong intermolecular COOH···OOC hydrogen bonds which made neighboring helices much closer. Therefore, a 3D dense framework with lower porosity of *ca.* 13%, compared with those of **2c** and **3b** (*ca.* 30%), was constructed. From the conversion, this type of dense framework was not observed in Co and Ni systems even though the reaction conditions, such as pH, concentration, and temperature, were controlled to be similar to those of Mn system. The different resulting frameworks obtained from the structural conversion might arise from the differences in the nature of each metal ion. For a solvated metal ion, the rate of solvent exchange is affected by the nature of solvent together with the solvation shell of metal ion, in which the size, charge, and electron configuration are directly characterized.[3,15,16] When only water was used as a solvent in the studied systems, the manganese(II) ion is prominent by its fast rate of water exchange together with its larger ionic radius (0.83 Å) compared with those of cobalt(II) and nickel(II) ions (0.74 Å and 0.69 Å, respectively).[3,4,16] The flexible coordination sphere of Mn^{2+} owing to its rate of water exchange which is much faster than those of Co^{2+} and Ni^{2+} might not allow Mn^{2+} to construct and maintain the framework that shows the isostructure with crystals **2c** and **3b.** However, Mn^{2+} ion preferentially forms the more rigid framework with the fixed coordination sphere in order to stabilize the whole structure. In general, the framework with lower porosity tends to have higher rigidity rather than the framework with higher porosity. Consequently, crystal **4b** that illustrates the lower porosity was reasonably formed. It was revealed that each [H**1**]$^{2-}$ anion in **4b** is surrounded by six [Mn(H$_2$O)$_4$]$^{2+}$ cations which is the maximum for six carboxylate arms of one Co$^{III}_2$Au$^{I}_3$ pentanuclear-complex anion, *via* both coordination bonds

and hydrogen bonds; whereas, only five $[Ni(H_2O)_4]^{2+}$ cations were observed around $[\mathbf{1}]^{3-}$ anion in **3b**. The higher number of connectivity observed in **4b** also supports the more rigidity of its framework. In addition, the hydration enthalpy of Mn^{2+} (1841 kJ mol^{-1}) is significant lower than those of Co^{2+} (2113 kJ mol^{-1}) and Ni^{2+} (2174 kJ mol^{-1}).[16] Thus, it is easier for Mn^{2+} to replace the water molecules by D-pen carboxyl groups through coordination bonds in the structural conversion process.

II-4. Conclusion.

In this chapter, four metallosupramolecular frameworks were successfully constructed from the combination of $[Co_2Au_3(\text{D-pen-}N,S)_6]^{3-}$ ($[\mathbf{1}]^{3-}$) pentanuclear-complex anions and aqua nickel(II) or aqua manganese(II) cations. An isostructural pair of porous ionic crystals, $[Ni(H_2O)_6]_2[\{Ni(H_2O)_4\}\{Co_2Au_3(\text{D-pen-}N,S)_6\}_2]$ (**3a**) and $[Mn(H_2O)_6]_2[\{Mn(H_2O)_4\}\{Co_2Au_3(\text{D-pen-}N,S)_6\}_2]$ (**4a**), were produced before the stepwise structural conversion to the different frameworks. Crystal **3a** illustrated a similar conversion to that of $[Co(H_2O)_6]_2[Co(H_2O)_4\{Co_2Au_3(\text{D-pen-}N,S)_6\}_2]$ (**2b**), described in Chapter I, in which the dense framework of $[\{Ni(H_2O)_4\}_3\{Co_2Au_3(\text{D-pen-}N,S)_6\}_2]$ (**3b**) with a decreased porosity to *ca.* 30% was formed. Interestingly, crystal **4a** converted to the different framework of $[\{Mn(H_2O)_4\}\{Co_2Au_3(\text{D-Hpen-}N,S)(\text{D-pen-}N,S)_5\}]$ (**4b**), presenting a lower porosity of *ca.* 13%. The difference in the resulting frameworks after the structural conversion observed in Ni^{II} and Mn^{II} systems are related to the differences in the nature of metal ions. The flexible coordination sphere of Mn^{2+} owing to the rapid rate of water exchange makes Mn^{2+} to form a more rigid framework in order to stabilize the whole structure. In addition, the selective adsorptions of H_2O and CO_2 were observed for all obtained metallosupramolecular frameworks (**3a**, **3b**, **4a**, and **4b**), reflecting their superhydrophilic characteristics.

II-5. References.

[1] (a) L. H. Gade, *Angew. Chem., Int. Ed.* **2000**, *39*, 2658-2678. (b) E. J. L. McInnes, S. Piligkos, G. A. Timco, R. E. P. Winpenny, *Coord. Chem. Rev.* **2005**, *249*, 2577-2590. (c) H. Li, T. J. Marks, *Proc. Natl. Acad. Sci. U. S. A.* **2006**, *103*, 15295-15302. (d) M. D. Ward, *Coord. Chem. Rev.* **2007**, *251*, 1663-1677. (e) H. Hofneier, U. S. Schubert, *Chem. Soc. Rev.* **2004**, *33*, 373-399. (f) C. F. Yocum, *Coord. Chem. Rev.* **2008**, *252*, 296-305. (g) Y.-G. Huang, F.-L. Jiang, M.-C. Hong, *Coord. Chem. Rev.* **2009**, *253*, 2814-2834. (h)

T. Nabeshima, *Bull. Chem. Soc. Jpn.* **2010**, *83*, 969-991.

[2] (a) O. M. Yaghi, H. Li, *J. Am. Chem. Soc.* **1995**, *117*, 10401-10402. (b) J. S. Seo, D. Whang, H. Lee, S. I. Jun, J. Oh, Y. J. Jeon, K. Kim, *Nature* **2000**, *404*, 982-986. (c) O. M. Yaghi, M. O'Keeffe, N. W. Ockwig, H. K. Chae, M. Eddaoudi, J. Kim, *Nature* **2003**, *423*, 705-714. (d) O. Delgado-Friedrichs, M. O'Keeffe, O. M. Yaghi, *Phys. Chem. Chem. Phys.* **2007**, *9*, 1035-1043. (e) J. J. Perry IV, J. A. Perman, M. J. Zaworotko, *Chem. Soc. Rev.* **2009**, *38*, 1400-1417. (f) D. J. Tranchemontagne, J. L. Mendoza-Cortés, M. O'Keeffe, O. M. Yaghi, *Chem. Soc. Rev.* **2009**, *38*, 1257-1283.

[3] (a) F. Basolo, R. C. Johnson, *Coordination Chemisry; the Chemistry of Metal Complexes*, Benjamin, NY, **1964**. (b) D. F. Shriver, P. W. Atkins, *Inorganic Chemistry* (Third edition), Oxford University Press, **1999**.

[4] R. J. Deeth, *Coord. Chem. Rev.* **2001**, *212*, 11-34.

[5] (a) G. M. Sheldrick, *Acta Cryst.* **2008**, *A64*, 112-122. (b) G. M. Sheldrick, *Acta Cryst.* **2015**, *C71*, 3-8.

[6] C. Kabuto, S. Akine, T. Nemoto, E. Kwon, *Nihon Kessho Gakkaishi* **2009**, *51*, 218-224.

[7] A. L. Spek, *Acta Cryst.* **2009**, *D65*, 148-155.

[8] Z. Otwinowski, W. Minor, *Methods Enzymol.* **1997**, *276A*, 307-326.

[9] K. Nakamoto, *Infrared and Raman Spectra of Inorganic and Coordination Compounds*, Wiley, New York, **1997**.

[10] G. R. Desiraju, T. Steiner, *The Weak Hydrogen Bond in Structural Chemistry and Biology*, Oxford University Press, Oxford, **1999**.

[11] (a) R. J. Davey, P. T. Cardew, D. McEwan, D. E. Sadler, *Angew. J. Cryst. Growth* **1986**, *79*, 648-653. (b) J. W. Mullin, *Crystallization*, Butterworth, London, **1993**.

[12] A. L. Spek, *J. Appl. Cryst.* **2003**, *36*, 7-13.

[13] (a) J. Canivet, J. Bonnefoy, C. Daniel, A. Legrand, B. Coasne, D. Farrusseng, *New J. Chem.* **2014**, *38*, 3102-3111. (b) J. Canivet, A. Fateeva, Y. Guo, B. Coasne, D. Farrusseng, *Chem. Soc. Rev.* **2014**, *43*, 5594-5617. (c) N. C. Burtch, H. Jasuja, K. S. Walton, *Chem. Rev.* **2014**, *114*, 10575-10612.

[14] (a) A. Nalaparaju, X. S. Zhao, J. W. Jiang, *J. Phys. Chem. C* **2010**, *114*, 11542-11550. (b) R. Plessius, R. Kromhout, A. L. D. Ramos, M. Ferbinteanu, M. C. Mittelmeijer-Hazeleger, R. Krishna, G. Ronthenberg, S. Tananse, *Chem. Eur. J.* **2014**, *20*, 7922-7925. (c) J. J. Gutiérrez-Sevillano, S. Calero, R. Krishna, *J. Phys. Chem. C* **2015**, *119*, 3658-3666.

[15] (a) R. Janes, E. A. Moore, *Metal-ligand bonding*, Cambridge, Royal Society of Chemistry, **2004**. (b) S. S. Zumdahl, D. J. DeCoste, *Chemical Principles* (Fifth edition), Houghton Mifflin Company, **2005**.

[16] (a) L. Dadci, H. Elias, U. Frey, A. Hoernig, U. Koelle, A. E. Merbach, H. Paulus, J. S. Schneider, *Inorg. Chem.* **1995**, *34*, 306-315. (b) D. R. Lide, *CRC handbook of Chemistry and Physics* (Eighty edition), CRC press, Boca Raton, **2000**.
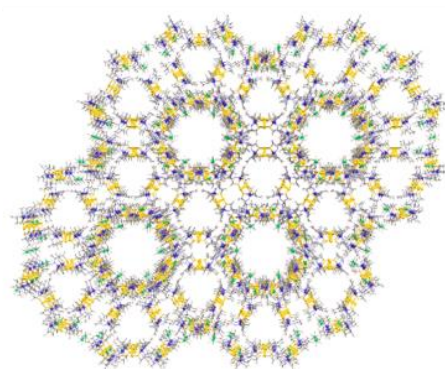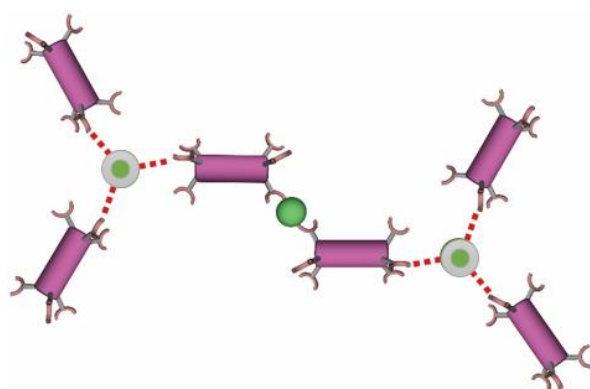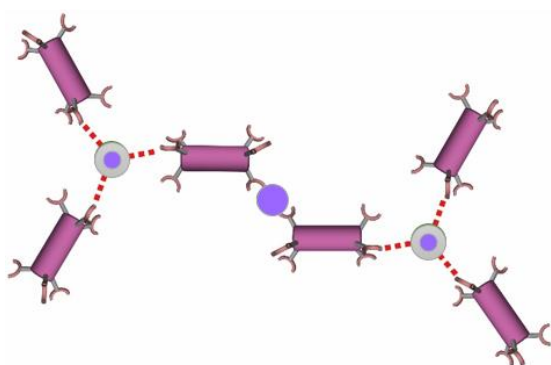
3a (porosity *ca.* 60%)
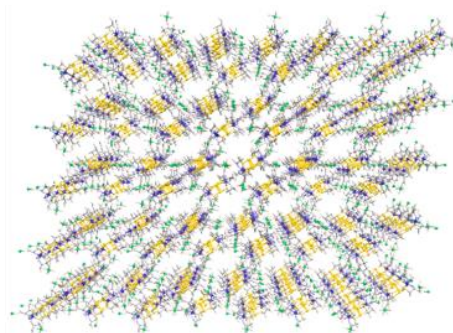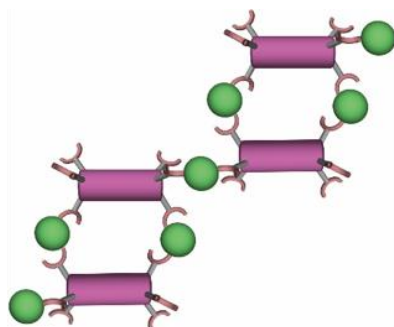
3b (porosity *ca.* 30%)

$[Co_2Au_3(D\text{-pen-}N,S)_6]^{3-}$ ($[\mathbf{1}]^{3-}$)

$[Ni(H_2O)_6]^{2+}$

$[Ni(H_2O)_4]^{2+}$
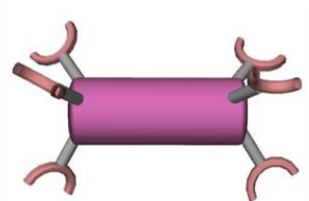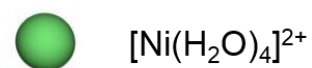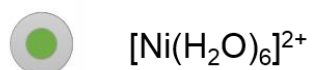
Scheme II-1. Structural conversion from the porous framework of **3a** to the dense framework of **3b**. Dashed lines indicate hydrogen bonds.
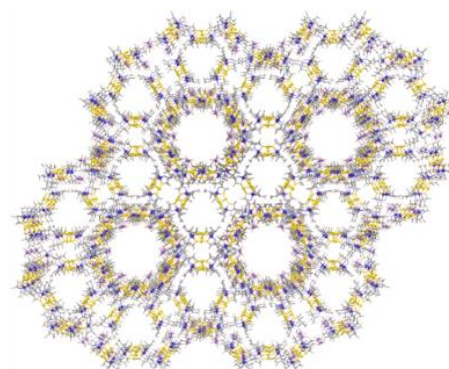
4a (porosity *ca.* 60%)
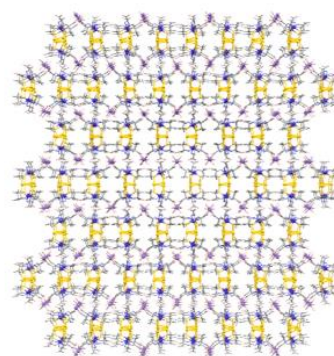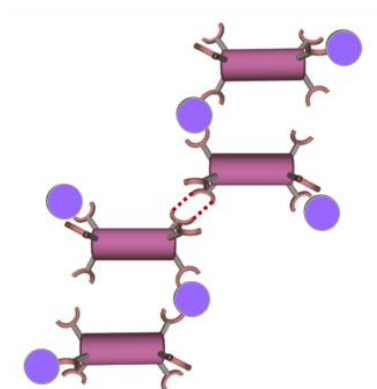
4b (porosity *ca.* 13%)

$[Co_2Au_3(\text{D-pen-}N,S)_6]^{3-}$ ($[\mathbf{1}]^{3-}$)

$[Mn(H_2O)_6]^{2+}$

$[Mn(H_2O)_4]^{2+}$
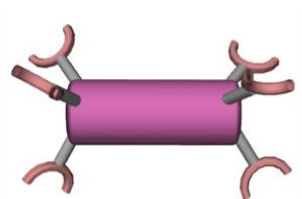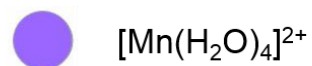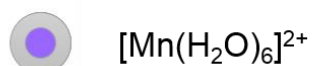
Scheme II-2. Structural conversion from the porous framework of **4a** to the dense framework of **4b**. Dashed lines indicate hydrogen bonds.
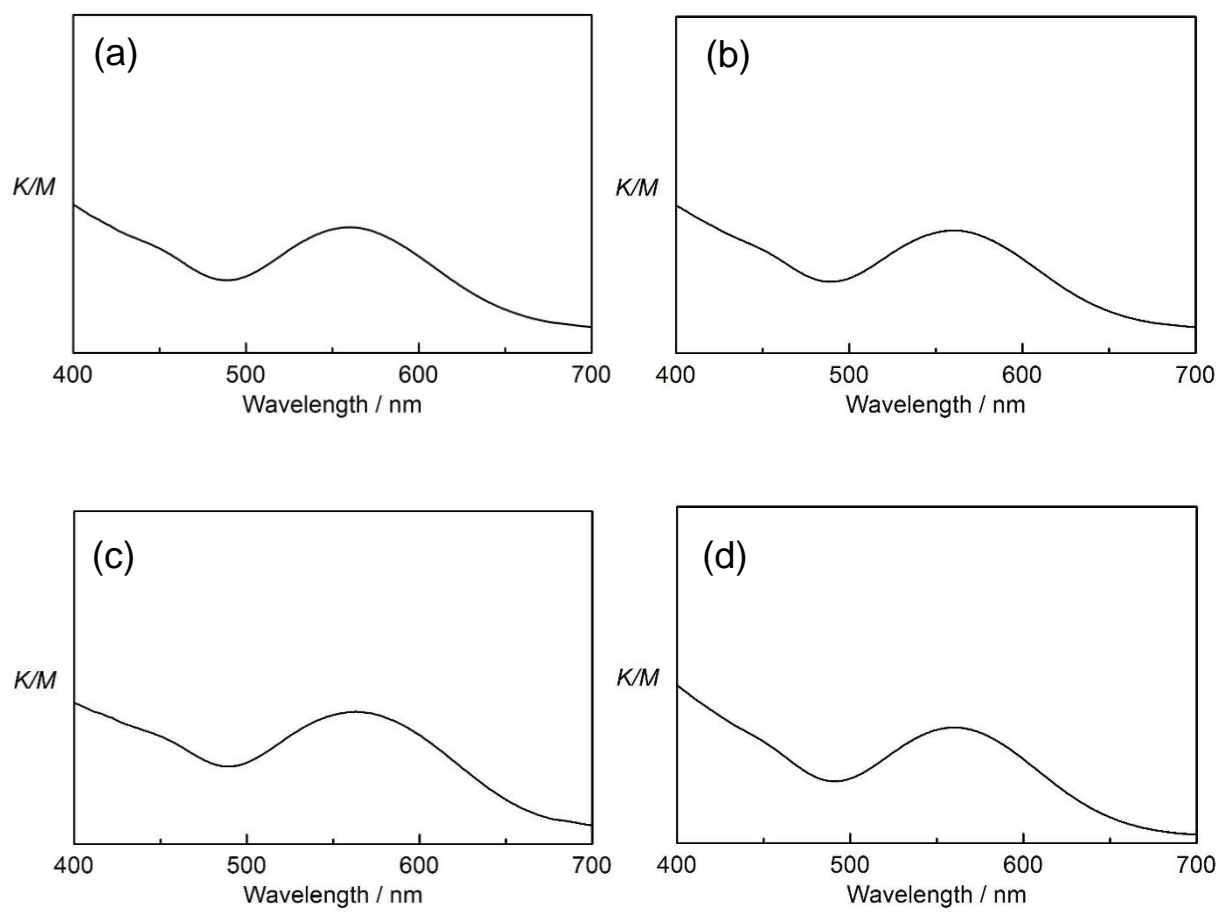
Figure II-1. Diffuse reflection spectra of (a) **3a**, (b) **3b**, (c) **4a**, and (d) **4b**.
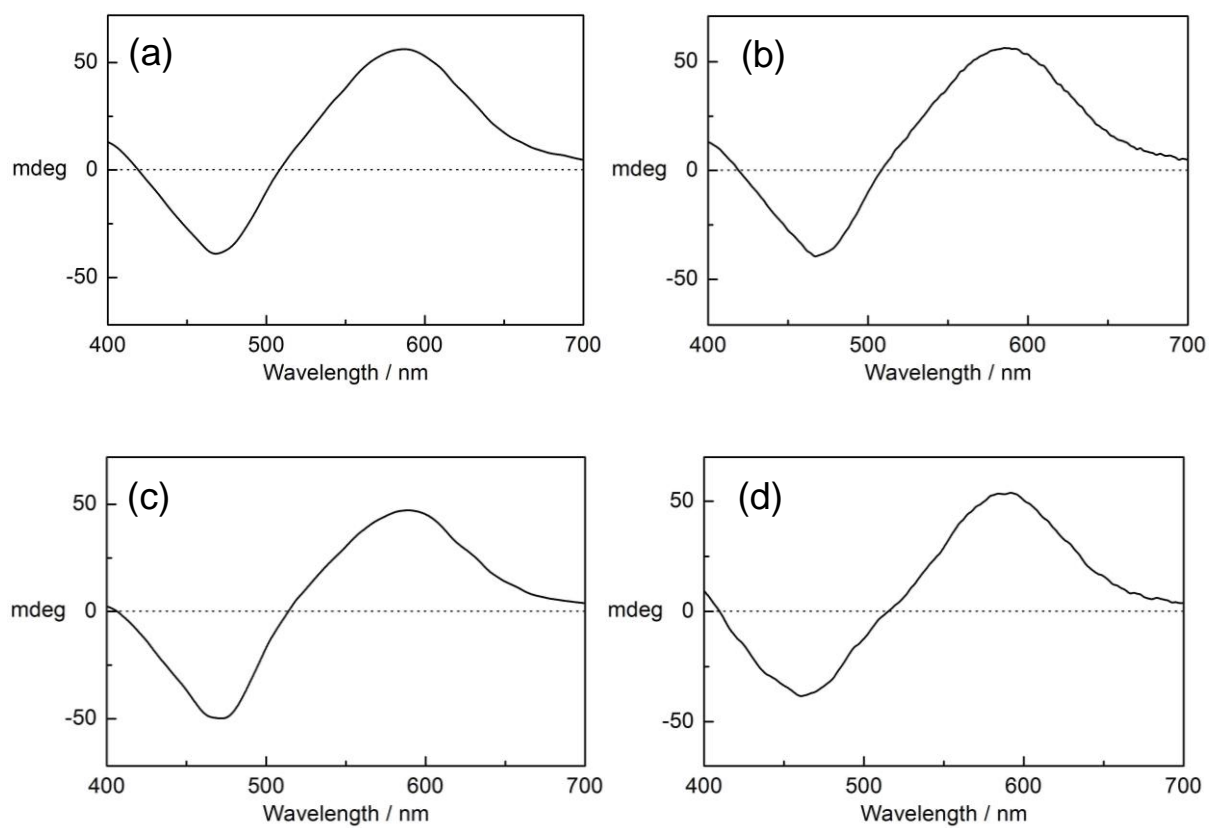
Figure II-2. Solid state CD spectra of (a) **3a**, (b) **3b**, (c) **4a**, and (d) **4b**.
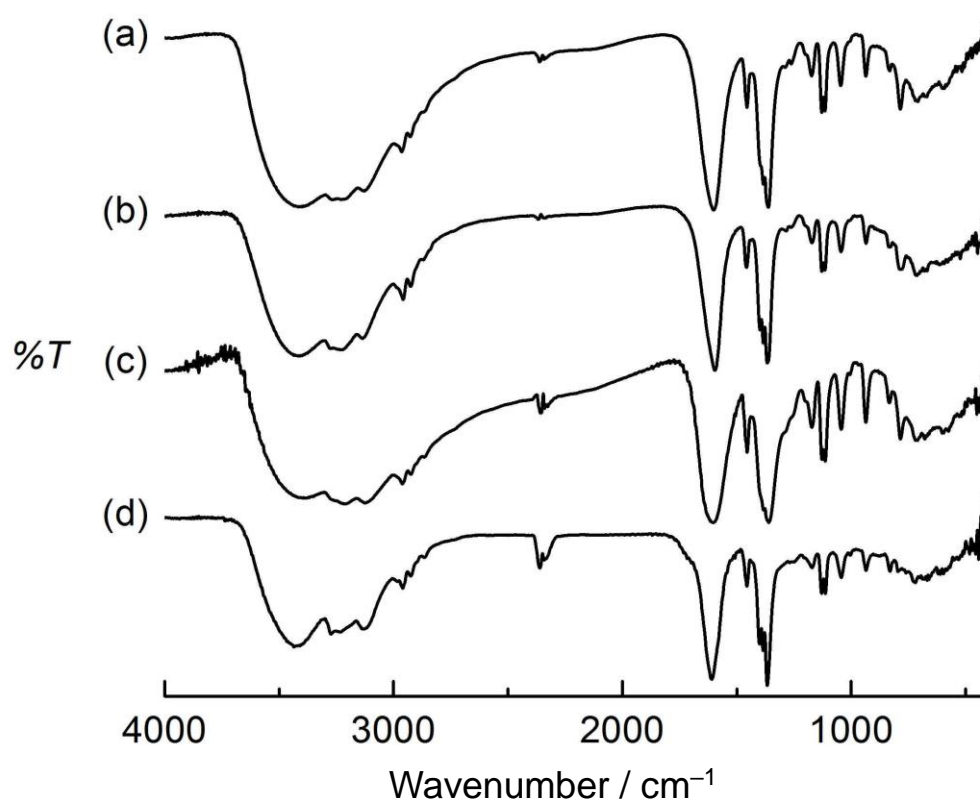
Figure II-3. IR spectra of (a) **3a**, (b) **3b**, (c) **4a**, and (d) **4b**.
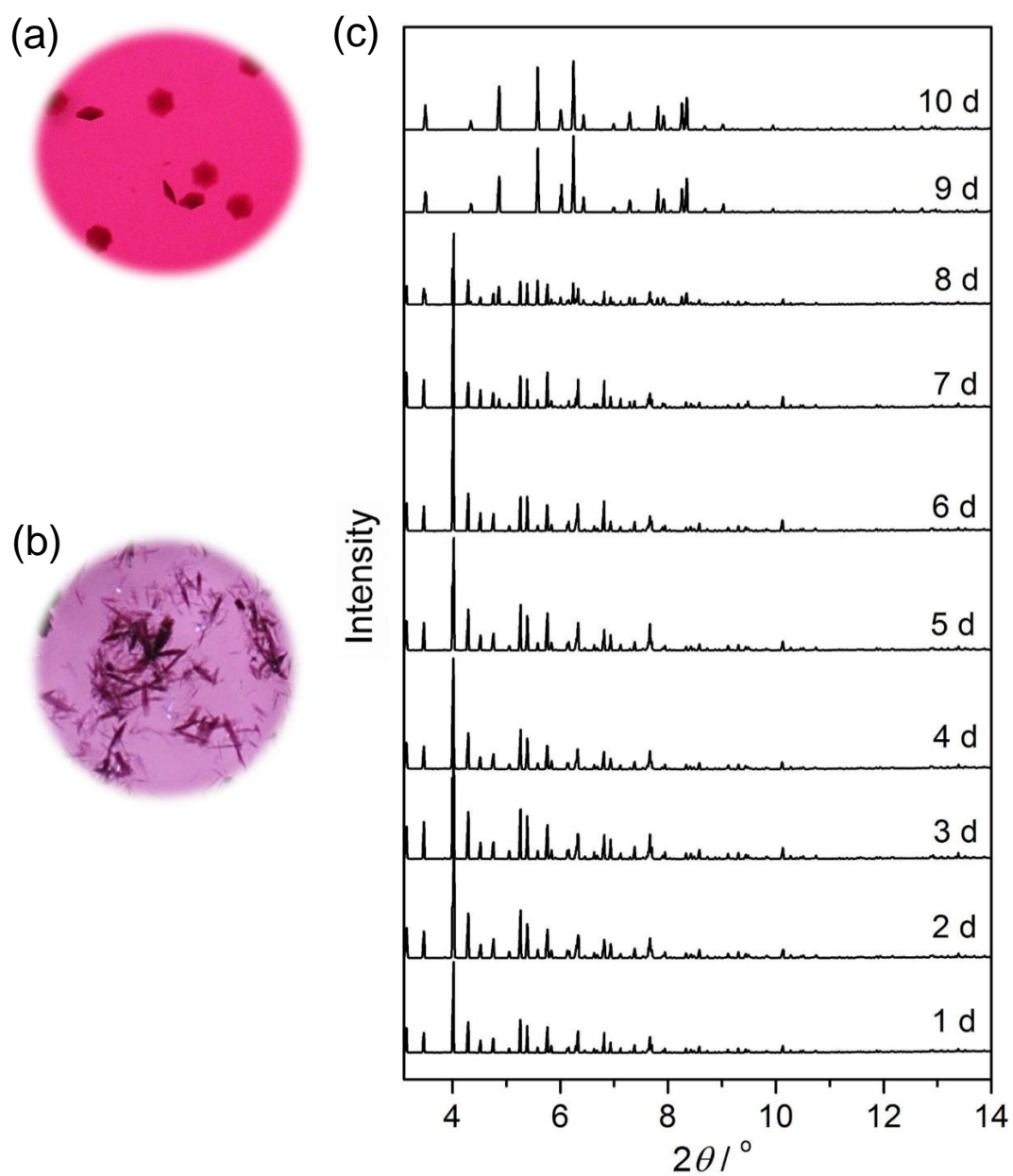
Figure II-4. Images of crystals (a) **3a** and (b) **3b**. (c) PXRD patterns showing structural conversion of **3a** in its mother liquor. Patterns observed at 7 and 8 days matched well with the mixture of **3a** and **3b**.
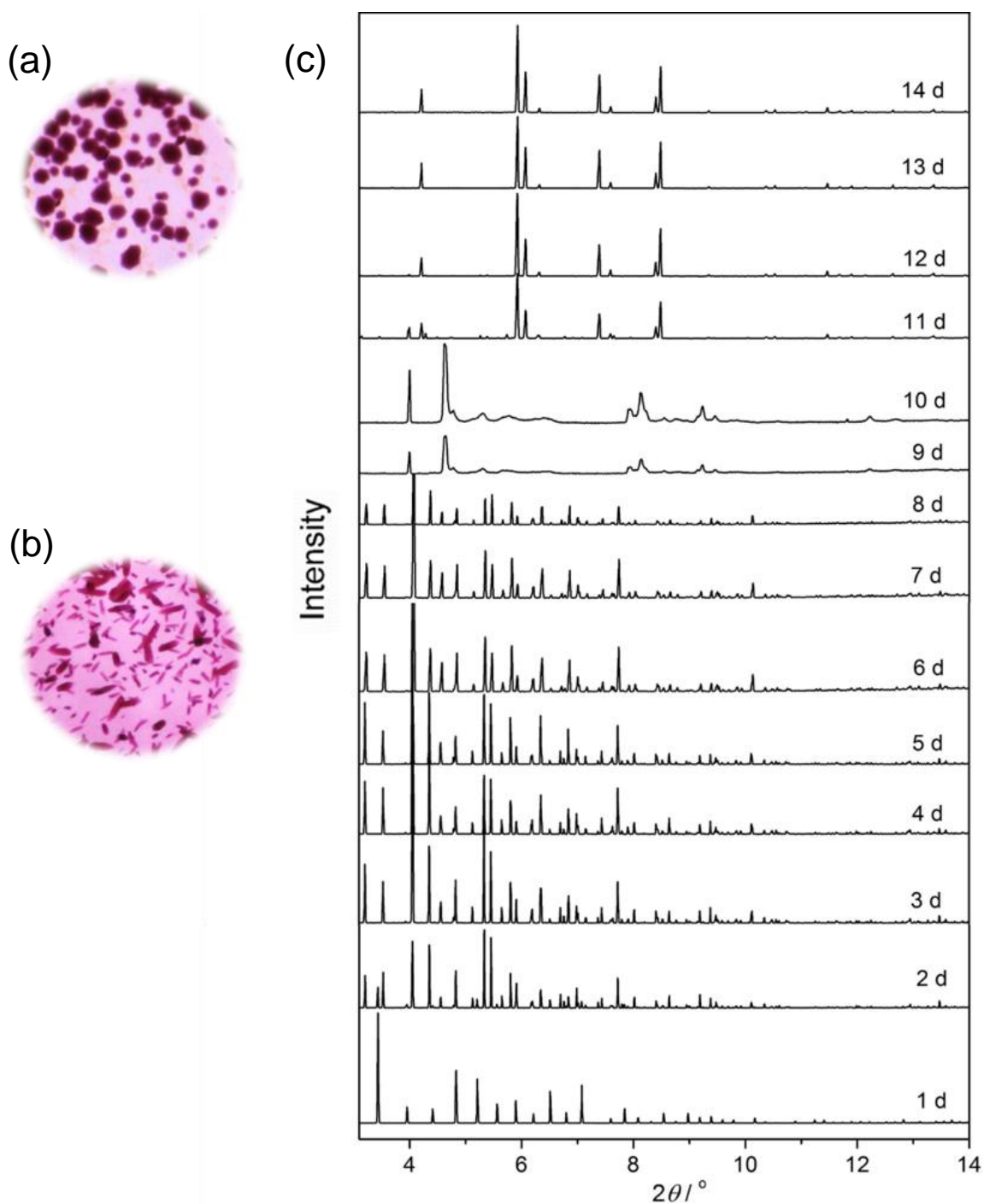
Figure II-5. Images of crystals (a) **4a** and (b) **4b**. (c) PXRD patterns showing structural conversion of **4a** in its mother liquor. Patterns observed at 2 and 11 days matched with the mixture of **4a*** & **4a** and unidentified phase & **4b**, respectively.
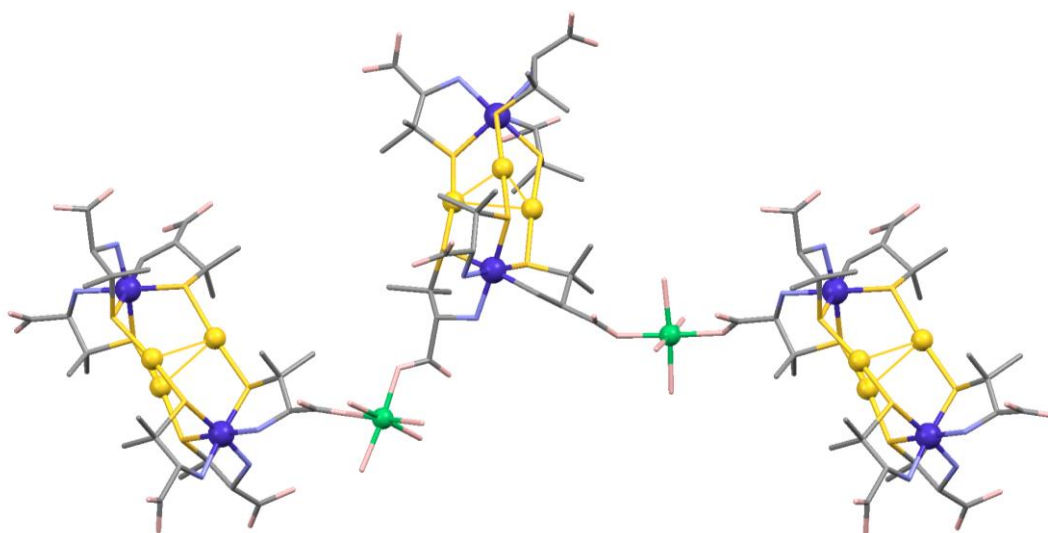
67
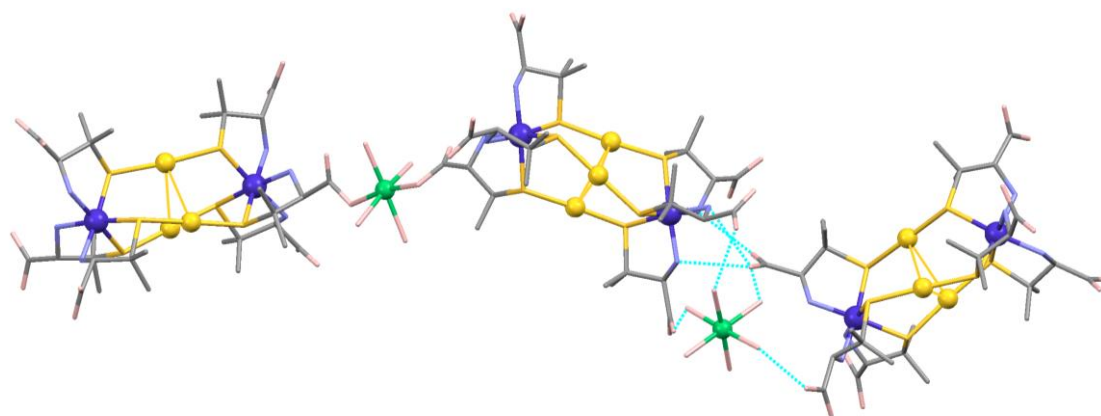
Figure II-6. A perspective view of the expanded asymmetric unit in **3a**. Color codes: Ni, green; Co, purple; Au, gold; S, yellow; O, pink; N, blue; C, gray. Dashed lines indicate hydrogen bonds.
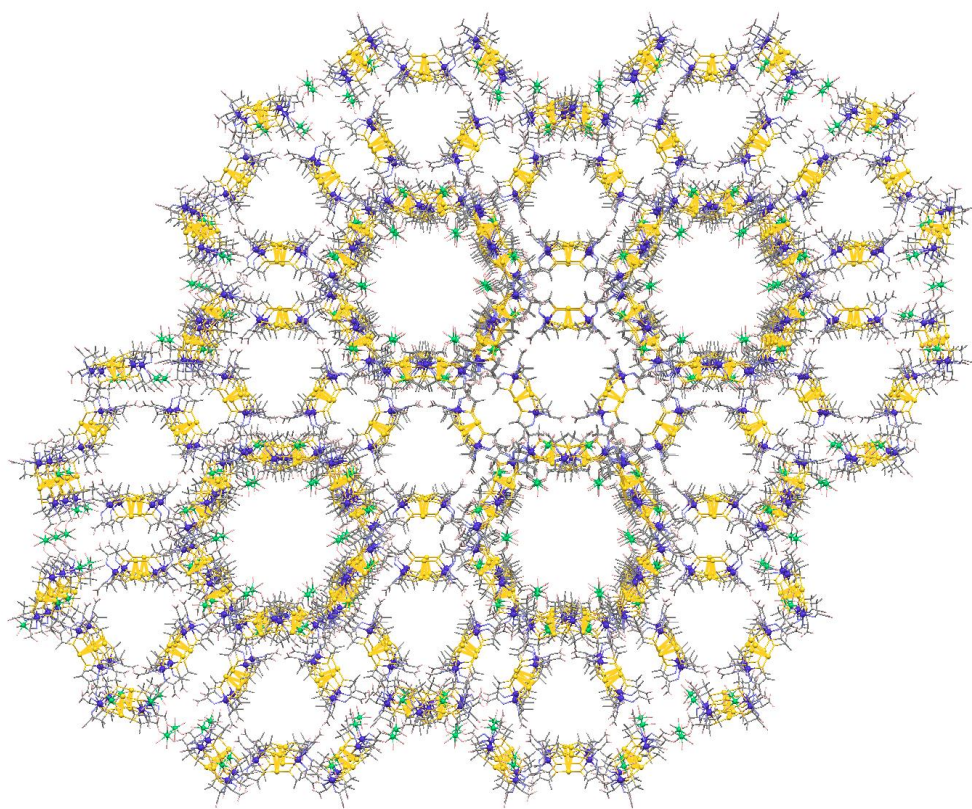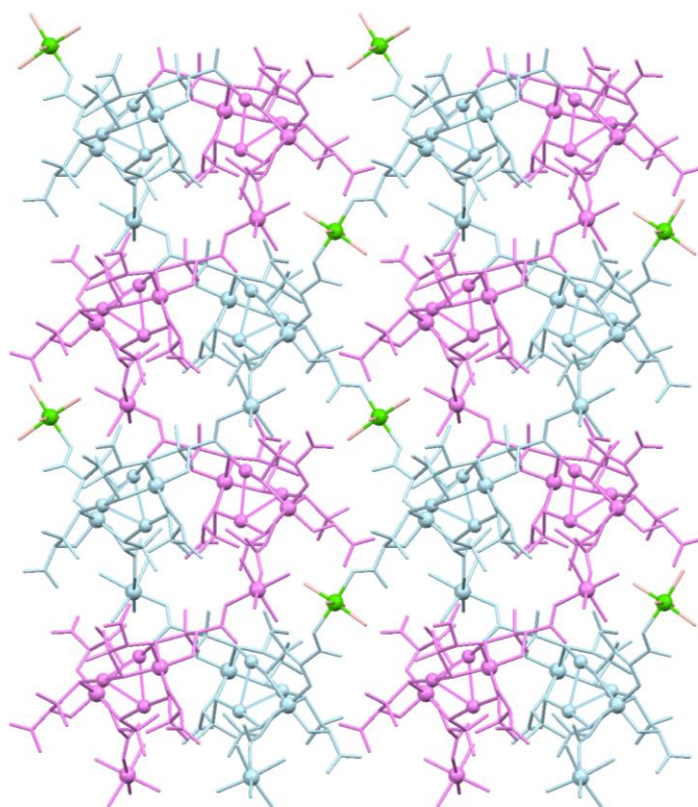
Figure II-7. A perspective view of a 1D channel structure in **3a**.
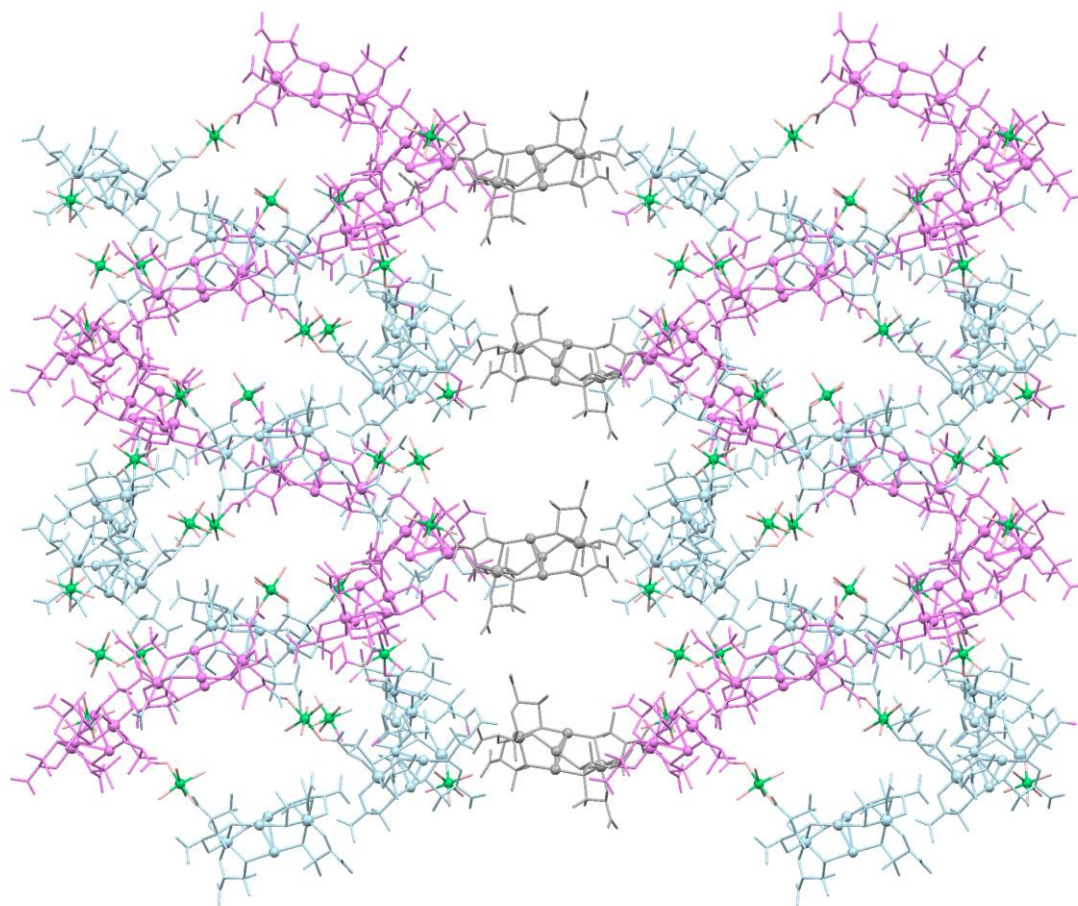
Figure II-8. A perspective view of two double helices (pink and light blue) connected by [**1**]$^{3-}$ anions (gray) in **3a**. Color codes: Ni, green; O, pink.
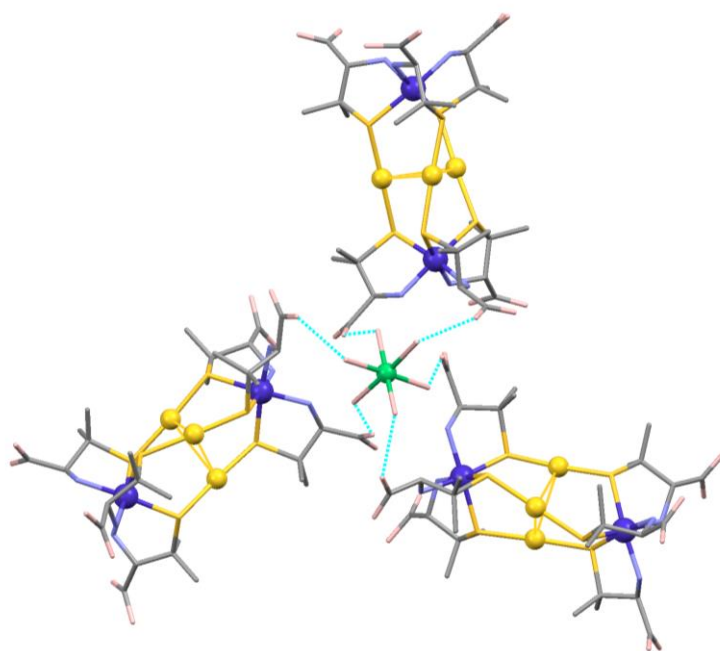
Figure II-9. A perspective view of the $[Ni(H_2O)_6]^{2+}$ cation connecting three $[\mathbf{1}]^{3-}$ anions through hydrogen bonds in **3a**. Color codes: Ni, green; Co, purple; Au, gold; S, yellow; O, pink; N, blue; C, gray. Dashed lines indicate hydrogen bonds.

Figure II-10. A perspective view of the expanded asymmetric unit in **3b**. Color codes: Ni, green; Co, purple; Au, gold; S, yellow; O, pink; N, blue; C, gray.

Figure II-11. A perspective view of two double helices (pink and light blue) connected by *trans*-[Ni(H$_2$O)$_4$]$^{2+}$ (green) cations in **3b**.
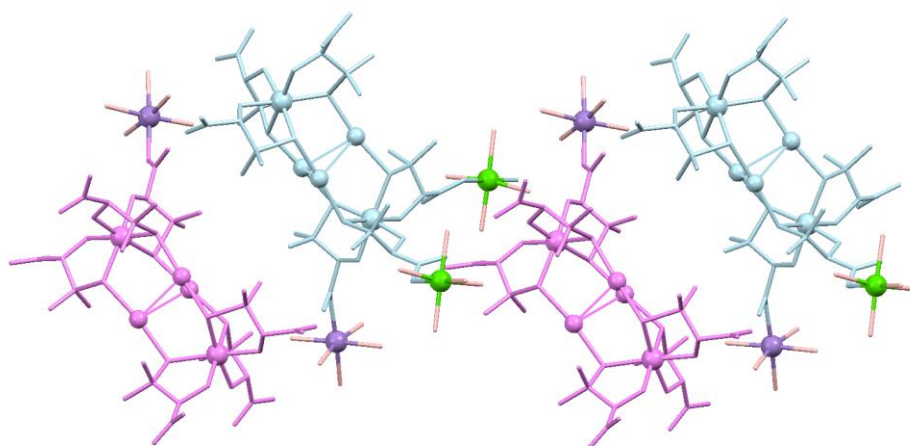
Figure II-12. Top view of the two double helices (pink and light blue) connected by *trans*-[Ni(H$_2$O)$_4$]$^{2+}$ (green) cations in **3b**.
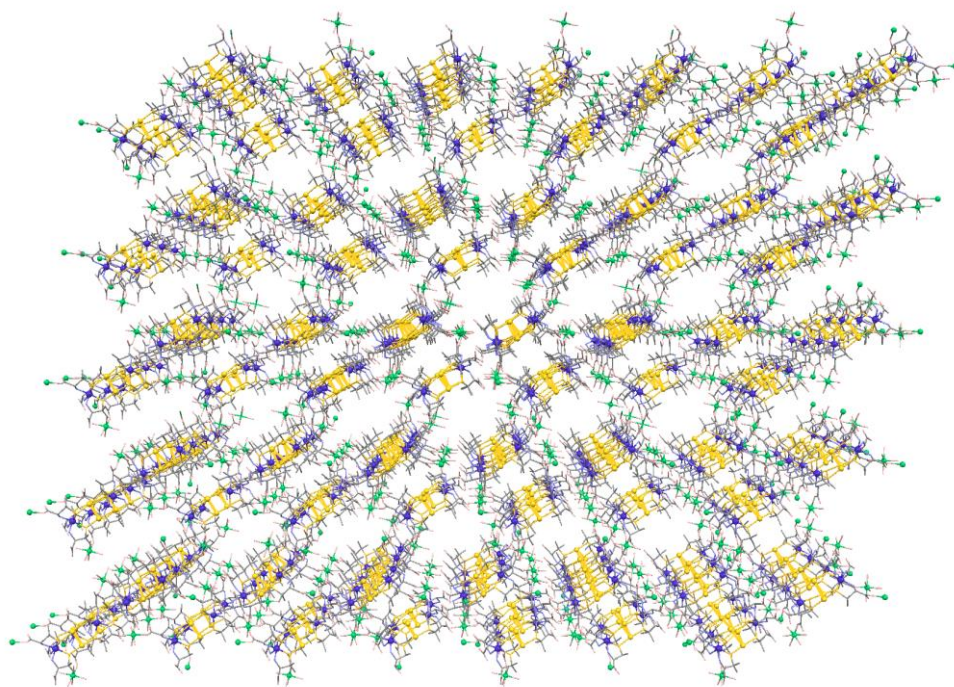
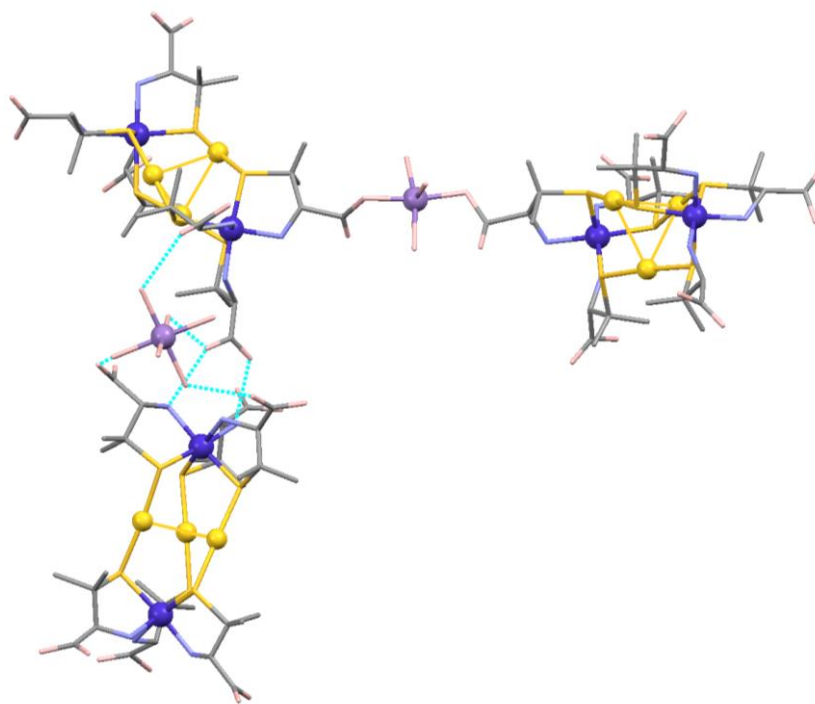**Figure II-13.** A perspective view of the 3D dense structure with 2D coordination polymers in **3b**.

Figure II-14. A perspective view of the expanded asymmetric unit in **4a**. Color codes: Mn, light purple; Co, purple; Au, gold; S, yellow; O, pink; N, blue; C, gray. Dashed lines indicate hydrogen bonds.
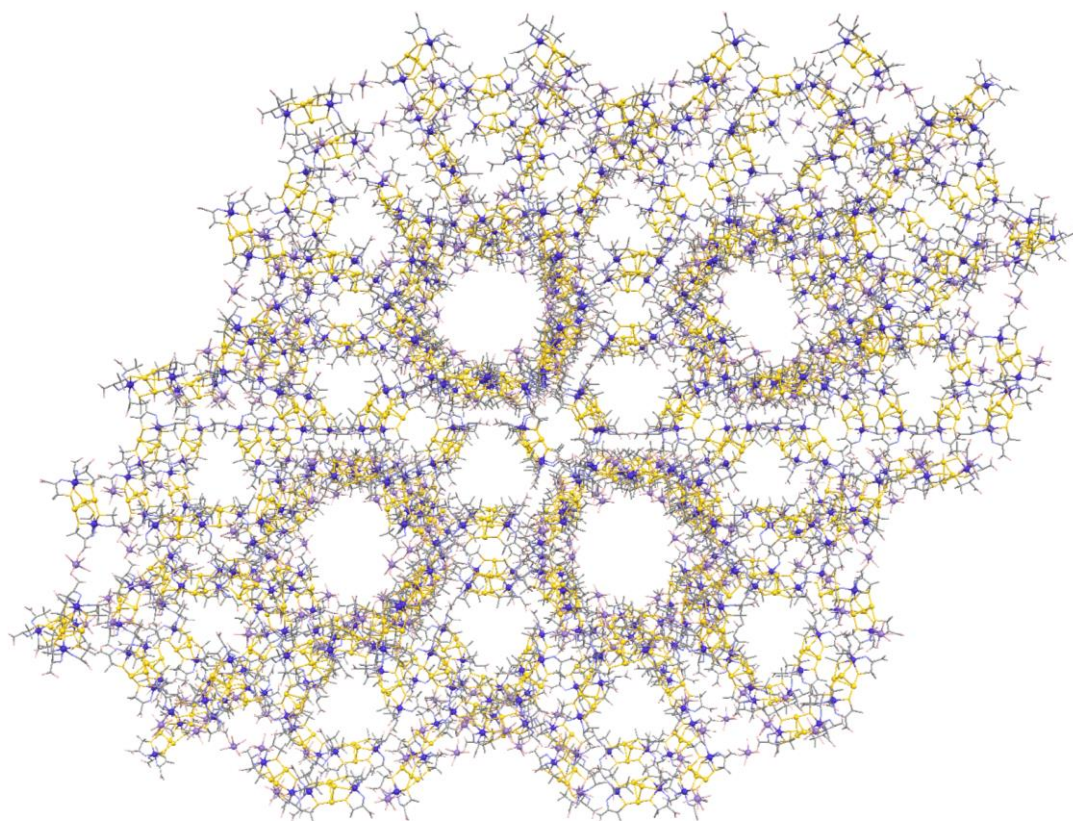
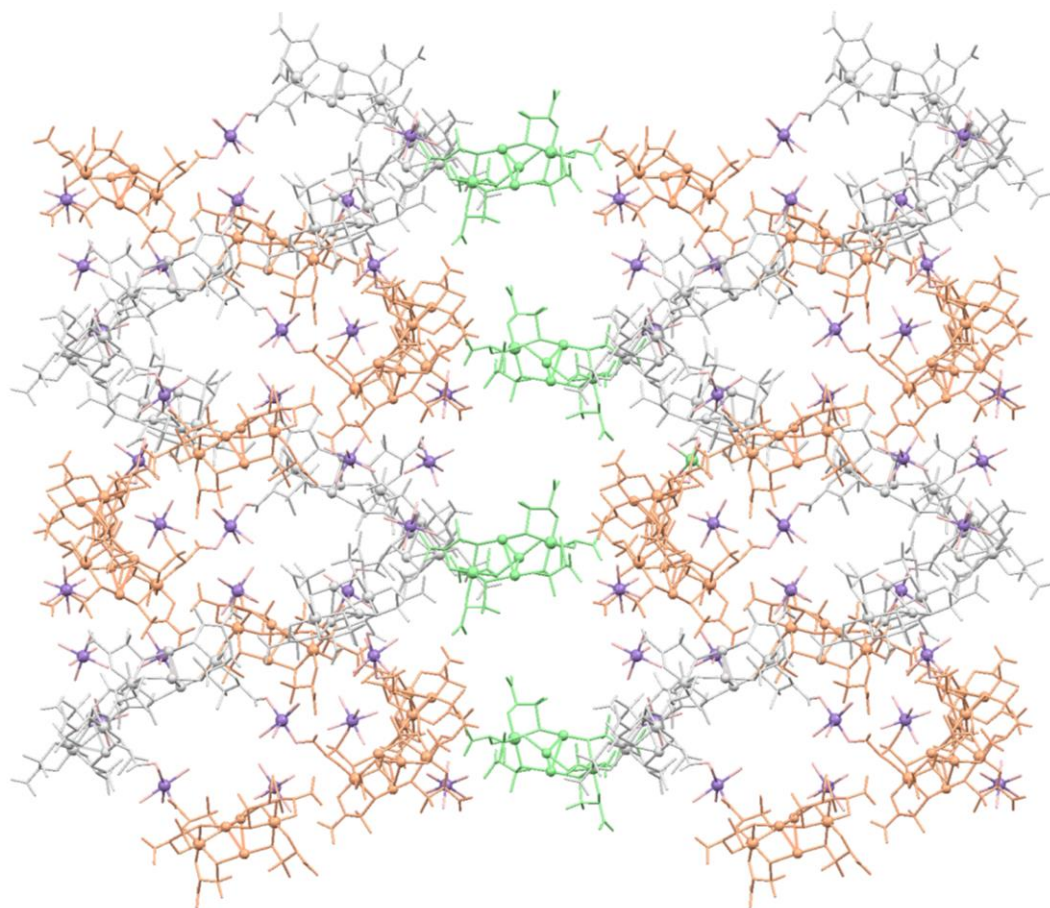**Figure II-15.** A perspective view of the 1D channel structure in **4a**.

Figure II-16. A perspective view of two double helices (orange and gray) connected by [**1**]$^{3-}$ anions (light green) in **4a**. Color codes: Mn, light purple; O, pink.
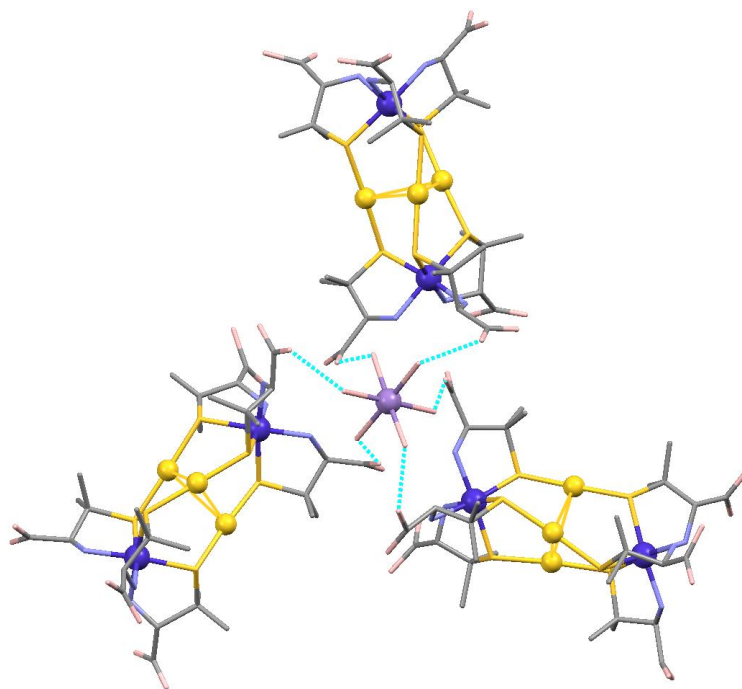
Figure II-17. A perspective view of the $[Mn(H_2O)_6]^{2+}$ cation connecting three $[\mathbf{1}]^{3-}$ anions through hydrogen bonds in **4a**. Color codes: Mn, light purple; Co, purple; Au, gold; S, yellow; O, pink; N, blue; C, gray. Dashed lines indicate hydrogen bonds.
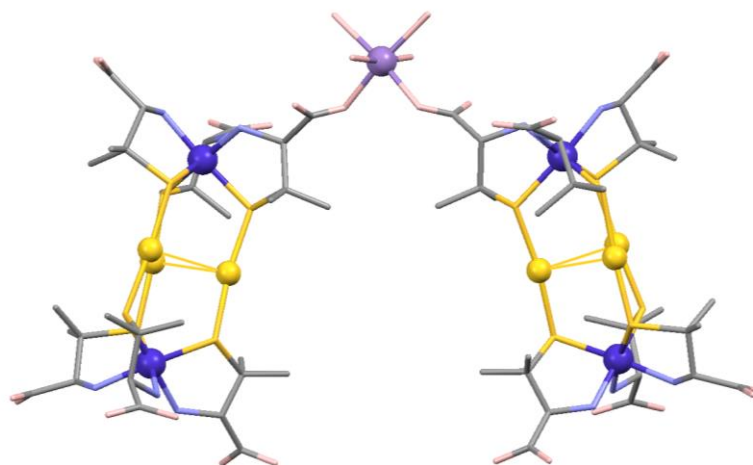

Figure II-18. A perspective view of the expanded asymmetric unit in **4b**. Color codes: Mn, light purple; Co, purple; Au, gold; S, yellow; O, pink; N, blue; C, gray.
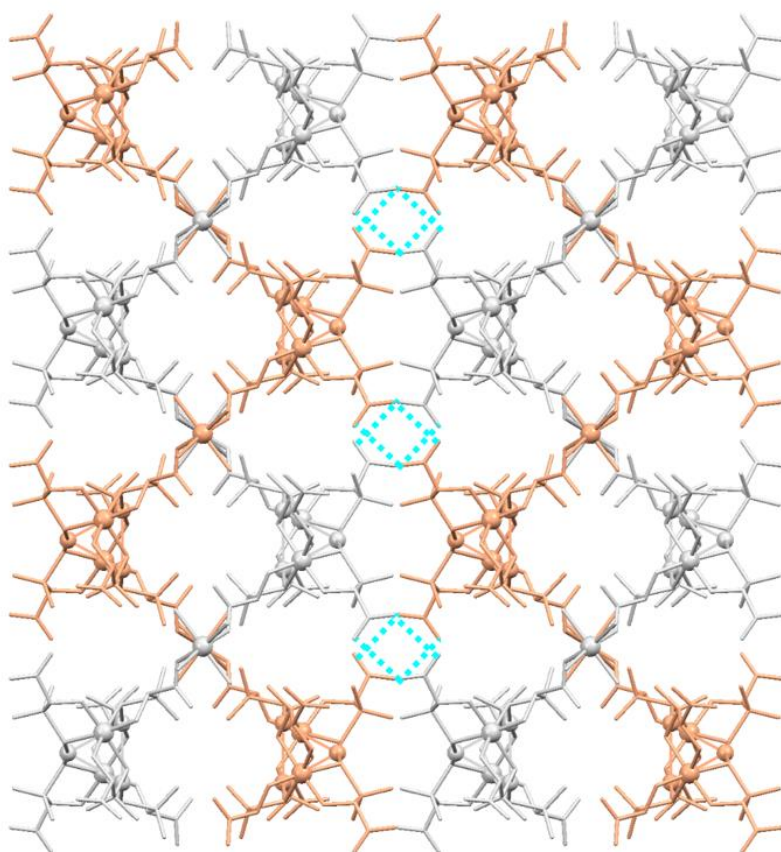
Figure II-19. A perspective view of two double helices (orange and gray) connected by intermolecular hydrogen-bonding interactions in **4b**. Dashed lines indicate hydrogen bonds.
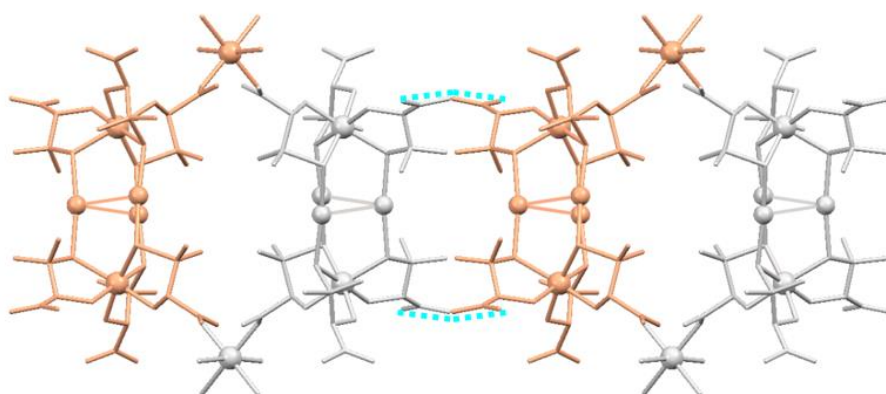

Figure II-20. Top view of the two double helices (orange and gray) connected by intermolecular hydrogen-bonding interactions in **4b**. Dashed lines indicate hydrogen bonds.
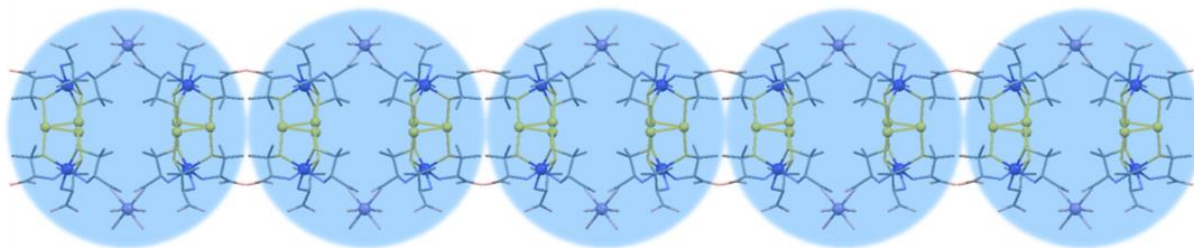
Figure II-21. The 2D sheet-like structure in **4b**. Transparent circles indicate each 1D coordination double helix.
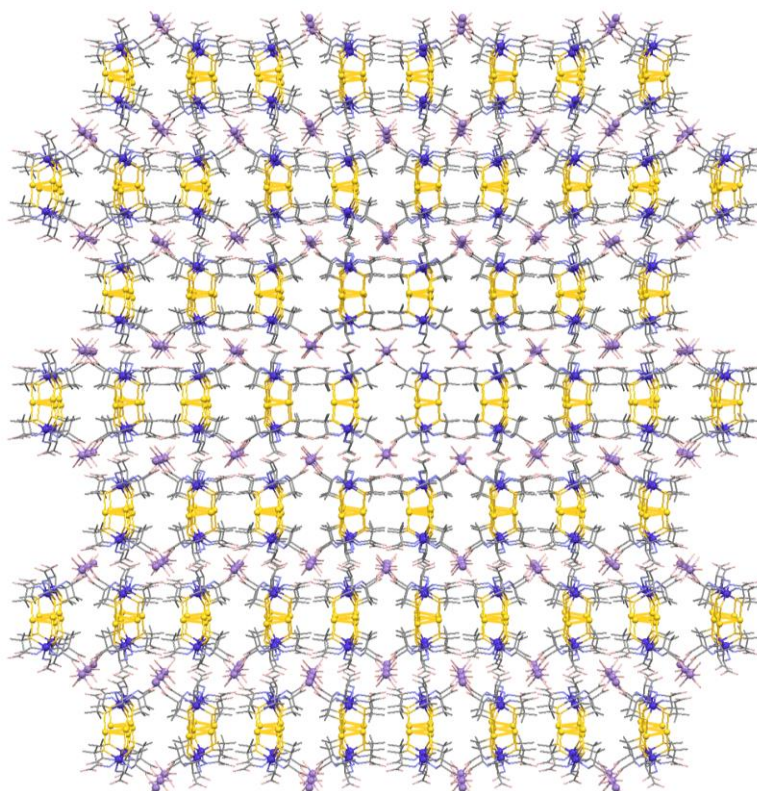

Figure II-22. A perspective view of the 3D dense structure with 1D coordination polymers in **4b**.
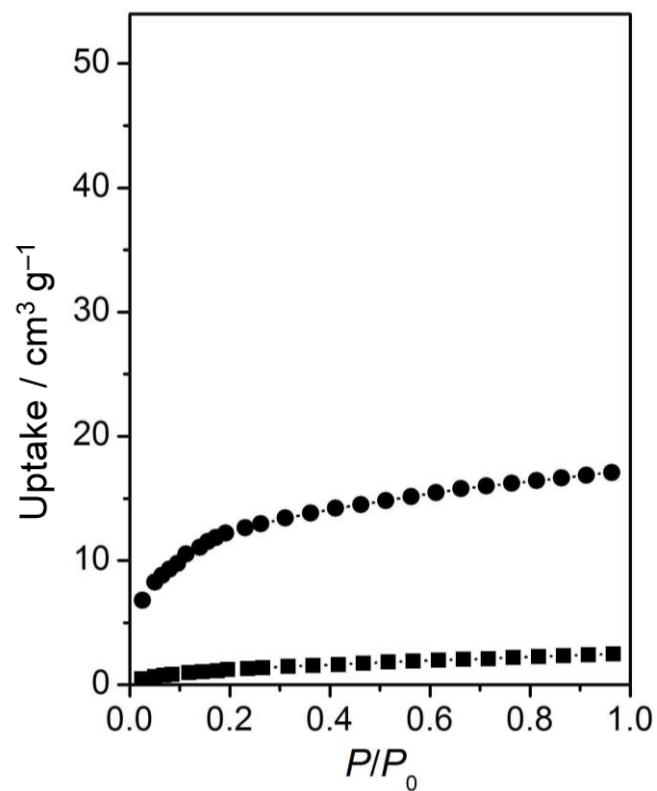
Figure II-23. Comparison of CO_2 adsorption isotherms at 195 K for **3a** (−●−) and **3b** (−■−).
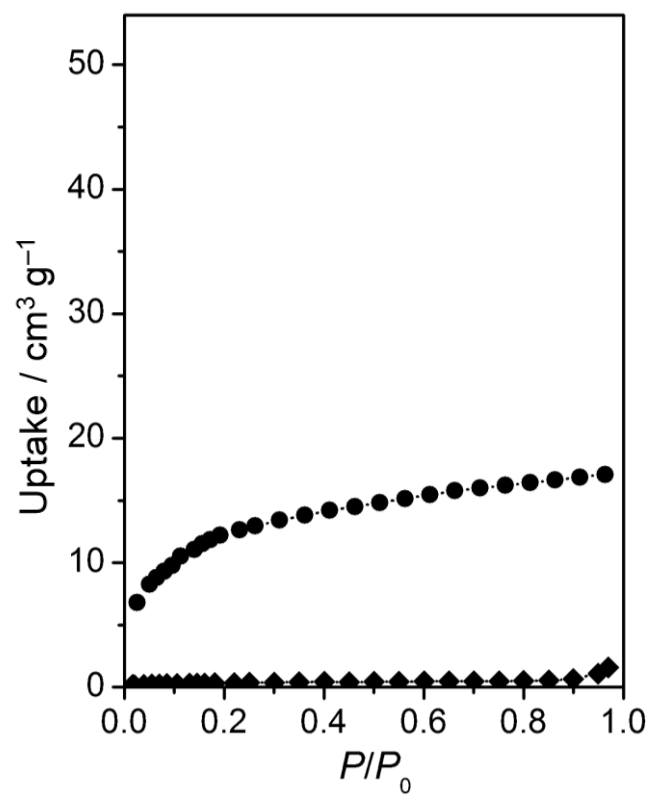
Figure II-24. Comparison of CO_2 at 195 K (−●−) and N_2 at 77 K (−◆−) adsorption isotherms for **3a**.

Figure II-25. Comparison of CO_2 at 195 K (–●–) and N_2 at 77 K (–◆–) adsorption isotherms for **3b**.

Figure II-26. Comparison of H_2O adsorption (solid symbols) and desorption (open symbols) isotherms at 298 K for **3a** (–●–) and **3b** (–■–).

Figure II-27. Vapor adsorption (solid symbols) and desorption (open symbols) isotherms of **3a** for H_2O (black), EtOH (blue), and acetone (red) vapors at 298 K.
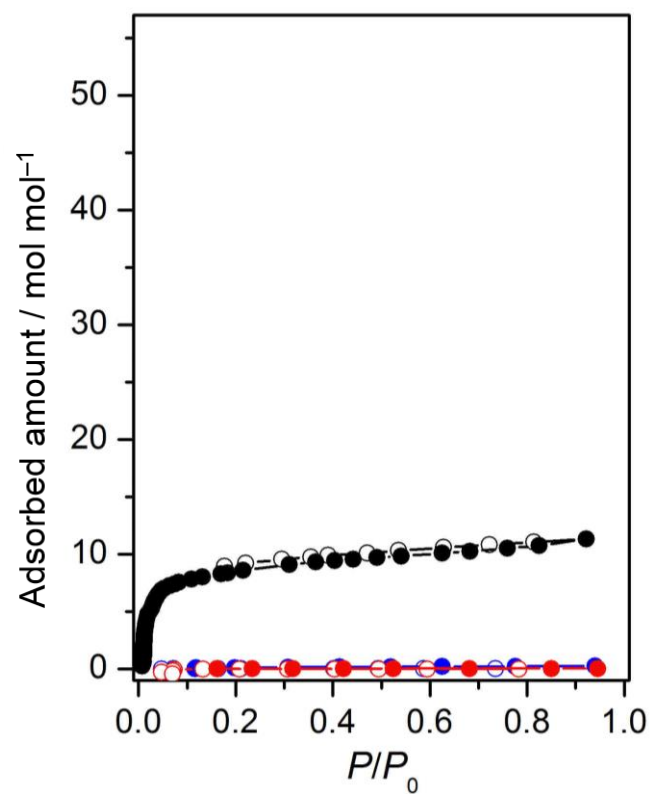
Figure II-28. Vapor adsorption (solid symbols) and desorption (open symbols) isotherms of **3b** for H_2O (black), EtOH (blue), and acetone (red) vapors at 298 K.
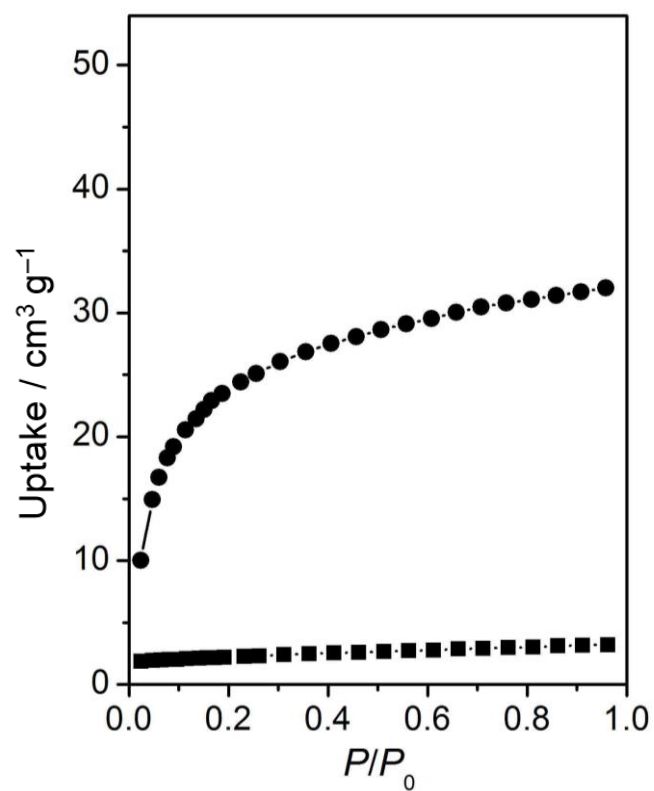
Figure II-29. Comparison of CO_2 adsorption isotherms at 195 K for **4a** (−●−) and **4b** (−■−).
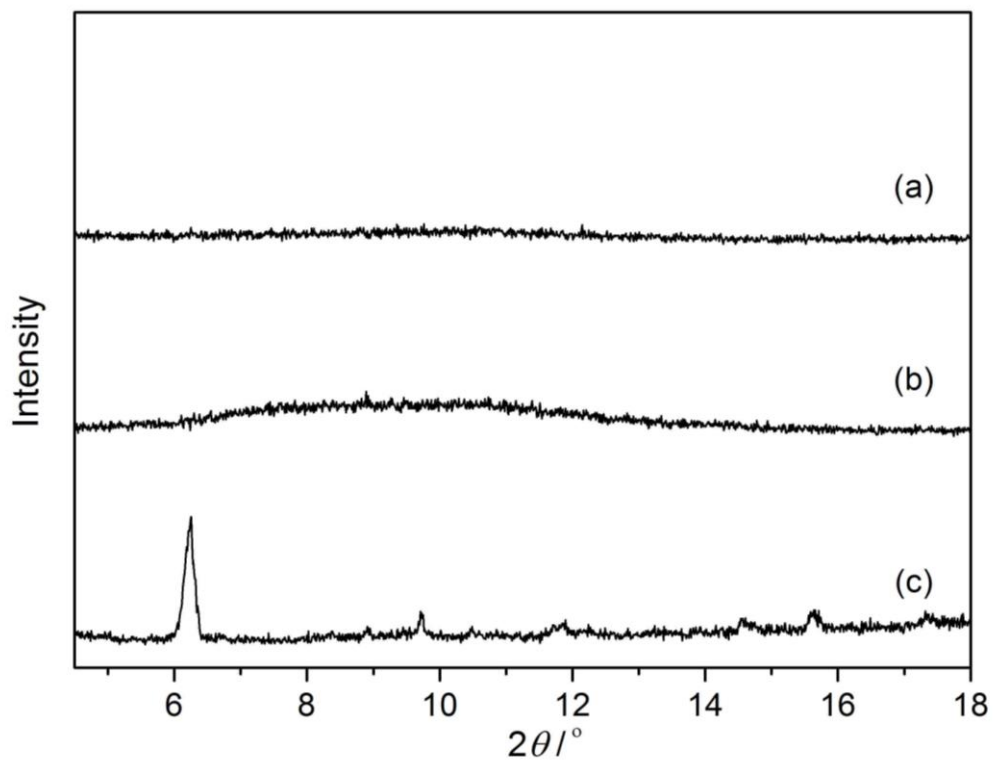
Figure II-30. Experimental PXRD patterns after heating at 120°C of (a) **2b**, (b) **3a**, and (c) **4a**.
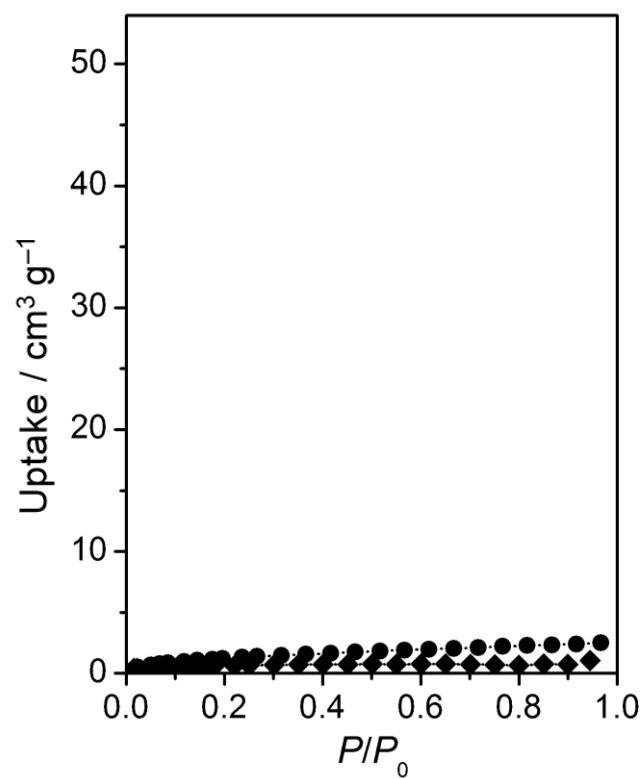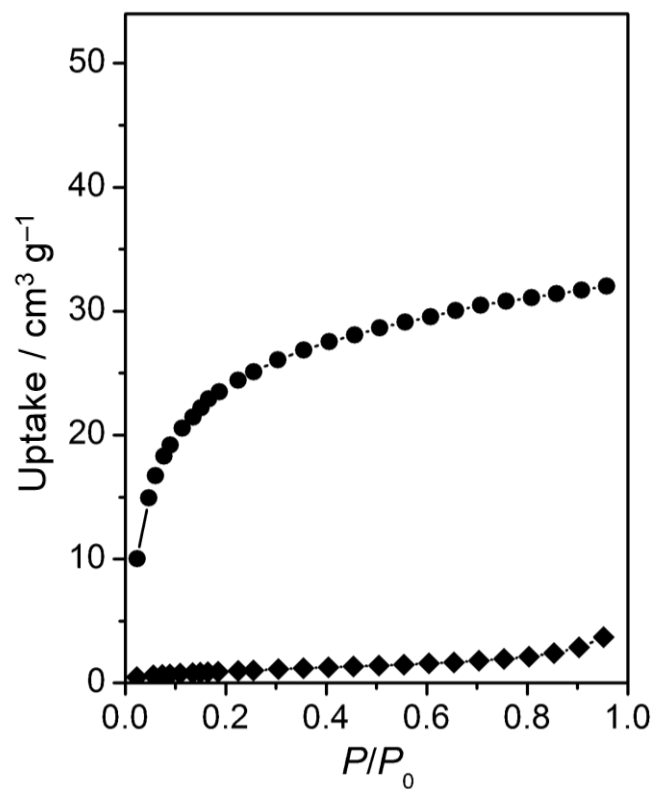
Figure II-31. Comparison of CO_2 at 195 K (–●–) and N_2 at 77 K (–◆–) adsorption isotherms for **4a**.
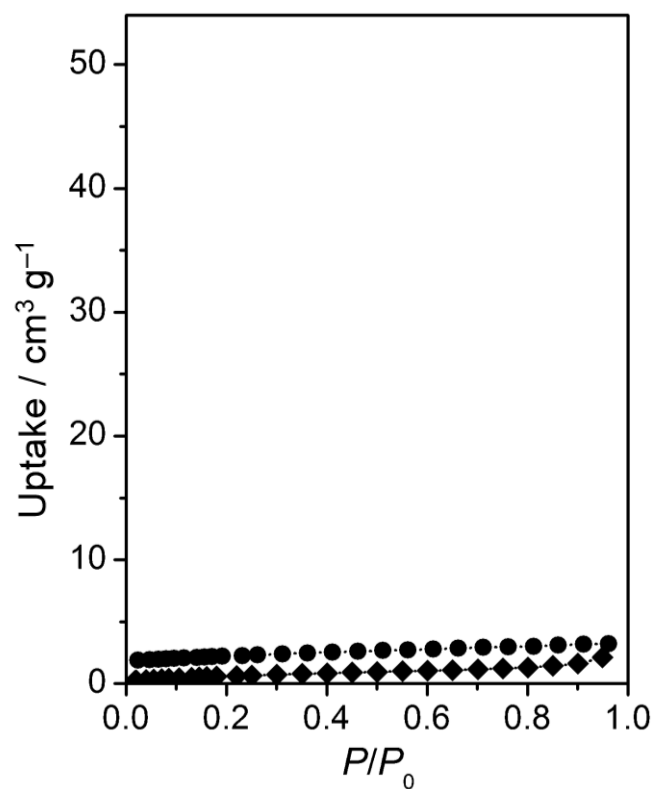
Figure II-32. Comparison of CO_2 at 195 K (–●–) and N_2 at 77 K (–◆–) adsorption isotherms for **4b**.
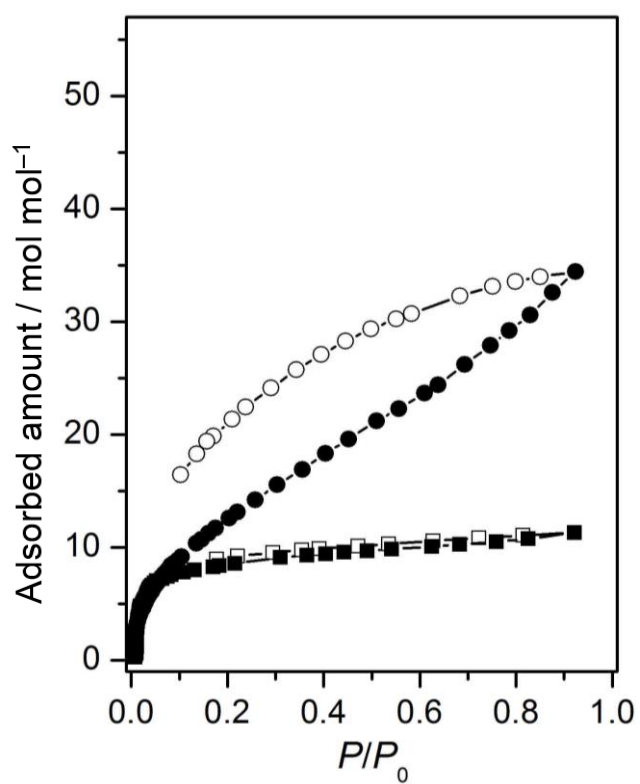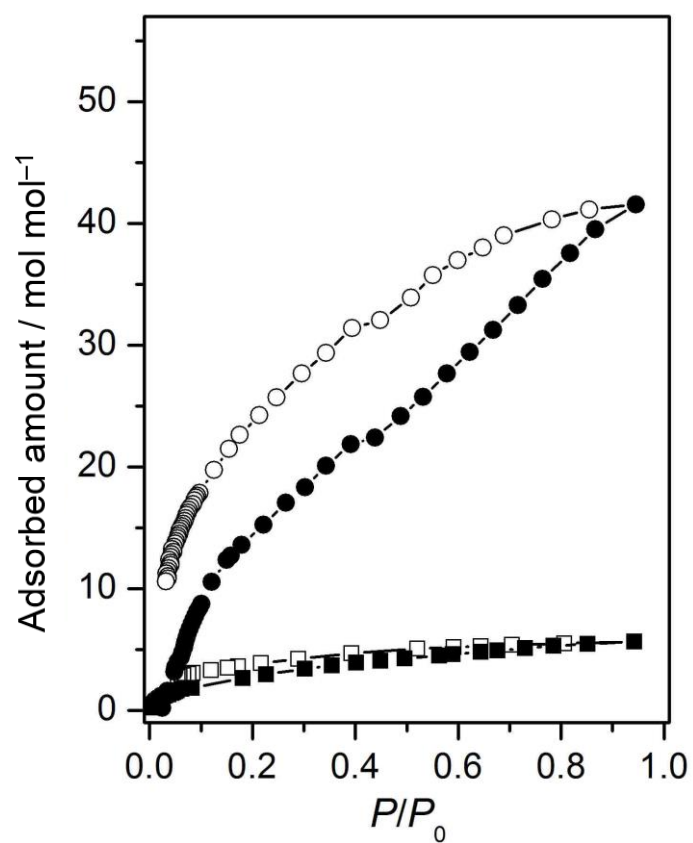
Figure II-33. Comparison of H_2O adsorption (solid symbols) and desorption (open symbols) isotherms at 298 K for **4a** (−●−) and **4b** (−■−).
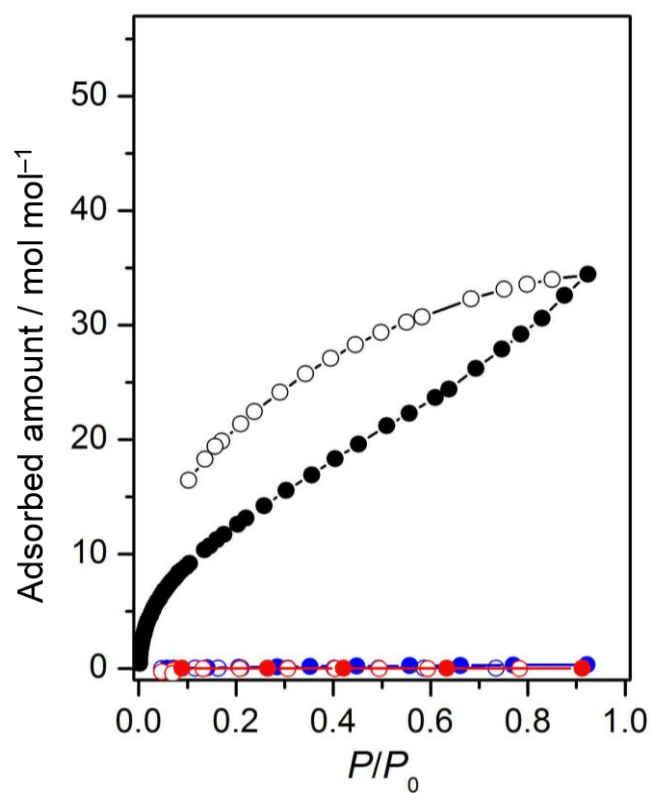
Figure II-34. Vapor adsorption (solid symbols) and desorption (open symbols) isotherms of **4a** for H_2O (black), EtOH (blue), and acetone (red) vapors at 298 K.
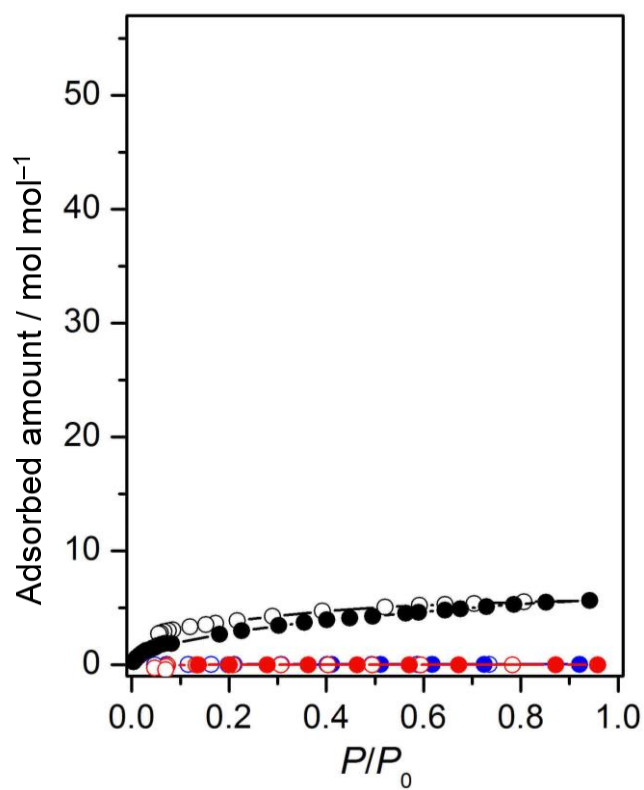
Figure II-35. Vapor adsorption (solid symbols) and desorption (open symbols) isotherms of **4b** for H_2O (black), EtOH (blue), and acetone (red) vapors at 298 K.

Table II-1. Crystallographic data of **3a** and **3b**.

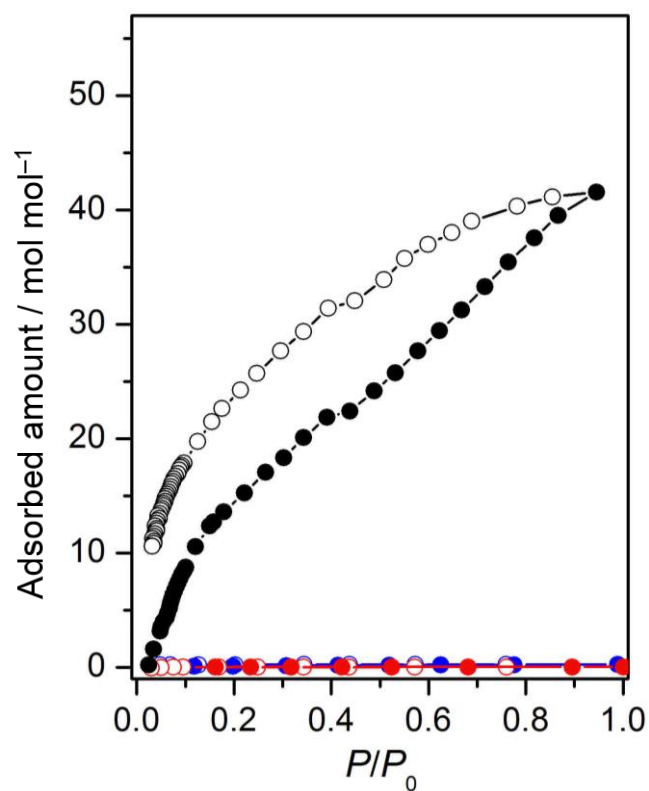|	3a	3b
Formula	$C_{60}H_{172}Au_6Co_4N_{12}O_{56}S_{12}Ni_3$	$C_{60}H_{178}Au_6Co_4N_{12}O_{59}S_{12}Ni_3$
Color, form	Purple, hexagonal block	Purple, needle
Formula weight	3936.48	3990.52
Crystal system	Hexagonal	Monoclinic
Space group	$P6_122$	$P2_1$
a / Å	45.3534(11)	19.0474(11)
b / Å	45.3534(11)	21.1071(12)
c / Å	30.0368(7)	32.6971(18)
α / °	90	90
β / °	90	97.538(7)
γ / °	120	90
V / Å^3	53506(3)	13031.8(13)
Z	6	4
T / K	100(2)	100(2)
F(000)	273312	63536
ρ_{calcd} / g cm^{-3}	17.614	16.841
μ(Mo Kα) / mm^{-1}	75.058	74.973
Crystal size / mm^3	0.18×0.13×0.08	0.05×0.02×0.01
Limiting indices	$-47 \leq h \leq 45$,	$-25 \leq h \leq 25$,
	$-62 \leq k \leq 57$,	$-29 \leq k \leq 28$,
	$-41 \leq l \leq 24$	$-35 \leq l \leq 43$
$2\theta_{max}$ / °	58.25	58.25
$R_1{}^a$ ($I>2\sigma(I)$)	0.0765	0.1134
w$R_2{}^b$ (all data)	0.2442	0.3086
GOF	1.502	1.105

[a]$R_1 = (\Sigma|(|F_o| - c|F_c|)|)/(\Sigma|F_o|)$

[b]$wR_2 = [\{\Sigma w(F_o{}^2 - cF_c{}^2)^2\}/(\Sigma w|F_o{}^2|^2)]^{1/2}$

Table II-2. Crystallographic data of **4a** and **4b**.

	4a	4b
Formula	$C_{60}H_{168}Au_6Co_4N_{12}O_{54}S_{12}Mn_3$	$C_{30}H_{73}Au_3Co_2N_6O_{21}S_6Mn$
Color, form	Purple, hexagonal block	Purple, stick
Formula weight	3889.18	1810.04
Crystal system	Hexagonal	Orthorhombic
Space group	$P6_122$	$I222$
a / Å	45.3619(4)	10.2937(6)
b / Å	45.3619(4)	27.1982(10)
c / Å	30.4028(2)	18.7136(18)
α / °	90	90
β / °	90	90
γ / °	120	90
V / Å^3	54178.4(10)	5239.2(6)
Z	6	4
T / K	100(2)	100(2)
F(000)	31739	3328
ρ_{calcd} / g cm^{-3}	2.225	2.210
μ(Mo Kα) / mm^{-1}	15.580	8.738
Crystal size / mm^3	0.20×0.10×0.04	0.10×0.03×0.02
Limiting indices	$0 \leq h \leq 55,$	$-17 \leq h \leq 6,$
	$-47 \leq k \leq 0,$	$-46 \leq k \leq 44,$
	$-32 \leq l \leq 32$	$-25 \leq l \leq 30$
$2\theta_{max}$ / °	52.02	72.00
$R_1{}^a$ ($I>2\sigma(I)$)	0.0929	0.0607
$wR_2{}^b$ (all data)	0.2791	0.1748
GOF	1.113	1.028

$^a R_1 = (\Sigma|(|F_o| - c|F_c|)|)/(\Sigma|F_o|)$

$^b wR_2 = [\{\Sigma w(F_o{}^2 - cF_c{}^2)^2\}/(\Sigma w|F_o{}^2|^2)]^{1/2}$

Table II-3. Summary of adsorbed amount for **2b**, **3a**, **3b**, **4a**, and **4b**.

	Adsorbed amount				
	Gas adsorptions ($cm^3 \ g^{-1}$)		Vapor adsorptions (mol mol^{-1})		
	CO_2	N_2	H_2O	EtOH	Acetone
2b	6.6	1.7	38	0.35	0.03
3a	17.1	1.6	34	0.34	0.03
3b	2.5	1.0	11	0.27	0.04
4a	32.0	3.6	42	0.26	0.05
4b	3.2	2.1	6	0.04	0.01

Chapter III. Combination of $Co^{III}_2Au^I_3$ complex anions and aqua zinc(II) cations.

III-1. Introduction.

In Chapter I and II, the combination of the rod-shaped $Co^{III}_2Au^I_3$ pentanuclear-complex anions ($[Co^{III}_2Au^I_3(D\text{-pen-}N,S)_6]^{3-}$; $D\text{-H}_2\text{pen}$ = D-penicillamine), as a molecular building block, and metal cations, such as Co^{2+}, Ni^{2+}, and Mn^{2+}, were mainly investigated in water media. However, it was found that solvent of water is not suitable for the reactions of $[Co^{III}_2Au^I_3(D\text{-pen-}N,S)_6]^{3-}$ with Zn^{2+} due to a rapid precipitation, in which X-ray quality crystals are not obtained. Therefore, an aqueous buffer system is examined in order to slow down the rate of crystallization. Moreover, buffer solutions can provide different pH values of reaction solutions precisely. Thus, it is interesting to study the influences of pH on the resulting frameworks.

As described in general introduction, metallosupramolecular frameworks have received much attention owing to their remarkable structures and properties which can lead to a wide range of applications.[1–3] However, a practical synthesis frequently faces difficulties in the control of interactions between metal ions and ligands because many external stimuli, such as pH, temperature, and pressure, play an important role in the formation of chemical bondings.[4-6] Therefore, a research on the creation of metallosupramolecular frameworks by controlling these external stimuli has been still a challenge. As one of the external stimuli, pH has a significant influence on the construction of metallosupramolecular frameworks. This is because the alteration of pH can tremendously affects the protonation level of organic ligands, which drastically changes coordination modes and conformations of ligands, geometries of metal centers, and hydrogen bonding interactions.[5,6] Several reports illustrated that pH of reaction solutions plays a key role in the self-assembly process of supramolecular systems. For example, Lehn *et al.* reported a pH-driven structural switching that possesses controllable and reversible modulation between contraction (coiled helix) and extension (uncoiled linear) of molecular motion in lead(II)/pyridine/pyrimidine supramolecular frameworks.[6b] Although several works have demonstrated the pH effects on coordination modes, structural conformations, and dimensions of resulting structures,[5,6] a systematic study on the production of hydrogen-bonded framework or coordination polymer influenced by pH has been less explored.

In this chapter, a study on the pH-controlled construction of two metallosupramolecular frameworks, $[\{Zn(H_2O)_4\}\{Co_2Au_3(D\text{-}Hpen\text{-}N,S)(D\text{-}pen\text{-}N,S)_5\}]$ **(5a)** and $Na_9[\{Zn(OAc)_2\}\{Co_2Au_3(D\text{-}pen\text{-}N,S)_6\}_2][Co_2Au_3(D\text{-}pen\text{-}N,S)_6]$ **(5b)**, based on the rod-shaped $[Co^{III}_2Au^I_3(D\text{-}pen\text{-}N,S)_6]^{3-}$ ($[\mathbf{1}]^{3-}$) anions and aqua zinc(II) cations is presented. This system illustrated a drastic change of the resulting frameworks by slightly changing pH of reaction solutions (Scheme III-1). The crystals obtained were fully characterized by single-crystal X-ray diffraction analyses. In addition, the physical characterizations on the basis of electronic absorption and CD in the solid state, along with IR, NMR, X-ray fluorescence, and elemental analyses were performed. The effects of solution pH on the resulting frameworks as well as the interconversion phenomena are discussed. Furthermore, the sorption behavior of products toward small molecules are also reported.

III-2. Experimental section.

III-2-1. Materials.

The starting complex, $Na_3[Co_2Au_3(D\text{-}pen\text{-}N,S)_6]$ ($Na_3[\mathbf{1}]$), was prepared by the method described in Chapter I. All other chemicals and solvents were commercially available and used without further purification.

III-2-2. Crystallizations.

(a) $[\{Zn(H_2O)_4\}\{Co_2Au_3(D\text{-}Hpen\text{-}N,S)(D\text{-}pen\text{-}N,S)_5\}]$ (5a).

To a purple solution containing $Na_3[\mathbf{1}]\cdot13H_2O$ (50 mg, 0.0301 mmol) in a sodium acetate buffer solution (2.5 mL, pH 4.5, $[OAc^-] = 0.5$ M), a colorless solution containing $Zn(OAc)_2\cdot2H_2O$ (10 mg, 0.045 mmol) in a sodium acetate buffer solution (2.5 mL, pH 4.5, $[OAc^-] = 0.5$ M) was added. The mixture was stirred at room temperature for 5 min which gave a clear dark purple solution. After the reaction solution was allowed to stand at room temperature for 1 day, purple square block crystals (**5a**) appeared which were collected by filtration and washed with acetone. Yield: 32 mg (58%). Anal. Calcd for $[\{Zn(H_2O)_4\}\{Co_2Au_3(D\text{-}Hpen\text{-}N,S)(D\text{-}pen\text{-}N,S)_5\}]\cdot5H_2O = C_{30}H_{73}N_6S_6O_{21}Co_2Au_3Zn$: C, 19.79; H, 4.04; N, 4.62%. Found: C, 19.75; H, 3.95; N, 4.60%. IR spectrum (cm^{-1}, KBr disk): 1609 (v_{COO}), 1717 (v_{COOH})^{sh}. The ^{23}Na NMR spectrum of **5a** in DCl/D$_2$O showed no signals from Na$^+$.

(b) Na9[{Zn(OAc)2}{Co2Au3(D-pen-*N*,*S*)6}2][Co2Au3(D-pen-*N*,*S*)6] (5b).

To a purple solution containing Na3[**1**]·13H2O (50 mg, 0.0301 mmol) in a sodium acetate buffer solution (2.5 mL, pH 5.5, [OAc⁻] = 0.9 M), a colorless solution containing Zn(OAc)2·2H2O (10 mg, 0.045 mmol) in a sodium acetate buffer solution (2.5 mL, pH 5.5, [OAc⁻] = 0.9 M) was added. The mixture was stirred at room temperature for 5 min which gave a clear dark purple solution. After the reaction solution was allowed to stand at room temperature for 2 weeks, purple hexagonal block crystals (**5b**) appeared which were collected by filtration and washed with acetone. Yield: 14 mg (23%). Anal. Calcd for Na9[{Zn(OAc)2}{Co2Au3(D-pen-*N*,*S*)6}2][Co2Au3(D-pen-*N*,*S*)6]·36H2O = C94H240N18S18O76Co6Au9Na9Zn: C, 19.42; H, 4.16; N, 4.34%. Found: C, 19.44; H, 4.11; N, 4.18%. IR spectrum (cm⁻¹, KBr disk): 1611 (ν_{COO}).

The ^{23}Na NMR spectrum of **5b** in D2O showed an intense signal from hydrated Na⁺ ion at δ 0.0 ppm (ppm from NaCl). The amount of Na⁺ ion in **5b** was evaluated to be 8.7 mol mol⁻¹ from the integration intensity of the ^{23}Na signal which matches well with the ideal value (9 mol mol⁻¹) for the chemical formula of **5b**.

III-2-3. Interconversion between 5a and 5b.

To a dark purple solution containing 12 mg (0.0066 mmol) of **5a**·5H2O in 10 mL of 0.5 M HCl aqueous solution was gradually added 0.5 M NaOH aqueous solution until solution pH reached 7. The obtained solution was evaporated to dryness by a rotary evaporator, and then a sodium acetate buffer solution (5 mL, pH 5.5, [OAc⁻] = 0.9 M) was added. After the resulting dark purple solution was allowed to stand at room temperature for 3 weeks, purple hexagonal block crystals appeared which were collected by filtration and washed with acetone. Yield: 4 mg (31%). The powder X-ray diffraction (PXRD) result of the obtained purple hexagonal block crystals is essentially similar to that of **5b**.

The reverse conversion from **5b** to **5a** was also investigated by the following procedure. The crystals of **5b**·36H2O in the amount of 15 mg (0.0026 mmol) was dissolved in a sodium acetate buffer solution (5 mL, pH 4.5, [OAc⁻] = 0.9 M) and gave a dark purple solution. After the resulting dark purple solution was allowed to stand at room temperature for 3 days, purple square block crystals appeared which were collected by filtration and washed with acetone. Yield: 3 mg (64%). The PXRD result of the obtained purple square block crystals is the same as that of **5a**.

III-2-4. Physical measurements.

The diffuse reflection spectra were recorded with a JASCO V-570 UV/VIS/NIR spectrometer at room temperature. The circular dichroism (CD) spectra in the solid state were performed on a JASCO J-820 spectropolarimeter at room temperature. The IR spectra were recorded with a JASCO FT/IR-4100 infrared spectrometer using KBr disks at room temperature. Elemental analyses (C, H, N) were performed using a Yanaco CHN Corder MT-5. The X-ray fluorescence analyses were conducted using a SHIMADZU Rayny EDX-720 spectrometer. The ^{1}H NMR spectra were recorded with a JEOL ECAMX-500SP spectrometer in D_2O. Sodium 4,4-dimethyl-4-silapentane-1-sulfonate (DSS) was used as the internal reference. The ^{23}Na NMR spectra were recorded with a JEOL JNM-ECS400 spectrometer in D_2O. Sodium chloride was used as the external reference. All measurements were performed at room temperature. The sorption isotherms of N_2 and CO_2 were measured with a BELSORP-mini II volumetric adsorption instrument. N_2 and CO_2 gases of high purity (99.9999%) were used. The sorption isotherms for H_2O, EtOH, and acetone were performed on a BELSORP-max volumetric adsorption instrument. High quality powder X-ray diffraction patterns were recorded at room temperature, in transmission mode [synchrotron radiation $\lambda = 0.999139(2)$ Å; 2θ range = 0–78°; step width = 0.005°; data collection time = 1 min] on a diffractometer equipped with a MYTHEN microstrip X-ray detectors (Dectris ltd.) at SPring-8 BL02B2 beamline. The crystals were loaded into glass capillary tubes (diameter = 0.3 mm). The samples were rotated during the measurements. The diffraction patterns were collected with a large Debye-Scherrer camera. The powder simulation patterns were generated from the single-crystal X-ray structures using Mercury 3.8.

III-2-5. X-ray structural determinations.

Single-crystal X-ray diffraction data for **5a** were recorded on a Rigaku Mercury 2 CCD detector with a synchrotron radiation ($\lambda = 0.6997$ Å) at BL02B1 beamline in SPring-8 with the approval of the Japan Synchrotron Radiation Research Institute (JASRI). The intensity data were collected by the ω-scan and were processed with a Rapid Auto software program. The structure of **5a** was solved by direct methods using SHELXS-2014.[7] The structure refinements were carried out using full-matrix least-squares (SHELXL-2014).[7] All calculations were performed using the Yadokari-XG software package.[8] All non-hydrogen atoms were refined anisotropically. Hydrogen atoms were included in the calculated positions except those of water molecules.

Single-crystal X-ray diffraction experiment for **5b** was performed on an ADSC Q210 CCD area detector with a synchrotron radiation (λ = 0.7000 Å) at 2D beamline in Pohang Accelerator Laboratory (PAL). The intensity data were collected by the ω-scan technique and the diffraction images were processed by using HKL3000.[9] Absorption correction was performed by using HKL3000.[9] The structure of **5b** was solved by direct methods using SHELXS-2014.[7] The structure refinements were carried out using full-matrix least-squares (SHELXL-2014).[7] All calculations were performed using the Yadokari-XG software package.[8] All non-hydrogen atoms were refined anisotropically. Hydrogen atoms were included in the calculated positions except those of water molecules. The crystal structure possesses a large void space in a one dimensional structure composed of Na^+ cations, $[Co_2Au_3(\text{D-pen-}N,S)_6]^{3-}$ anions, and $\{Zn(OAc)_2\}$ moieties. The void space should be filled by the solvated water molecules and a part of $[Na(H_2O)_n]^+$ ions based on the elemental, fluorescence X-ray, and thermogravimetric analyses. However, they are severely disordered and only several solvated water molecules could be modeled in the void space. The SQUEEZE report indicated a solvent-accessible volume of 29526 A^3 per cell,[10] corresponding to 61.2% of the unit-cell volume. Crystal data are summarized in Table III-1.

III-3. Results and discussion.

III-3-1. Syntheses and characterizations.

(a) [{Zn(H₂O)₄}{Co₂Au₃(D-Hpen-*N,S*)(D-pen-*N,S*)₅}] (5a).

The reaction of Na₃[**1**] and $Zn(OAc)_2$ in a sodium acetate buffer solution at pH 4.5 (HOAc/NaOAc=1:1) gave water-insoluble purple square block crystals (**5a**). The crystallization of **5a** occurred within a day with the yield of *ca.* 60%. The diffuse reflection and the solid state CD spectra of **5a** were similar to those of Na₃[**1**], indicating that the S-bridged pentanuclear structure of [**1**]$^{3-}$ retained in **5a** (Figure III-1 and Figure III-2). In the IR spectrum, **5a** illustrates an intense C=O stretching band at 1609 cm^{-1} with the shoulder at 1717 cm^{-1}. The former and the latter correspond to the deprotonated COO$^-$ and protonated COOH groups, indicative of the partial protonation of carboxylate groups in **5a** (Figure III-3).[11] From these results, together with the X-ray fluorescence analysis showing the existence of Zn, Co, and Au, and the elemental analysis data, it is expected that **5a** contains a 1:1 adduct of Zn^{2+} and the monoprotonated form of $Co^{III}_2Au^I_3$ pentanuclear-complex anion,

[Co$_2$Au$_3$(D-Hpen-*N,S*)(D-pen-*N,S*)$_5$]$^{2-}$ ([H**1**]$^{2-}$), in which one of six D-pen carboxyl groups is protonated. The observed anion in the partially protonated form as [H**1**]$^{2-}$ is similar to that in previous crystal, [{Mn(H$_2$O)$_4$}{Co$_2$Au$_3$(D-Hpen-*N,S*)(D-pen-*N,S*)$_5$}] (**4b**), demonstrated in Chapter II. The homogeneity of the bulk sample **5a** was confirmed by PXRD measurement. It was found that the experimental diffraction pattern matched well with the simulated pattern based on the single-crystal X-ray data (Figure III-4). In addition, it was revealed that a similar reaction of Na$_3$[**1**] and Zn(OAc)$_2$ in a sodium acetate buffer solution at pH 5.0 (HOAc/NaOAc=1:2) also yielded purple square block crystals of **5a**.

(b) Na$_9$[{Zn(OAc)$_2$}{Co$_2$Au$_3$(D-pen-*N,S*)$_6$}$_2$][Co$_2$Au$_3$(D-pen-*N,S*)$_6$] (5b).

The purple hexagonal block crystals of **5b** that are soluble in water were obtained when the pH of a sodium acetate buffer solution containing Na$_3$[**1**] and Zn(OAc)$_2$ was slightly increased to 5.5 (HOAc/NaOAc=1:6). The crystallization of **5b** occurred within 2 weeks with a yield of *ca.* 25%. The diffuse reflection and solid state CD spectra of **5b** are similar to those of Na$_3$[**1**], indicating that the S-bridged pentanuclear structure of [**1**]$^{3-}$ anionic building blocks retained in **5b** (Figure III-1 and Figure III-2), and are essentially the same as those of **5a**. However, the IR spectrum displays only an intense C=O stretching band at 1611 cm^{-1} (Figure III-3), indicating the existence of fully deprotonated carboxyl groups in **5b**.[11] The results from X-ray fluorescence and elemental analyses match well with the formula of the 3:1 adduct of [**1**]$^{3-}$ and Zn^{2+}. The ^{23}Na and ^{1}H NMR spectra of **5b** in D$_2$O showed the presence of Na$^+$ and OAc$^-$ ions, respectively. The homogeneity of the bulk sample **5b** was confirmed by PXRD measurement. It was found that the experimental diffraction pattern matched well with the simulated pattern based on the single-crystal X-ray data (Figure III-5). In addition, the similar reactions of Na$_3$[**1**] and Zn(OAc)$_2$ in a sodium acetate buffer solution at pH 6.0 and 6.5 also gave **5b**.

III-3-2. Crystal structures.

(a) [{Zn(H$_2$O)$_4$}{Co$_2$Au$_3$(D-Hpen-*N,S*)(D-pen-*N,S*)$_5$}] (5a).

The crystal structure of **5a** was studied by single-crystal X-ray diffraction analysis. In addition to the water molecules of crystallization, crystal **5a** contains *cis* configurational [Zn(H$_2$O)$_4$]$^{2+}$ cations that are directly bound to rod-shaped Co$^{III}_2$Au$^I_3$ pentanuclear-complex anions ([Co$_2$Au$_3$(D-Hpen-*N,S*)(D-pen-*N,S*)$_5$]$^{2-}$; [H**1**]$^{2-}$) (Figure III-6). In this context, it should

be noted that the partial protonation of D-pen carboxyl groups to form $[H1]^{2-}$ observed in **5a** did not cause a change in the conformation of $Co^{III}_2Au^I_3$ pentanuclear-complex anion. In **5a**, $[H1]^{2-}$ anions are alternately connected by the $[Zn(H_2O)_4]^{2+}$ cations through coordination bonds of deprotonated carboxylate groups (av. Zn–OOC = 2.03 Å), forming a 2-fold helix along the crystallographic *a* axis. Additionally, the two helices are intertwined and connected to each other through $OH_2\cdots OOC$ hydrogen bonds (av. O$\cdots$O = 2.72 Å), forming a right-handed double helix structure (Figure III-7 and Figure III-8). Each double helix is hydrogen-bonded to each other through COOH$\cdots$OOC intermolecular hydrogen-bonding interactions (av. O$\cdots$O = 2.88 Å) by using the protonated carboxylate group to form a 2D sheet-like structure (Figure III-9). Finally, the 2D sheets are stacked through the $NH_2\cdots OOC$ hydrogen bonds (av. N$\cdots$O = 2.98 Å), completing a 3D dense framework (Figure III-10). The crystal porosity of **5a** without including the crystallization water molecules was estimated to be *ca.* 13%, based on the calculation with PLATON program.[12] In addition, it was shown that the overall packing structure in **5a** is reminiscent of that in **4b**, demonstrated in Chapter II.

(b) $Na_9[\{Zn(OAc)_2\}\{Co_2Au_3(D\text{-}pen\text{-}N,S)_6\}_2][Co_2Au_3(D\text{-}pen\text{-}N,S)_6]$ (5b).

Single-crystal X-ray analysis demonstrated that **5b** consists of tetrahedral $\{Zn(OAc)_2\}$ units, rod-shaped $Co^{III}_2Au^I_3$ pentanuclear-complex anions ($[Co^{III}_2Au^I_3(D\text{-}pen\text{-}N,S)_6]^{3-}$; $[1]^{3-}$), in addition to the aqua Na^+ cations and water molecules of crystallization (Figure III-11). In **5b**, $[1]^{3-}$ are hydrogen-bonded (av. N$\cdots$O = 2.89 Å) to each other, thus constructing a six-fold helix with right handedness along the *c* axis. In addition, the two helices are bridged by the $\{Zn(OAc)_2\}$ moieties (av. Zn–O_{OAc} = 1.99 Å) through coordination bonds (av. Zn–O_{pen} = 1.97 Å), resulting in a double helix structure with a large 1D pore with a diameter of *ca.* 20 Å (Figure III-12). The double helices are further connected by other $[1]^{3-}$ anions *via* $NH_2\cdots OOC$ hydrogen bonds (av. N$\cdots$O = 2.91 Å), completing a 3D framework presenting 1D pore channels (Figure III-13). The crystal porosity of **5b** was evaluated to be *ca.* 61%, based on the calculation with PLATON program.[12] This 1D channel structure is supported by the aqua sodium(I) cations, each of which makes $OH_2\cdots OOC$ hydrogen bonds (av. O$\cdots$O = 2.82 Å) to the two $[1]^{3-}$ anions and one $\{Zn(OAc)_2\}$ unit in the double helix, and additional one $[1]^{3-}$ anion that links the double helix. The spatial arrangement of $[1]^{3-}$ anions in **5b** is reminiscent of that in previous porous ionic crystal, $[Co(H_2O)_6]_2[Co(H_2O)_4\{Co_2Au_3(D\text{-}pen\text{-}N,S)_6\}_2]$ (**2b**), demonstrated in Chapter I.

The structural difference between **5b** and **2b** was the substitution of linking

trans-[Co(H$_2$O)$_4$]$^{2+}$ units and free [Co(H$_2$O)$_6$]$^{2+}$ ions in **2b** by {Zn(OAc)$_2$} units and [Na$_2$(H$_2$O)$_{10}$]$^{2+}$ ions in **5b**. However, the stability of **5b** and **2b** were sharply different. The powder X-ray diffraction study demonstrated that **5b** keeps its crystallinity after heating at 120°C for 12 h, while **2b** collapses immediately even at room temperature (Figure III-5 and Figure III-14). As mentioned above, there exist multiple hydrogen bonds between acetate O atoms from {Zn(OAc)$_2$} and aqua ligands in [Na$_2$(H$_2$O)$_{10}$]$^{2+}$ units in **5b** (Figure III-11), while no direct hydrogen bonding interaction was observed between *trans*-[Co(H$_2$O)$_4$]$^{2+}$ units and free [Co(H$_2$O)$_6$]$^{2+}$ ions in **2b**. This is the reason why **5b** and **2b** show large difference in stability.

III-3-3. Interconversion between 5a and 5b.

A structural conversion from **5a** to **5b** was investigated by dissolving crystal **5a** in 0.5 M HCl aqueous solution, followed by a neutralization with 0.5 M NaOH aqueous solution. After the obtained solution was evaporated to dryness, a crystallization process was achieved in a sodium acetate buffer solution with pH 5.5. The water-soluble purple hexagonal block crystals were obtained after 3 weeks. The crystals were characterized as **5b** based on X-ray fluorescence and elemental analyses which match well with the formula of the 3:1 adduct of [**1**]$^{3-}$ and Zn^{2+} in **5b**. The IR spectrum displays only an intense C=O stretching band at 1611 cm^{-1}, indicating the existence of fully deprotonated carboxyl groups in the obtained crystals.[11] The observed results are reasonable due to a prevention of the protonation at D-pen carboxyl groups under the employed higher pH. The observed PXRD pattern is similar to that of **5b**. Thus, a conversion from a dense framework of **5a** to a porous framework of **5b** could be accomplished.

A reverse conversion from **5b** to **5a** was also investigated. The water–soluble crystal **5b** was dissolved in a sodium acetate buffer solution with pH 4.5 which gave a dark purple solution. The water-insoluble purple square block crystals were produced after 3 days. X-ray fluorescence and elemental analyses of the obtained crystals are in agreement with the formula of the 1:1 adduct of Zn^{2+} and [H**1**]$^{2-}$ in **5a**. The IR spectrum illustrates an intense C=O stretching band at 1609 cm^{-1} with the shoulder at 1717 cm^{-1}, indicative of the partial protonation of carboxylate groups.[11] The observed results show the protonation effect at the lower pH value leading to a formation of strong intermolecular COOH···OOC hydrogen bonds through the protonated D-pen carboxyl groups, thus forming a dense framework of **5a**. In addition, the observed PXRD pattern is very similar to that of **5a**. Thus, it is strongly

confirmed that the reverse conversion from **5b** to **5a** successfully occurred.

Consequently, the structural interconversion between dense framework of **5a** and porous framework of **5b** was successful which was evidenced by X-ray fluorescence and elemental analyses together with IR and PXRD measurements.

III-3-4. Sorption behavior.

The gas and vapor adsorption behaviors were investigated for both **5a** and **5b**. As shown in Figure III-15, the CO_2 adsorption isotherm for **5a** at 195 K displayed a type-I physical sorption isotherm illustrating a gradual increase and reached the amount of 8.7 cm^3 g^{-1} at P/P_0 = 0.99 with a low calculated BET surface area of 16 m^2 g^{-1}. A similar CO_2 adsorption isotherm was observed for **5b**, but the adsorption amount apparently increased with the saturated amount of 29.3 cm^3 g^{-1} at P/P_0 = 0.99, corresponding to its higher porosity. The BET surface area calculated from the CO_2 sorption isotherm was also significantly increased up to 66 m^2 g^{-1}. In contrast, the adsorption capacities of N_2 gas for both compounds (Figure III-16 and Figure III-17) are all poor at 77 K (<5.0 cm^3 g^{-1}). In addition, the adsorption characteristics of **5a** and **5b** toward small molecules were also studied. As shown in Figure III-18, an adsorption of H_2O vapor was observed for **5b** with the impressively high amount of 134 mol mol^{-1} (584 cm^3 g^{-1}) at P/P_0 = 0.90. Although the adsorption amount is lower than the champion record which has been reported on MOFs (PIZOF-2; 850 cm^3 g^{-1}),[13] this porous ionic framework interestingly showed high performance for water uptake comparable to that of MOFs with high capacity.[14] A reproducibility *via* a dissolution–crystallization process makes the ionic crystals have a substantial advantage over the MOFs that are commonly insoluble in most solvents and thus are not reproducible. A large hysteresis loop was clearly observed in an adsorption–desorption cycle which is common for nanoporous materials with large pores.[14] On the other hand, the H_2O adsorption amount was much smaller for **5a** (5 mol mol^{-1} at P/P_0 = 0.94), consistent with its lower porosity. Remarkably, both of them showed no preferential adsorption capacity toward EtOH and acetone vapors (Figure III-19 and Figure III-20), reflecting the superhydrophilic property of their frameworks.[15] A similar superhydrophilic behavior was also observed in **2b**, demonstrated previously in Chapter I. However, the adsorption capacity of **5b** is extremely higher than that of **2b** (38 mol mol^{-1} at P/P_0 = 0.99) due to the more stable framework of **5b**.

III-3-5. Influence of solution pH.

The key factors that caused a drastic difference in the resulting metallosupramolecular frameworks and their porosities between **5a** and **5b** are the protonation effect at the lower pH values (4.0-5.0), as well as the copresence of an excess amount of Na^+ and OAc^- ions in the reaction solution. In **5a**, the protonated D-pen carboxyl groups form strong intermolecular COOH···OOC hydrogen bonds that made neighboring helices much closer. Consequently, a dense framework with low porosity of *ca.* 13% was reasonably constructed. In this case, the copresence of the protonated and deprotonated carboxylate groups in the complex anion at the pH region of 4.5-5.0 is reasonable, since the pH was similar to the pKa value of a relating negatively charged complex with D-pen in $[Cu_{14}(D\text{-}pen\text{-}N,S)_{12}Cl]^{5-}$ (pKa = 4.5).[16] On the other hand, a comparatively higher pH value of 5.5 leads to a fully deprotonated form of D-pen in **5b**. Unlike in the case of **5a**, Na^+ and OAc^- ions were incorporated in **5b** which came from the employed sodium acetate buffer solution. Both Na^+ and OAc^- ions are also associated with the template-directed synthesis of **5b**, resulting in a 1D channel structure with significantly increased porosity up to *ca.* 61%. Therefore, at a glance, the formation of **5b** was accomplished with the aid of the stabilizing effect from a large amount of Na^+ and OAc^- ions in a basic sodium acetate buffer solution. However, it was found that crystal **5a** was selectively produced under the controlled synthetic conditions having the same concentration of Na^+ and OAc^- ions to that of **5b**, but pH values were lower (4.0-5.0). The observed results implied that pH that controls the protonation/deprotonation level of the carboxylate groups in D-pen is the dominant factor for the control of the resulting frameworks and their porosities in this system.

III-4. Conclusion.

In this chapter, the production of two metallosupramolecular frameworks, consisting of $[Co_2Au_3(D\text{-}pen\text{-}N,S)_6]^{3-}$ ($[\mathbf{1}]^{3-}$) anions and Zn^{2+} cations, with remarkably different porosities was successfully controlled only by a slight pH change. The coordination polymer of $[\{Zn(H_2O)_4\}\{Co_2Au_3(D\text{-}Hpen\text{-}N,S)(D\text{-}pen\text{-}N,S)_5\}]$ **(5a)** was produced in a sodium acetate buffer under the pH range of 4.0-5.0. When a slightly higher pH range (5.5-6.5) was applied, the porous ionic framework of $Na_9[\{Zn(OAc)_2\}\{Co_2Au_3(D\text{-}pen\text{-}N,S)_6\}_2][Co_2Au_3(D\text{-}pen\text{-}N,S)_6]$ **(5b)** that illustrates a 1D channel structure was obtained. The crystal porosity of **5a** (*ca.* 13%) was drastically increased in **5b** (*ca.* 61%). The dense framework of **5a** was stabilized by the protonation on the D-pen carboxyl groups at lower pH. On the other hand, at a higher pH, the protonation effect was

disappeared and the formation of the porous framework of **5b** was promoted by the guest templating effect of Na^+ and OAc^- ions. Such a systematic pH-controlled construction of metallosupramolecular frameworks, in which a drastic increase of crystal porosities from a dense coordination polymer to a porous ionic framework is accomplished, has never been observed previously. Notably, the exclusively selective adsorption of H_2O was observed for **5b**, which is attributable to the superhydrophilic opening channels in its stable framework.

III-5. References.

[1]   (a) S. Kitagawa, R. Kitaura, S. Noro, *Angew. Chem., Int. Ed.* **2004**, *43*, 2334-2375. (b) J. R. Li, R. J. Kuppler, H. C. Zhou, *Chem. Soc. Rev.* **2009**, *38*, 1477-1504. (c) R. Eguchi, S. Uchida, N. Mizuno, *Angew. Chem., Int. Ed.* **2012**, *51*, 1635-1639. (d) R. Eguchi, S. Uchida, N. Mizuno, *J. Phys. Chem. C* **2012**, *116*, 16105-16110. (e) S. Uchida, R. Kawahara, Y. Ogasawara, N. Mizuno, *Dalton Trans.* **2013**, *42*, 16209-16215. (f) H. Furukawa, K. E. Cordova, M. O'Keeffe, O. M. Yaghi, *Science* **2013**, *341*, 974-986.

[2]   (a) L. E. Kreno, K. Leong, O. K. Farha, M. Allendorf, R. P. Van Duyne, J. T. Hupp, *Chem. Rev.* **2012**, *112*, 1105-1125. (b) Y.-W. Li, J.-R. Li, L.-F. Wang, B.-Y. Zhou, Q. Chen, X.-H. Bu, *J. Mater. Chem. A* **2013**, *1*, 495-499. (c) Z. Dou, J. Yu, Y. Cui, Y. Yang, Z. Wang, D. Yang, G. Qian, *J. Am. Chem. Soc.* **2014**, *136*, 5527-5530.

[3]   (a) N. Guillou, Q. Gao, P. M. Forster, J. S. Chang, M. Noguès, S. E. Park, G. Férey, A. K. Cheetham, *Angew. Chem., Int. Ed.* **2001**, *40*, 2831-2834. (b) A. Proust, R. Thouvenot, P. Gouzerh, *Chem. Commun.* **2008**, 1837-1852. (c) J. Lee, O. K. Farha, J. Roberts, K. A. Scheidt, S. T. Nguyen, J. T. Hupp, *Chem. Soc. Rev.* **2009**, *38*, 1450-1459. (d) Z.-J. Liu, S. Yao, Z.-M. Zhang, E.-B. Wang, *RSC Adv.* **2013**, *3*, 20829-20835. (e) R. Kawahara, K. Niinomi, J. N. Kondo, M. Hibino, N. Mizuno, S. Uchida, *Dalton Trans.* **2016**, *45*, 2805-2809.

[4]   (a) N. Stock, S. Biswas, *Chem. Rev.* **2012**, *112*, 933-969. (b) D. Kim, X. Song, J. H. Yoon, M. S. Lah, *Cryst. Growth Des.* **2012**, *12*, 4186-4193. (c) P.-Z. Li, X.-J. Wang, Y. Li, Q. Zhang, R. H. D. Tan, W. Q. Lim, R. Ganguly, Y. Zhao, *Microporous Mesoporous Mater.* **2013**, *176*, 194-198. (d) Y.-X. Sun, W.-Y. Sun, *Chin. Chem. Lett.* **2014**, *25*, 823-828.

[5]   (a) R.-Q. Zhong, R.-Q. Zou, M. Du, T. Yamada, G. Maruta, S. Takeda, Q. Xu, *Dalton Trans.* **2008**, 2346-2354. (b) H. Wang, Y.-Y. Wang, G.-P. Yang, C.-J. Wang, G.-L. Wen,

Q.-Z. Shi, S. R. Batten, *CrystEngComm* **2008**, *10*, 1583-1594. (c) B. Zheng, J. Bai, Z. Zhang, *CrystEngComm* **2010**, *12*, 49-51. (d) J.-X. Yang, X. Zhang, J.-K. Cheng, J. Zhang, Y.-G. Yao, *Cryst. Growth Des.* **2012**, *12*, 333-345. (e) H.-N. Wang, G.-S. Yang, X.-L. Wang, Z.-M. Su, *Dalton Trans.* **2013**, *42*, 6294-6297. (f) K. P. Rao, M. Higuchi, J. Duan, S. Kitagawa, *Cryst. Growth Des.* **2013**, *13*, 981-985. (g) C. Patzschke, C. M. Forsyth, S. R. Batten, A. L. Chaffee, *CrystEngComm* **2014**, *16*, 6296-6299.

[6]   (a) V. Amendola, L. Fabbrizzi, P. Pallavicini, *Coord. Chem. Rev.* **2001**, *216–217*, 435-448. (b) M. Barboiu, J.-M. Lehn, *Proc. Natl. Acad. Sci. USA* **2002**, *99*, 5201–5206. (c) S.-T. Wu, L.-S. Long, R.-B. Huang, L.-S. Zheng, *Cryst. Growth Des.* **2007**, *7*, 1746-1752. (d) R.-G. Lin, L.-S. Long, R.-B. Huang, L.-S. Zheng, *Inorg. Chem. Commun.* **2007**, *10*, 1257-1261. (e) Q. Chu, G.-X. Liu, T. Okamura, Y.-Q. Huang, W.-Y. Sun, N. Ueyama, *Polyhedron* **2008**, *27*, 812-820. (f) K. C.-F. Leung, C.-P. Chak, C.-M. Lo, W.-Y. Wong, S. Xuan, C. H. K. Cheng, *Chem. Asian J.* **2009**, *4*, 364-381. (g) S.-L. Li, K. Tan, Y.-Q. Lan, J.-S. Qin, M.-N. Li, D.-Y. Du, H.-Y. Zang, Z.-M. Su, *Cryst. Growth Des.* **2010**, *10*, 1699-1705.

[7]   (a) G. M. Sheldrick, *Acta Cryst.* **2008**, *A64*, 112-122. (b) G. M. Sheldrick, *Acta Cryst.* **2015**, *C71*, 3-8.

[8]   C. Kabuto, S. Akine, T. Nemoto, E. Kwon, *Nihon Kessho Gakkaishi* **2009**, *51*, 218-224.

[9]   Z. Otwinowski, W. Minor, *Methods Enzymol.* **1997**, *276A*, 307-326.

[10]   A. L. Spek, *Acta Cryst.* **2009**, *D65*, 148-155.

[11]   K. Nakamoto, *Infrared and Raman Spectra of Inorganic and Coordination Compounds*, Wiley, New York, **1997**.

[12]   A. L. Spek, *J. Appl. Cryst.* **2003**, *36*, 7-13.

[13]   H. Furukawa, F. Gándara, Y.-B. Zhang, J. Jiang, W. L. Queen, M. R. Hudson, O. M. Yaghi, *J. Am. Chem. Soc.* **2014**, *136*, 4369-4381.

[14]   (a) J. Canivet, J. Bonnefoy, C. Daniel, A. Legrand, B. Coasne, D. Farrusseng, *New J. Chem.* **2014**, *38*, 3102-3111. (b) J. Canivet, A. Fateeva, Y. Guo, B. Coasne, D. Farrusseng, *Chem. Soc. Rev.* **2014**, *43*, 5594-5617. (c) N. C. Burtch, H. Jasuja, K. S. Walton, *Chem. Rev.* **2014**, *114*, 10575-10612.

[15]   (a) A. Nalaparaju, X. S. Zhao, J. W. Jiang, *J. Phys. Chem. C* **2010**, *114*, 11542-11550. (b) R. Plessius, R. Kromhout, A. L. D. Ramos, M. Ferbinteanu, M. C. Mittelmeijer-Hazeleger, R. Krishna, G. Ronthenberg, S. Tananse, *Chem. Eur. J.* **2014**, *20*, 7922-7925. (c) J. J. Gutiérrez-Sevillano, S. Calero, R. Krishna, *J. Phys. Chem.*

C **2015**, *119*, 3658-3666.

[16] N. Yoshinari, K. Tatsumi, A. Igashira-Kamiyama, T. Konno, *Chem. Eur. J.* **2010**, *16*, 14252-14255.
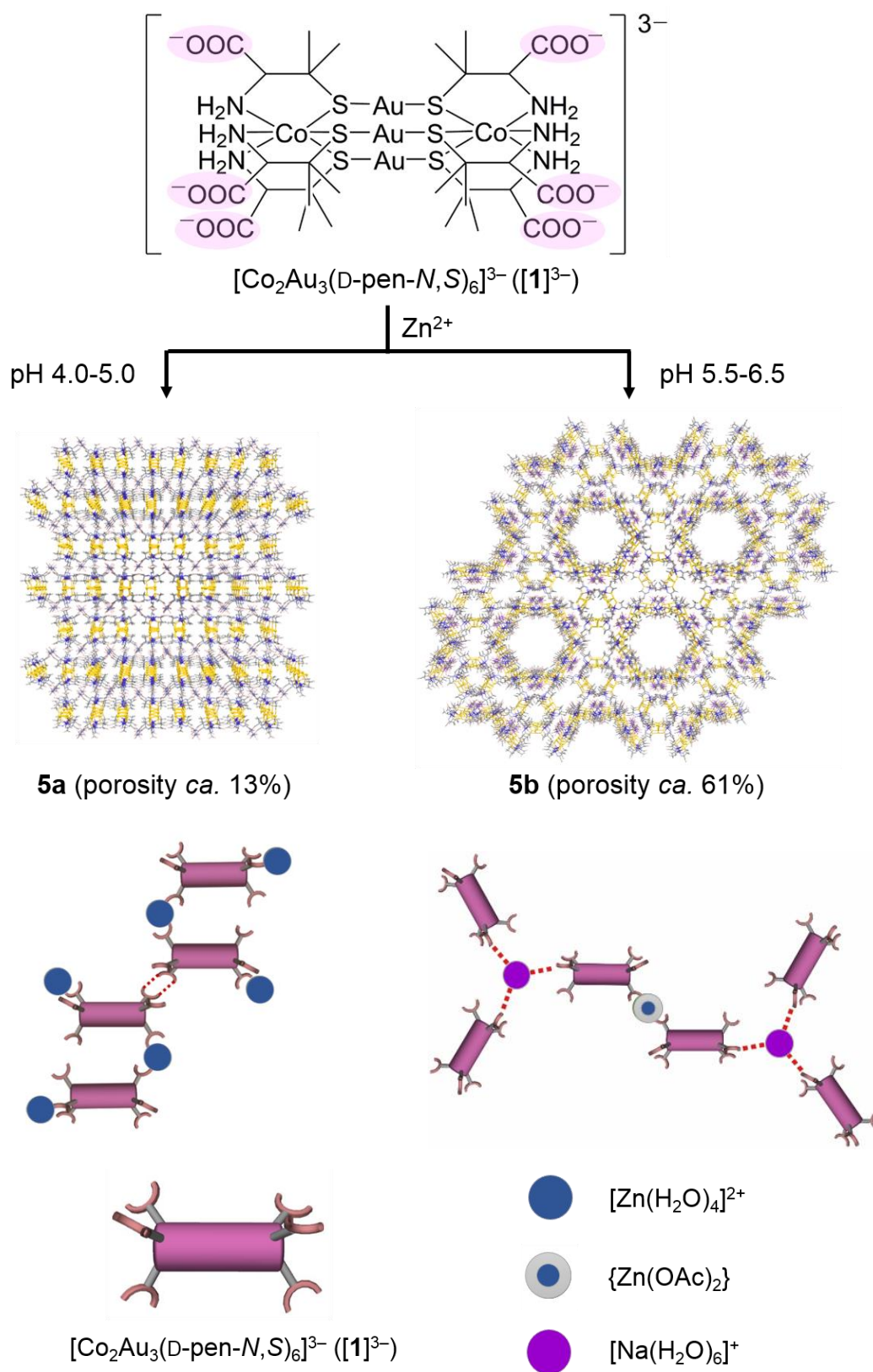
Scheme III-1. Two different metallosupramolecular frameworks constructed from the combination of $[\mathbf{1}]^{3-}$ anions and Zn^{2+} cations under the varied pH values. Dashed lines indicate hydrogen bonds.
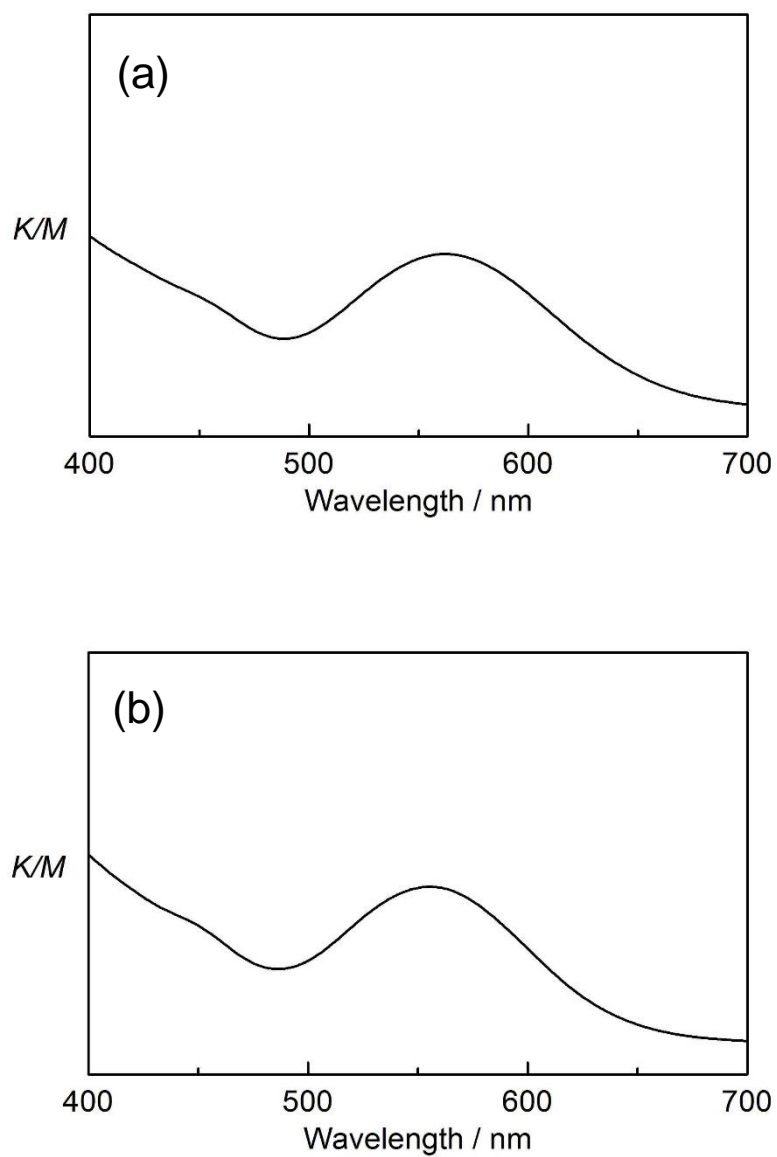
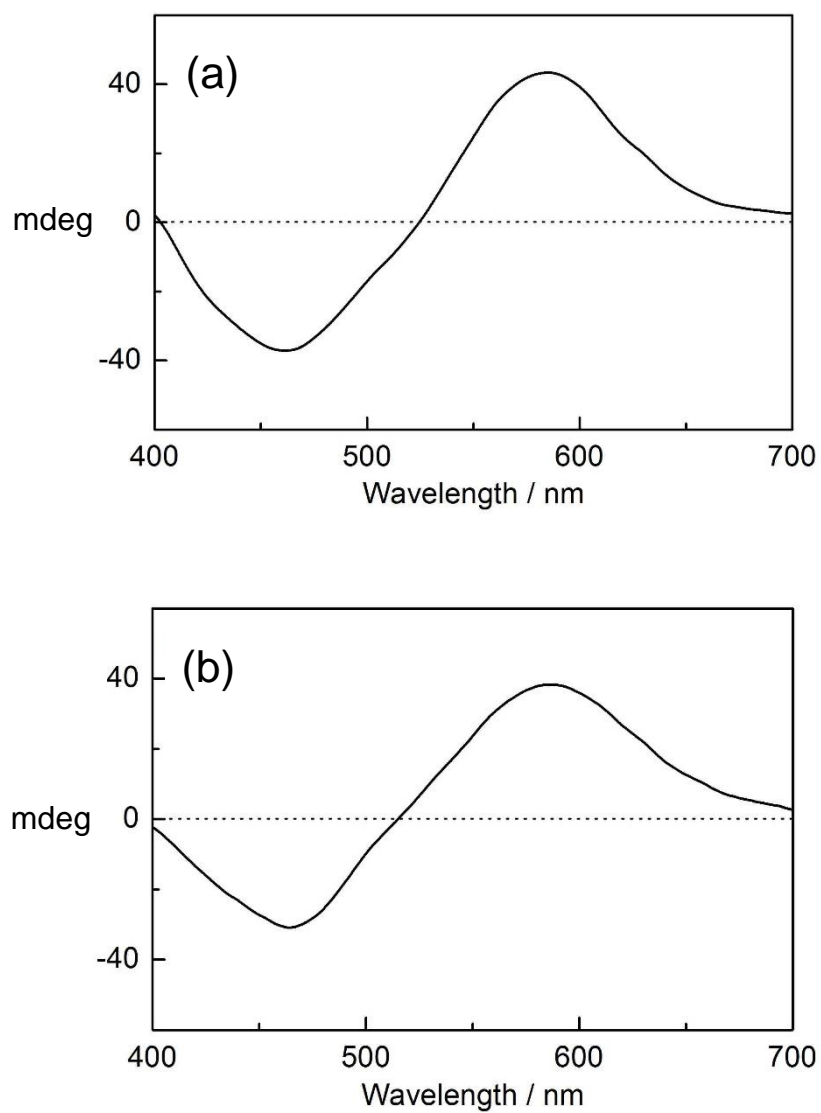**Figure III-1.** Diffuse reflection spectra of (a) **5a** and (b) **5b**.
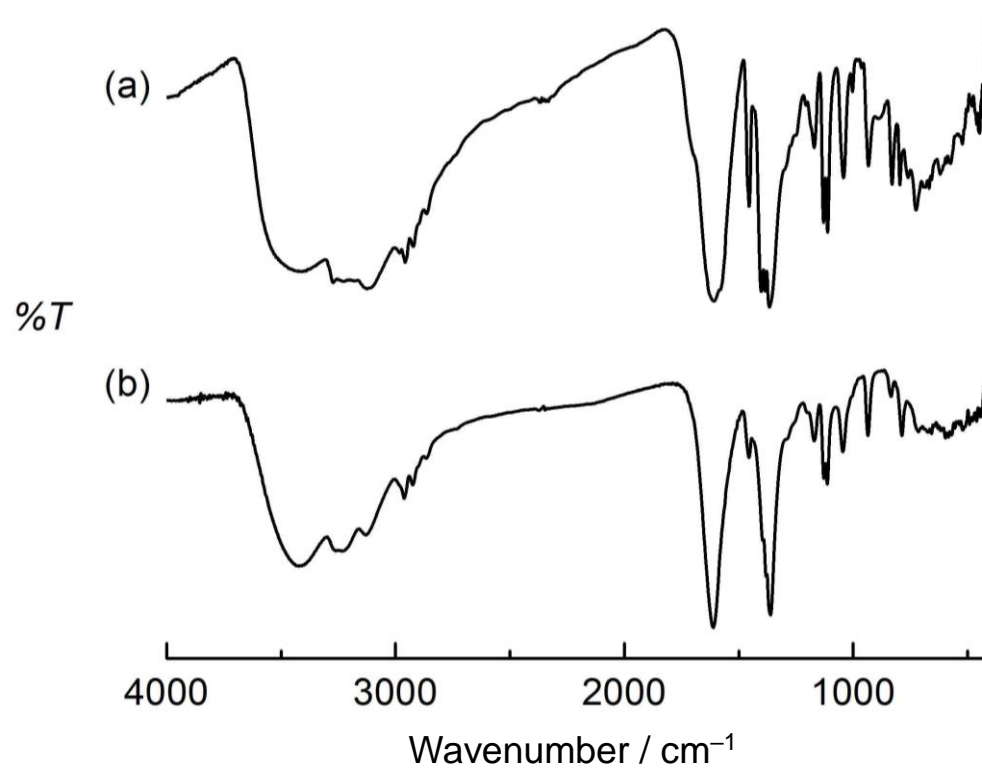
Figure III-2. Solid state CD spectra of (a) **5a** and (b) **5b**.

Figure III-3. IR spectra of (a) **5a** and (b) **5b**.
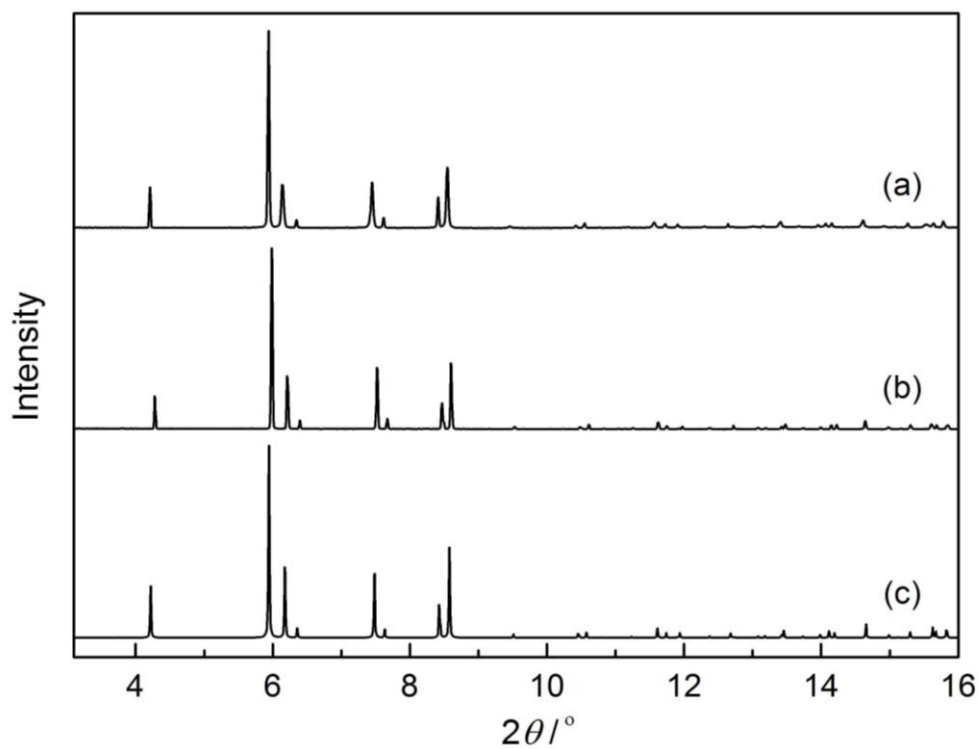
Figure III-4. Experimental PXRD patterns (a) after and (b) before heating at 120°C, and (c) simulated PXRD pattern of **5a**.
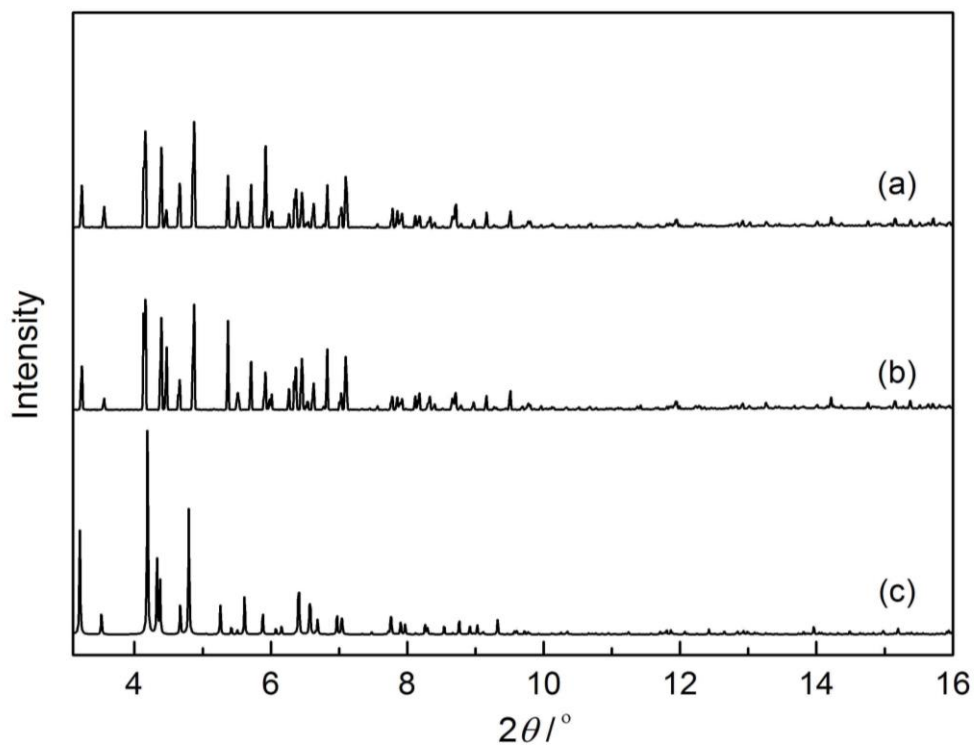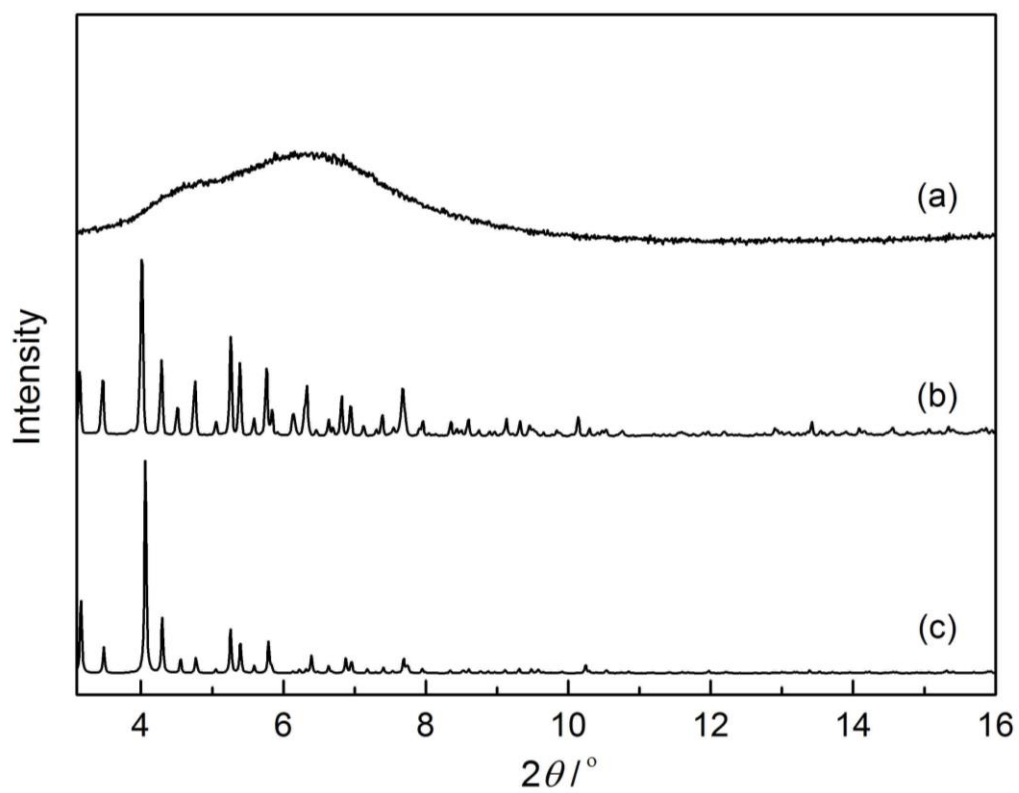

Figure III-5. Experimental PXRD patterns (a) after and (b) before heating at 120°C, and (c) simulated PXRD pattern of **5b**.
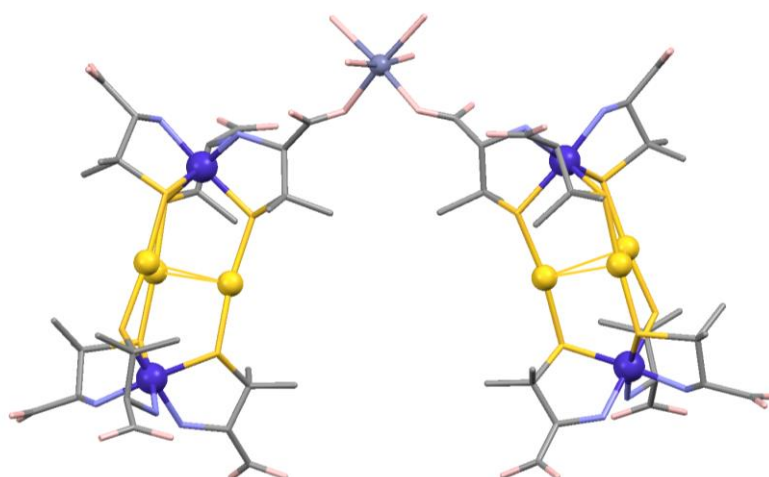
**Figure III-6.** A perspective view of the expanded asymmetric unit in **5a**. Color codes: Zn, dark blue; Co, purple; Au, gold; S, yellow; O, pink; N, blue; C, gray.
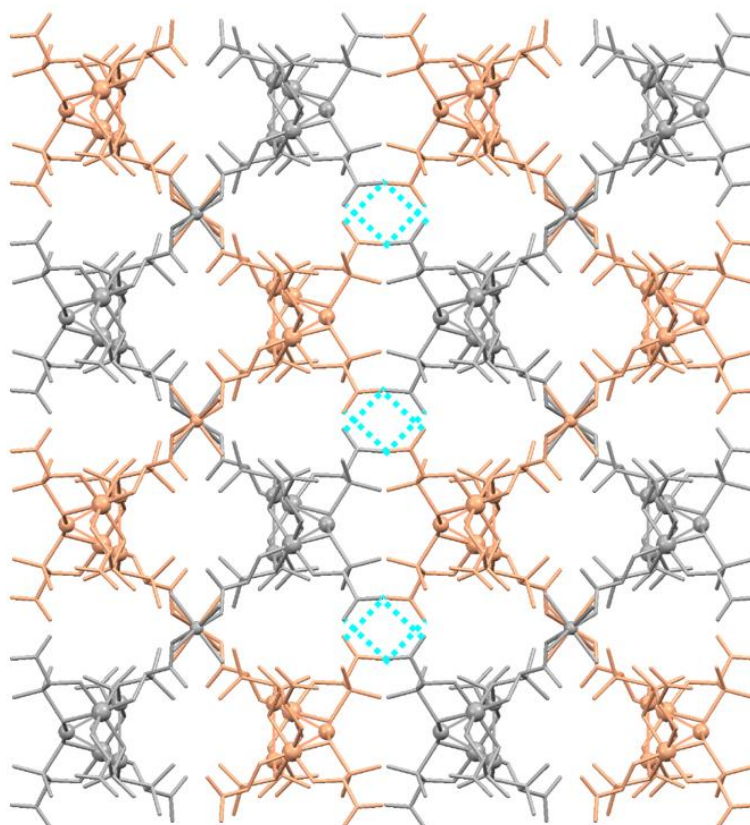
Figure III-7. A perspective view of two double helices (orange and gray) connected by intermolecular hydrogen-bonding interactions in **5a**. Dashed lines indicate hydrogen bonds.
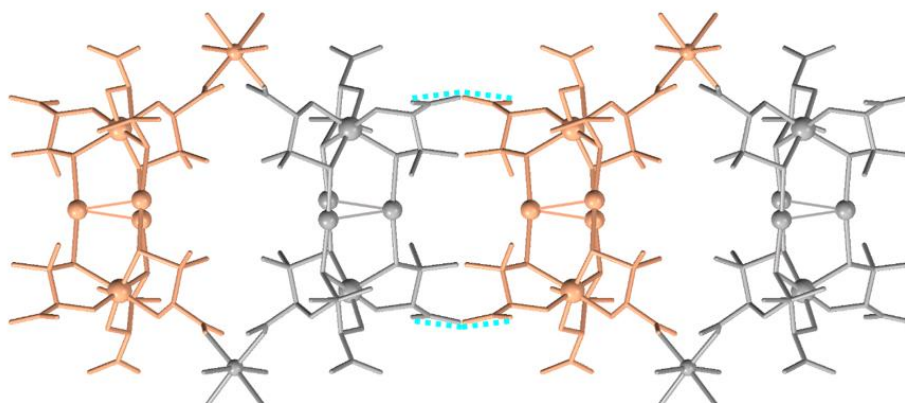
Figure III-8. Top view of the two double helices (orange and gray) connected by intermolecular hydrogen-bonding interactions in **5a**. Dashed lines indicate hydrogen bonds.
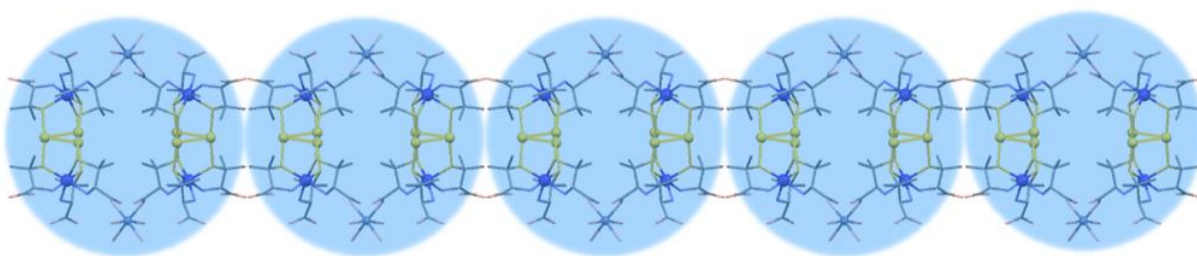
Figure III-9. A 2D sheet-like structure in **5a**. Color codes: Zn, dark blue; Na, light purple; Co, purple; Au, gold; S, yellow; O, pink; N, blue; C, gray. Blue circles indicate each 1D coordination double helix.
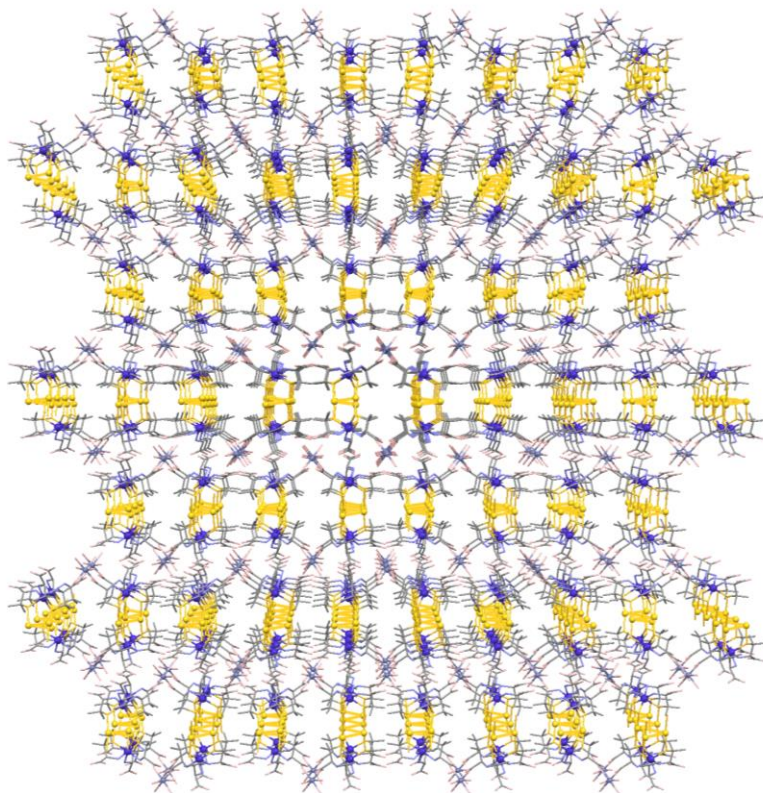
Figure III-10. A perspective view of the 3D dense structure with 1D coordination polymers in **5a**.
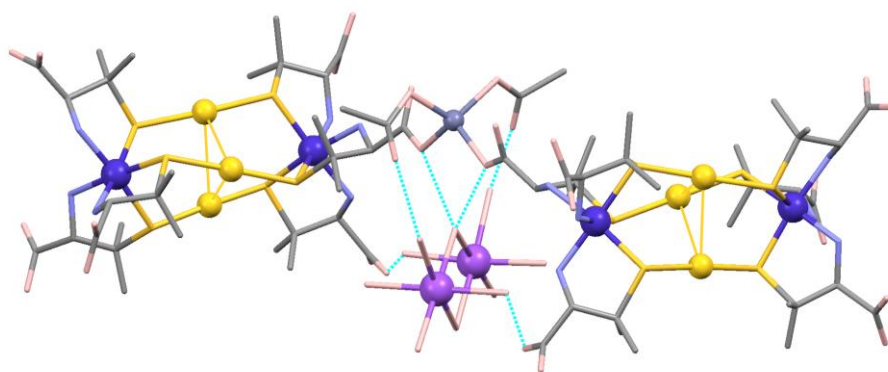
Figure III-11. A perspective view of the expanded asymmetric unit in **5b**. Color codes: Zn, dark blue; Na, light purple; Co, purple; Au, gold; S, yellow; O, pink; N, blue; C, gray. Dashed lines indicate hydrogen bonds.
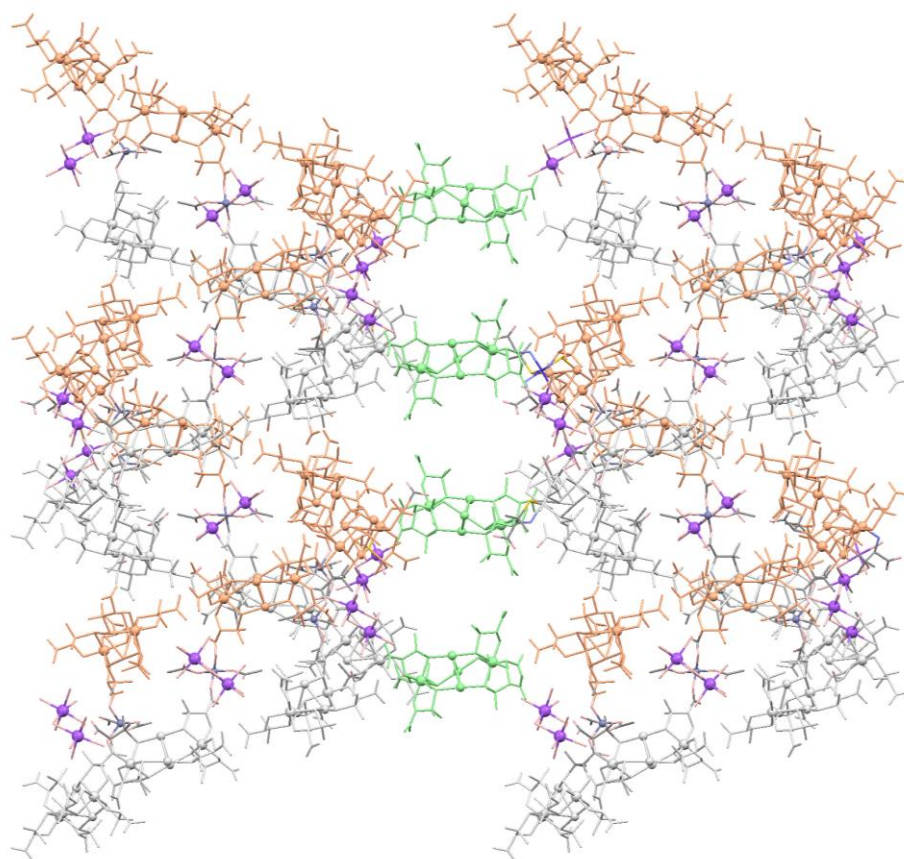
Figure III-12. A perspective view of two double helices (orange and gray) connected by [**1**]$^{3-}$ anions (green) in **5b**. Color codes: Zn, dark blue; Na, light purple; O, pink. Dashed lines indicate hydrogen bonds.
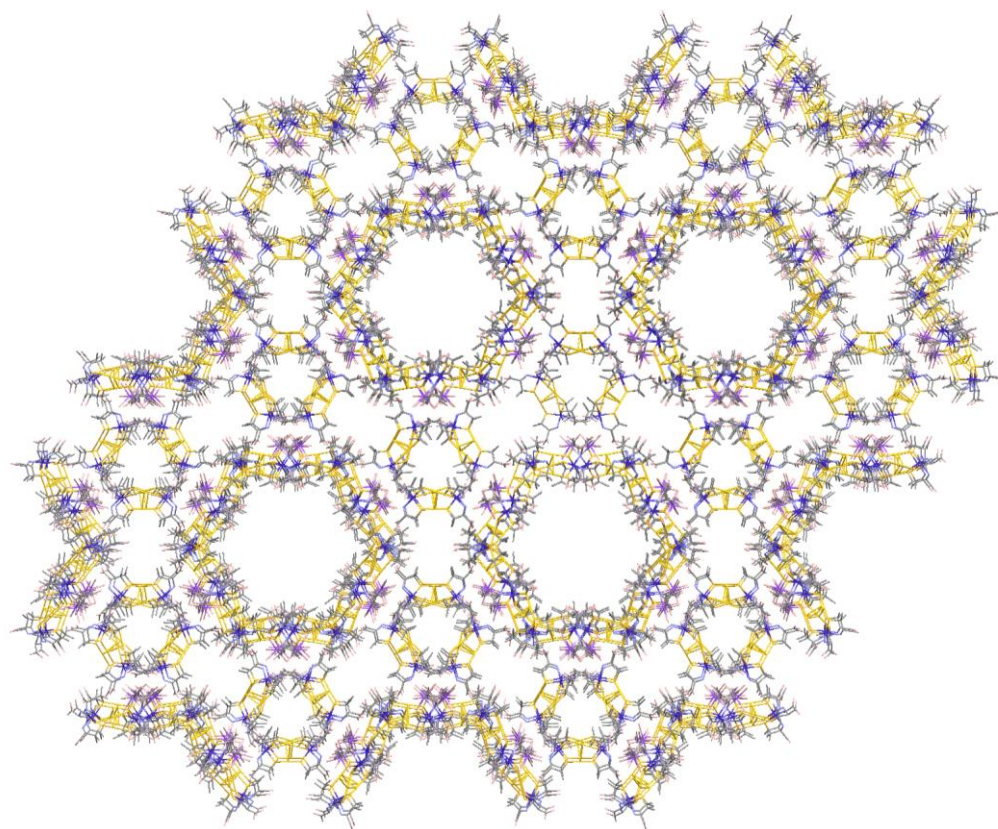
Figure III-13. A perspective view of the 1D channel structure in **5b**.

Figure III-14. Experimental PXRD patterns (a) after and (b) before heating at 120°C, and (c) simulated PXRD pattern of **2b**.
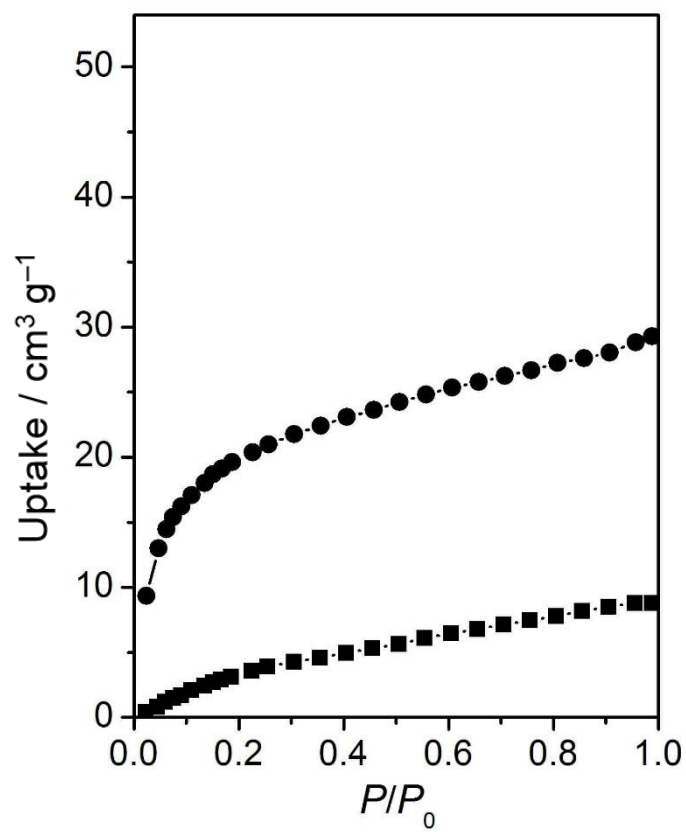
Figure III-15. Comparison of CO_2 adsorption isotherms at 195 K for **5a** (–■–) and **5b** (–●–).
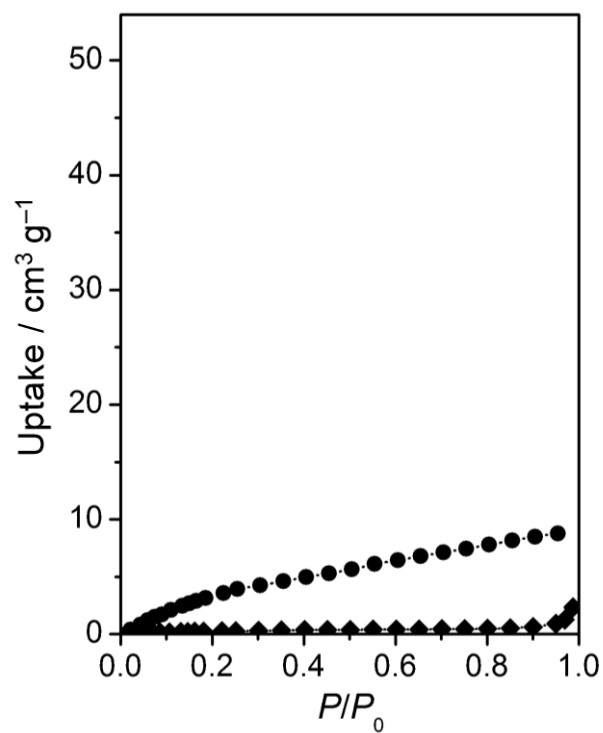
Figure III-16. Comparison of CO_2 at 195 K (−●−) and N_2 at 77 K (−◆−) adsorption isotherms for **5a**.
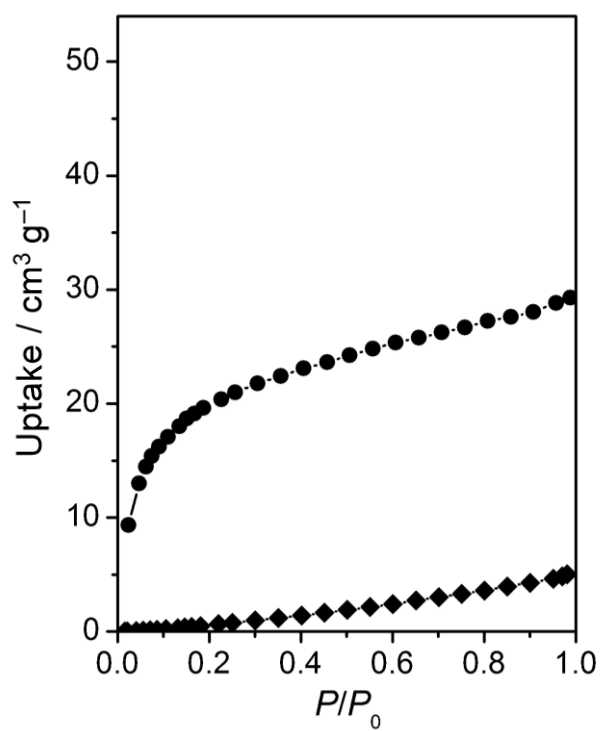
Figure III-17. Comparison of CO_2 at 195 K (−●−) and N_2 at 77 K (−◆−) adsorption isotherms for **5b**.
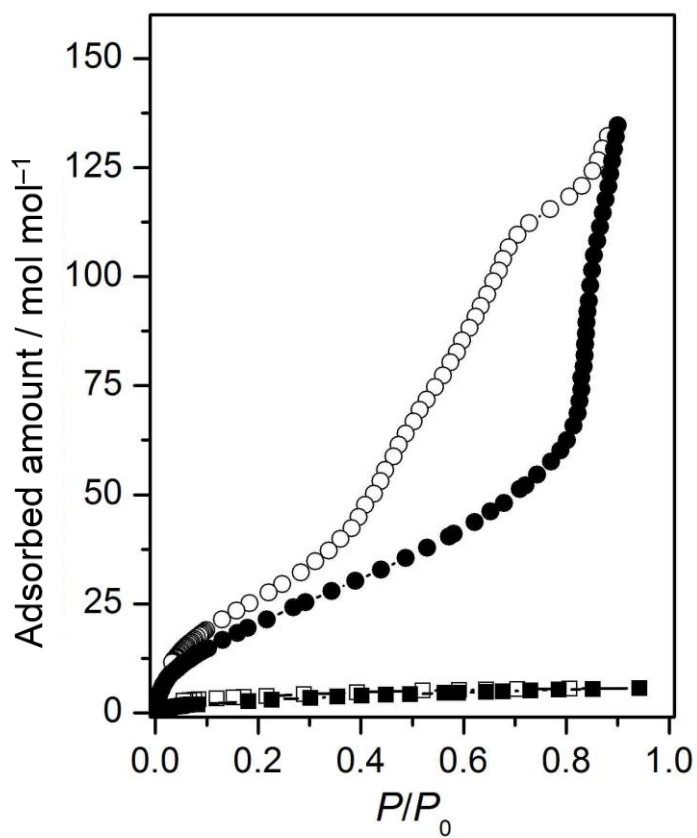
Figure III-18. Comparison of H$_2$O adsorption (solid symbols) and desorption (open symbols) isotherms at 298 K for **5a** (–■–) and **5b** (–●–).
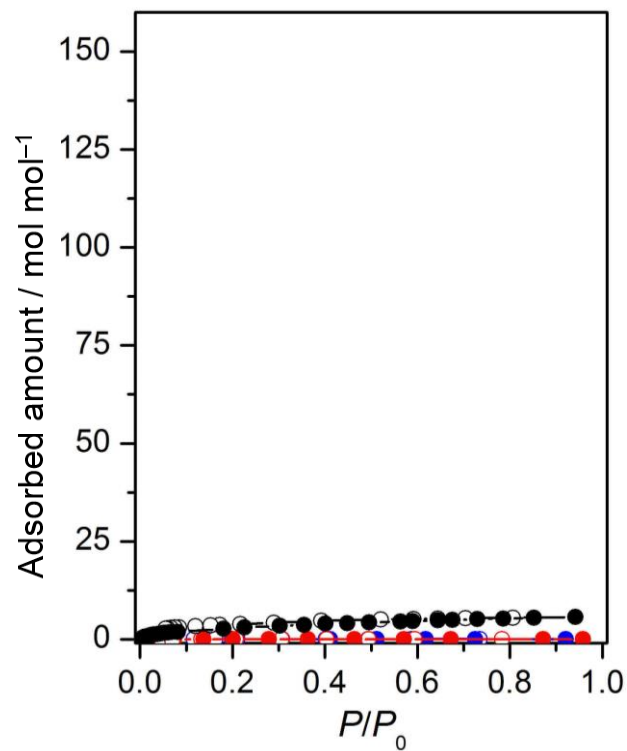
Figure III-19. Vapor adsorption (solid symbols) and desorption (open symbols) isotherms of **5a** for H_2O (black), EtOH (blue), and acetone (red) vapors at 298 K.
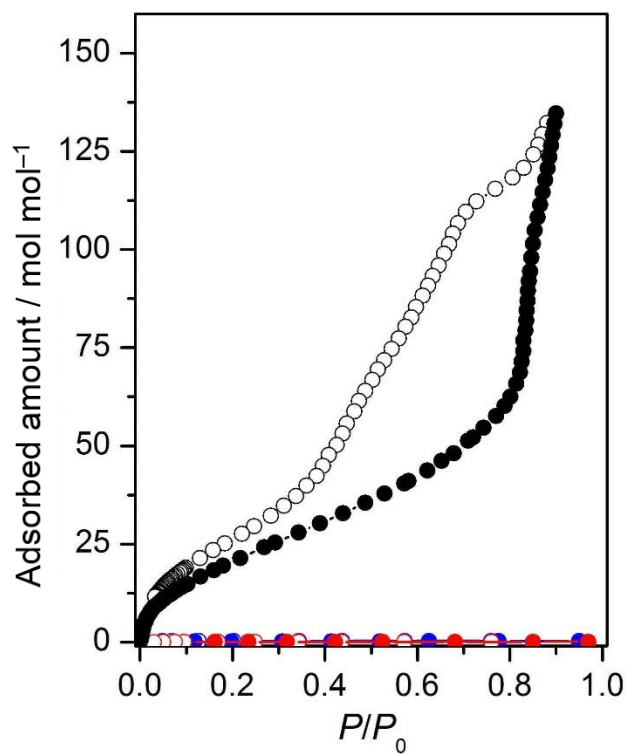
Figure III-20. Vapor adsorption (solid symbols) and desorption (open symbols) isotherms of **5b** for H_2O (black), EtOH (blue), and acetone (red) vapors at 298 K.

117

Table III-1. Crystallographic data of **5a** and **5b**.

	5a	5b
Formula	$C_{30}H_{52}Au_3Co_2N_6O_{18.5}S_6Zn$	$C_{94}H_{240}Au_9Co_6N_{18}Na_2O_{124}S_{18}Zn$
Color, form	Purple, square block	Purple, hexagonal block
Formula weight	1759.32	6421.84
Crystal system	Orthorhombic	Hexagonal
Space group	$I222$	$P6_122$
a / Å	10.307(3)	44.24850(10)
b / Å	18.544(5)	44.24850(10)
c / Å	27.144(7)	28.44460(10)
α / °	90	90
β / °	90	90
γ / °	90	120
V / Å^3	5188(2)	48231.1(3)
Z	16	18
T / K	100(2)	100(2)
F(000)	21776	30024
ρ_{calcd} / g cm^{-3}	14.068	2.162
μ(Mo Kα) / mm^{-1}	46.617	9.043
Crystal size / mm^3	0.10×0.06×0.06	0.18×0.15×0.11
Limiting indices	$-13 \leq h \leq 12$, $-24 \leq k \leq 23$, $-35 \leq l \leq 34$	$-64 \leq h \leq 56$, $-56 \leq k \leq 60$, $-37 \leq l \leq 37$
$2\theta_{max}$ / °	54.08	66.79
R_1[a] $(I>2\sigma(I))$	0.0378	0.0777
wR_2[b] (all data)	0.0816	0.2320
GOF	0.954	1.073

[a]$R_1 = (\Sigma|(|F_o| - c|F_c|)|)/(\Sigma|F_o|)$

[b]$wR_2 = [\{\Sigma w(F_o^2 - cF_c^2)^2\}/(\Sigma w|F_o^2|^2)]^{1/2}$

Concluding Remarks.

The studies presented in this thesis focused on the construction of novel metallosupramolecular frameworks, in which both coordination and hydrogen bonds are utilized, by employing the rod-shaped $Co^{III}_2Au^I_3$ pentanuclear complex with D-penicillaminate, $[Co^{III}_2Au^I_3(\text{D-pen-}N,S)_6]^{3-}$ ($[1]^{3-}$; D-H_2pen = D-penicillamine), as a molecular building block. The combinations of the $Co^{III}_2Au^I_3$ pentanuclear-complex anions that possess six carboxylate arms and the different kinds of simple aqua transition metal cations, $[M(H_2O)_n]^{2+}$ (M = Co^{2+}, Ni^{2+}, Mn^{2+}, Zn^{2+}), were investigated under varied synthetic conditions. This research expanded the methodology for the design and construction of metallosupramolecular frameworks, in which a series of unique metallosupramolecular structures with different porosities are created depending on not only the nature of metal ions but also the synthetic parameters.

In Chapter I, the kinetic synthesis of the highly porous metallosupramolecular framework of $[Co(H_2O)_6]_3[Co_2Au_3(\text{D-pen-}N,S)_6]_2$ (**2a**) was accomplished by the combination of $[1]^{3-}$ and $[Co(H_2O)_n]^{2+}$ under highly concentrated conditions. The ionic crystal **2a** illustrated the extremely high porosity of *ca.* 80%, in which the anionic $[1]^{3-}$ and cationic $[Co(H_2O)_6]^{2+}$ species are alternately linked solely by COO···HO hydrogen bonds. This is owing to the presence of terminal, non-coordinating carboxylate groups in the rod-shaped chiral $[1]^{3-}$ anion that can form screwed, 3-connected hydrogen bonds around the aqua groups in the octahedral $[Co(H_2O)_6]^{2+}$ cation. Impressively, this is the highest porosity so far reported for ionic crystals consisting of cationic and anionic species without the formation of coordination bonds. Moreover, it was found that crystal **2a** was kinetically produced and stepwise structural converted to the thermodynamically more stable products with denser frameworks, $[Co(H_2O)_6]_2[\{Co(H_2O)_4\}\{Co_2Au_3(\text{D-pen-}N,S)_6\}_2]$ (**2b**; porosity *ca.* 60%) and $[\{Co(H_2O)_4\}_3\{Co_2Au_3(\text{D-pen-}N,S)_6\}_2]$ (**2c**; porosity *ca.* 30%), induced by the coordination of the carboxylate groups toward the Co^{II} centers. Such a unique stepwise conversion, in which all three solid phases are crystallographically characterized, is quite rare. In addition, the selective capture of H_2O over EtOH or acetone, as well as that of CO_2 over N_2, was recognized for **2a**, which is ascribed to its highly porous framework with superhydrophilic opening channels.

In order to study about the effects of different metal ions on the construction of metallosupramolecular frameworks, other metals were used as cationic species in Chapter II. The combinations of $[1]^{3-}$ and $[Ni(H_2O)_n]^{2+}$ or $[Mn(H_2O)_n]^{2+}$ successfully produced four metallosupramolecular frameworks. An isostructural pair of porous ionic crystals, $[Ni(H_2O)_6]_2[\{Ni(H_2O)_4\}\{Co_2Au_3(D\text{-}pen\text{-}N,S)_6\}_2]$ **(3a)** and $[Mn(H_2O)_6]_2[\{Mn(H_2O)_4\}\{Co_2Au_3(D\text{-}pen\text{-}N,S)_6\}_2]$ **(4a)**, was produced under similar synthetic conditions, followed by the structural conversion to different frameworks. Crystal **3a** showed a similar conversion to that of $[Co(H_2O)_6]_2[\{Co(H_2O)_4\}\{Co_2Au_3(D\text{-}pen\text{-}N,S)_6\}_2]$ **(2b)**, described in Chapter I, in which the dense framework of $[\{Ni(H_2O)_4\}_3\{Co_2Au_3(D\text{-}pen\text{-}N,S)_6\}_2]$ **(3b)** with a low porosity of *ca.* 30% was formed. Notably, crystal **4a** was converted to the different framework of $[\{Mn(H_2O)_4\}\{Co_2Au_3(D\text{-}Hpen\text{-}N,S)(D\text{-}pen\text{-}N,S)_5\}]$ **(4b)**, presenting a lower porosity of *ca.* 13%. The structural conversion occurred in the Mn^{II} complexes was different from that in Co^{II} or Ni^{II} complex, leading to the different frameworks with different porosities. This should be ascribed to the differences in the nature of each metal ion. The flexible coordination sphere of Mn^{2+} ion owing to its larger ionic radius, together with its faster rate of water exchange than those of Co^{2+} and Ni^{2+} ions, allowed Mn^{2+} ion to form a more rigid framework in order to stabilize the whole structure. Expressly, the selective adsorptions of H_2O and CO_2 were observed for all metallosupramolecular frameworks obtained (**3a**, **3b**, **4a**, and **4b**), reflecting their superhydrophilic characteristics.

In Chapter III, the effects of pH on the construction of metallosupramolecular frameworks were investigated by means of the reactions of $[1]^{3-}$ with $[Zn(H_2O)_n]^{2+}$ in sodium acetate buffer solutions. This is due to the rapid crystallization in water system, in which X-ray quality crystals could not be obtained. As a result, the production of two different metallosupramolecular frameworks, $[\{Zn(H_2O)_4\}\{Co_2Au_3(D\text{-}Hpen\text{-}N,S)(D\text{-}pen\text{-}N,S)_5\}]$ **(5a)** and $Na_9[\{Zn(OAc)_2\}\{Co_2Au_3(D\text{-}pen\text{-}N,S)_6\}_2][Co_2Au_3(D\text{-}pen\text{-}N,S)_6]$ **(5b)**, with remarkably different porosities was successfully controlled only by a slight pH change. Under the pH range of 4.0-5.0, the coordination polymer of **5a** that is isostructural with $[\{Mn(H_2O)_4\}\{Co_2Au_3(D\text{-}Hpen\text{-}N,S)(D\text{-}pen\text{-}N,S)_5\}]$ **(4b)** described in Chapter II, with a low porosity of *ca.* 13% was produced. The construction of the porous ionic framework of **5b** with a drastically increased porosity up to *ca.* 61% was achieved when a slightly higher pH range of 5.5-6.5 was applied. The dense framework of **5a** was stabilized by the protonation on the

D-pen carboxyl groups at a lower pH. On the other hand, at a higher pH, the protonation effect was disappeared and the formation of porous framework of **5b** was promoted by the guest templating effect of Na^+ and OAc^- ions. Moreover, the most notable result in this system is the systematic pH-controlled construction of metallosupramolecular frameworks, in which a drastic increase of crystal porosities from a dense coordination polymer to a porous ionic framework was accomplished, has never been observed previously. Furthermore, **5b** exhibited the extremely high performance for water uptake, comparable to that of highly porous MOFs, which is attributable to the superhydrophilic opening channels in its stable framework sustained by the existence of multiple hydrogen bonds.

Finally, this study demonstrated the expanded methodology for the construction of novel metallosupramolecular frameworks by the introduction of the rod-shaped heterometallic multinuclear complex that offers the multiple carboxylate arms, as a molecular building block, in the combinations with different kinds of aqua metal cation. Thanks to the feasible utilization of both coordination and hydrogen bonds, a series of unique metallosupramolecular frameworks illustrating a high flexibility and stability were created, in which the diversities from a dense framework to a highly porous frameworks controlled by kinetics, metal types, and solution pH were established. The successful production of various metallosupramolecular frameworks earned the benefits from the well-designed heterometallic multinuclear building block of the rod-shaped $Co^{III}_2Au^I_3$ pentanulear-complex anion. This is owning to the presence of multiple carboxylate arms, good stability and retention of chirality, and high solubility, together with the well-fixed conformation, which is proper to form a variety of intermolecular interactions not only coordination bond but also hydrogen-bonding interaction with the aqua metal cations. Moreover, the highly selective captures of H_2O and CO_2 were recognized for the resulting metallosupramolecular frameworks, especially for the porous frameworks. This is attributable to the superhydrophilic property of the opening channels, surrounded not only by the D-pen amine and carboxyl groups of the employed $Co^{III}_2Au^I_3$ pentanulear-complex anion but also by the aqua groups in aqua metal cations. Such a superhydrophilicity of the opening channels is highly applicable for the inclusion of hydrophilic molecules. Ultimately, the methodology presented in this thesis would guide to a great progress in the design and creation of new classes of metallosupramolecular frameworks which may convey to functional expansions.

Acknowledgement.

August 2016

Sireenart Surinwong